DEVELOPMENT OF THE PRELIMINARY GUIDELINES FOR THE EVALUATION AND REPAIR OF PORTABLE CONCRETE BARRIERS

A Thesis

by

SRISHTI BHUTANI

Submitted to the Graduate and Professional School of
Texas A&M University
in partial fulfillment of the requirements for the degree of

MASTER OF SCIENCE

Chair of Committee,	Stefan Hurlebaus
Committee Members,	Chiara Silvestri Dobrovolny
	Anastasia Muliana
Head of Department,	Zachary Grasley

December 2021

Major Subject: Civil Engineering

ABSTRACT

Portable concrete barriers (PCBs) are roadway safety hardware designed to contain and redirect vehicles during accidents and prevent vehicles from entering the construction zone, while protecting drivers. The Texas Department of Transportation (TxDOT) requires a set of formal guidelines governing the evaluation and repair of PCBs. Arriving at the guidelines is a multi-task research procedure. Objectives of this project are: (i) to conduct a non-destructive evaluation (NDE) of selected PCBs (ii) to develop preliminary evaluation guidance for the classification of PCBs and to propose repair procedures for minor damages, (iii) to develop calibrated finite element models of PCB in LS-DYNA (an advanced general-purpose multi-physics simulation software package) and study the behavior of damaged and undamaged PCB assembly when subjected to impact by MASH vehicles, (iv) to identify the most critical pre-existing damage or a combination of damages and further evaluate its effect on the crashworthiness of the PCB by carrying out predictive finite element analysis (FEA) simulations.

NDE was conducted to analyze the internal structure of selected damaged PCBs and see whether a correlation existed between the NDE results and the damages observed in the component crash test with the surrogate test vehicle. Based on the findings of the latest literature review and observations from the component crash test, a preliminary evaluation and repair guidance was drafted for PCBs. Finite element model of the PCB assembly was developed in LS-DYNA, it was validated by running a crash

simulation with surrogate vehicle, which replicated the results of the component crash test previously conducted. Predictive simulations were carried out to impact the undamaged and pre-damaged models of 210-foot-long PCB assembly with MASH vehicle models under the Test Level-3 (TL-3) impact conditions. Crash data obtained was further processed in TRAP (Test Risk Assessment Program) and compared with the corresponding prescribed limits given in MASH. The location and extent of pre-existing damages in the PCB were decided based on the provisions outlined in the preliminary guidance. The researcher recommends verifying the FEA results of this research study by carrying out full-scale crash testing under MASH TL-3 impact conditions.

DEDICATION

I dedicate this research study to my parents, Brigadier (Dr.) Rajeev Kumar Bhutani and Mrs. Deepa Bhutani without whose unconditional support I could not have completed the master's course, my sister, Dr. Akanksha Bhutani who never hesitated to share her experiences with me, my furry companion, Gullu whose innocence helped me stay positive during my toughest time, the numerous mentors who guided me to the correct path whenever I made mistakes and my truly genuine friends from India and the US, each of whom inspired me in their own unique way to never give up in the face of difficulties and emotional distress. This work wouldn't have been possible without the endless morale support that I got from this incredible team of people that backed me up at various stages.

ACKNOWLEDGEMENTS

I would like to thank my advisor Dr. Stefan Hurlebaus who introduced me to the Computational Mechanics Institute of the Roadside Safety and Physical Security Division at Texas A&M Transportation Institute (TTI). Dr. Hurlebaus provided the technical support by educating me on the basics of NDT equipment. He made sure I had round the clock access to the Sensors Laboratory at Centre of Infrastructure Renewal (CIR) where the NDT devices and the computer system with the associated image processing software were located. His inputs and the literature materials he supplied on repair methodologies, cracking in portable concrete barriers and corrosion evaluation of rebars helped me immensely in drafting the guidelines for the evaluation and repair of barriers. I would like to thank Dr. Chiara Silvestri Dobrovolny who provided me the opportunity to work under her guidance on the TxDOT Project 0-7059: Develop Guidelines for Inspection, Repair and Use of Portable Concrete Barriers (PCBs). Dr. Dobrovolny's continuous feedback on simulations and various intermediate reports not only helped me in getting realistic results but also immensely improved my knowledge of computational mechanics and understanding of the dynamic behavior of the portable concrete barrier-vehicle system.

Since this individual project is a part of TxDOT project 0-7059 awarded to TTI, researchers of TTI had a major role to play in supporting this project. I would like to thank Dr. Roger Bligh and Dr. Nauman Sheikh who participated in the periodic review meetings where they provided valuable insights on the crash simulations. Their vast

experience in the field of crash testing and computational research benefitted me in a huge way. I would like to acknowledge the help provided by Dr. Husain Aldahlki who made sure I got access to the data and resources gathered from the DOT survey he undertook along with other researchers during January-May 2020. Dr. Aldahlki extended great support and guidance in debugging the finite element model. I would like to thank Sofo Cakalli whose insights helped me identify and fix the initial fundamental issues that I faced while developing the model in LS-DYNA. Further, I would like to acknowledge the support extended by TTI Laboratory. Not only the laboratory staff gave me access to the crash videos and data records, but they also made sure I got an easy access to the PCBs on the TTI proving ground for the conduction of non-destructive testing (NDT) and supplied the tools required to mark the barrier prior to the conduction of NDT.

Since this project is a computational effort on a major scale, it would not have been possible without the necessary computational resources and specialized software. The numerical models were developed with the help of a non-linear dynamic analysis program called LS-DYNA, provided by ANSYS LST. The computer simulations were run on a super-computer with the support provided by Texas A&M High Performance Research Computing (HPRC) using SUs allocated by Dr. Stefan Hurlebaus and Dr. Akram Abuodeh (TTI). The raw data from the crash simulations in LS-DYNA was further processed in a software developed by TTI called Test Risk Assessment Program (TRAP).

CONTRIBUTORS AND FUNDING SOURCES

Contributors

This work was supervised by a thesis committee consisting of Dr. Stefan Hurlebaus of the Department of Civil & Environmental Engineering [advisor], Dr. Chiara Silvestri Dobrovolny of Texas A&M Transportation Institute [committee member] and Professor Dr. Anastasia Muliana of the Department of Mechanical Engineering [committee member].

The steel stress strain curve data provided in Chapter 7 was provided by Dr. Nauman Sheikh, TTI. The FEM models of the MASH vehicles namely, RAM Pickup Truck and Toyota Yaris Passenger Car were developed by GMU and were directly included in the assembly. The geometric details of the secondary components of the connection such as the angle plates were modelled by the Graduate Assistant Researcher Aniruddha Zalani.

All other work conducted for the thesis was completed by the student independently.

Funding Sources

Graduate study was supported by the funding provided to Texas A&M Transportation Institute by the Texas Department of Transportation [TxDOT] for the Project 0-7059 Develop Guidelines for the Inspection, Use and Repair of Portable Concrete Barriers.

Contents of this work are solely the responsibility of the authors and do not necessarily represent the official views of the TxDOT.

NOMENCLATURE

AASHTO	American Association of State Highway and Transportation Officials
ATSSA	American Traffic Safety Services Association
CEB	Comité européen du béton - European Committee for Concrete
CIP	Critical Impact Point
CNRB	Constrained Nodal Rigid Body
DOT	Department of Transportation
FEA	Finite Element Analysis
FE	Finite Element
FHWA	Federal Highway Administration
FIP	Fédération Internationale de la Précontrainte
GPR	Ground Penetrating Radar
GSSI	Geophysical Survey Systems, Inc.
IN.	Inches
MAXPAR	Maximum parametric coordinate
MPH	Miles per hour
NDT	Non-Destructive Testing
PCB	Portable Concrete Barrier
RADAR	Radio Detection and Ranging
SBOPT	Segment based contact option

SCDOT	South Carolina Department of Transportation
SOFSCL	Scale factor for constraint forces of soft constraint
TRAP	Test Risk Assessment Program
TTI	Texas A&M Transportation Institute
TxDOT	Texas Department of Transportation

TABLE OF CONTENTS

Page

LIST OF FIGURES

Page

LIST OF TABLES

Page

1. INTRODUCTION

Portable concrete barriers (PCBs) are roadway safety hardware designed to protect workers in construction zones from traffic. A PCB assembly contains and redirects vehicles during accidents and prevents vehicles from entering the construction zone, while protecting drivers. Continuing to use severely damaged barriers and not replacing them in a timely manner can pose a safety risk, while replacing them too early underestimates their design life and adds to the overhead cost of the project. PCBs are made of precast shaped sections (e.g., F shape, single slope, and low profile) joined together with the help of appropriate connections to form a continuous longitudinal barrier.

Having a set of guidelines for the inspection and use of PCBs helps the engineer in charge determine if the PCB is appropriate to use at several work stages, such as upon delivery to the project site, during initial setup, during phase changes, and periodically throughout the duration of the project. To assess the condition of the PCB, the engineer is required to thoroughly assess the condition of the concrete surface and reinforcement; match the findings with the expectations of acceptability, repairability, and unacceptability laid down by the guidelines; and accordingly classify the PCB as acceptable, acceptable with repair, or unacceptable. Conditional assessment of a component of the PCB consists of looking for specific defects and their extent. For example, to assess the condition of the concrete surface of the PCB, the engineer in

charge should look for defects such as spalls and cracks. To assess the condition of the reinforcement, the engineer should check whether the reinforcing bar (rebar) is exposed or covered. The engineer should also check the condition of the steel plate to see if it has any initial discontinuity or signs of early or advanced stage corrosion, and whether the connection between the JJ hooks of the two barrier segments is rotated or straight.

Over the time, different transportation agencies such as State Departments of Transportation (DOTs), American Association of State Highway and Transportation Officials (AASHTO), Federal Highway Administration (FHWA), American Traffic Safety Services Association (ATSSA) have come up with their own set of guidelines to help the engineer on site determine the suitability of the PCB. In a survey conducted by the researchers of Texas A&M Transportation Institute (TTI), all the state DOTs were contacted and asked whether they had a formal guidance related to the inspection, evaluation, and repair of PCBs. In case, they did not have a formal guidance, they were asked what procedure they followed to inspect, evaluate, and repair the PCB. Regarding the evaluation and repair guidance, 27 state DOTs responded back while the other 23 state DOTs did not revert to the survey questions. Out of the 27 state DOTs which responded back, 16 state DOTs were found to have a formal evaluation guidance and 11 state DOTs did not have any formal evaluation guidance. Out of the 16 state DOTs with evaluation guidance, 5 state DOTs directed the researchers to the document which they used for inspection while 3 state DOTs said they followed guidelines laid down by ATSSA. Agencies with no formal evaluation guidance relied on the judgement of the maintenance, work zone or construction staff, visual inspection of concrete

surface/connecting loops/pins and criteria adopted by other DOTs. Regarding repair guidance, 8 out of 27 state DOTs were found to have a formal guidance and 18 state DOTs did not have any formal guidance. 1 state DOT reverted with ‘other’ response. Agencies with no formal guidance on repair either relied on the judgement of the maintenance, work zone or construction staff, visual inspection or would have the damaged PCB segments replaced by the contractor (1). On reviewing the publicly available documents of various DOTs, it was seen that different DOTs had different acceptance criteria for the concrete surface. Regarding pre-existing concrete spalls, DOTs had different thresh hold values for the acceptable size/extent. The acceptable size varied with respect to the location of the spall in different documents. While DOTs of states such as New York, Florida, New Jersey, South Carolina, Wisconsin, Iowa, and Virginia classified PCBs into two categories namely acceptable and unacceptable, DOTs of states such as Kansas, Ohio, Illinois, Indiana, Oregon, and Washington classified PCBs into three categories namely acceptable, marginal, and unacceptable. All these DOTs instruct to inspect the connections on a qualitative basis only i.e., if the connection is bent, deformed, or rotated, PCB is rejected. DOTs of states such as Virginia, Indiana, Oregon, Washington, and Wisconsin do not give out any critical sizes of pre-existing concrete spall, rather their guidelines are qualitative in nature. Except New York DOT, all the other DOTs instruct to inspect cracks on a qualitative basis only. Multiple open transverse cracks are considered as unacceptable by all the DOTs, whereas multiple hairline cracks are considered as either acceptable or marginal.

It may be concluded that the evaluation guidelines suggested by different DOTs lay down different quantitative criteria for acceptance and in parts, are very subjective to the knowledge of the inspector evaluating the PCB. Wherever the DOTs have suggested some critical sizes/areas/volumes of pre-existing concrete damage, the numbers are found to be different in different guidelines and when compared, these sizes/areas/volumes are not even close to each other. It is very difficult to comprehend which recommendation would be most practical without running an engineering analysis or an actual crash test.

Among these DOT guidelines, the least conservative (or the most critical) pre-existing damage or a combination of damages will be identified, and its effect on the crashworthiness of the barrier system will be assessed by carrying out an engineering analysis with MASH TL-3 impact conditions.

The main objective of this research study is to develop preliminary guidelines for the evaluation and repair of TxDOT PCBs. This guidance shall be based on the current practices of other state DOTs complemented with the observations made from the results of the component crash test conducted at the TTI proving ground and findings of a predictive engineering analysis performed to determine the crashworthiness of full-scale barrier systems with different damage modes. In case there is a contradiction between the DOT guidelines and findings of the engineering analysis, the latter shall govern. All the objectives of this project are summarized below:

(i) To conduct a non-destructive evaluation of selected PCBs.

(ii) To develop a preliminary evaluation guidance for the classification of

PCBs and to propose repair procedures for minor damages.

(iii) To develop calibrated finite element models of PCB and predict the crashworthiness of full-scale PCB systems (with different damage modes) under MASH TL-3 impact conditions through FEA simulations.

1.1 References

1. Dobrovolny Chiara Silvestri, Bligh Roger, Hurlebaus Stefan, Aldahlki Husain, Agarwal Hemangi, Moran Sana, Technical Memorandum 2 for TxDOT Project 0-7059, “Develop Guidelines for Inspection, Repair and Use of Portable Concrete Barrier”.

2. COMMON DAMAGES FOUND IN PORTABLE CONCRETE BARRIERS

2.1 Spalling

2.1.1. Description

Spalling is the breaking of flakes of concrete from the barrier body. Spalled concrete zones look like depressions along the barrier surface and corners. Figure 1 and Figure 2 show spalled zones at different locations in PCBs.

(a) **(b)**

Figure 1. Spalling Observed in Crash Barriers in Bogie Tests: (a) Spall on the Middle Base of the Barrier; (b) Spall on the Toe of the Barrier.

(a) **(b)**

Figure 2. Real-Life Spalling Observed in Crash Barriers from a Stockyard: (a) Spall on the Middle Base of the Barrier; (b) Spall on the Toe of the Barrier.

2.1.2. Causes

2.1.2.1. Transportation, Handling, and Placement of Portable Concrete Barrier Segments

Portions of PCBs are likely to get spalled off by varying degrees depending on the extent to which they are impacted when they are being transported from the precast yard to the jobsite and placed next to each other by forklift or crane.

The heavy weight of PCBs makes their transportation and handling inconvenient and expensive. Weight of a PCB ranges from 4800 lb. to over 20,000 lb. depending on the segment length and cross-sectional dimensions. In addition to the weight, the size of PCBs also plays an important role in deciding the number

of PCB segments that can be transported in a single truckload. The typical width of a PCB is approximately 24 inches. The available length and width of a trailer are 40 ft and 7.5 ft, respectively. This allows three PCB segments to fit along the width of a trailer (1). Given the considerations of size and weight, several truckloads are required to achieve the desired protected length. An increase in the number of trips needed to transport PCBs from the yard to the jobsite therefore increases the chances of the PCBs getting damaged during transit and placement.

2.1.2.2. Corrosion of Rebars Embedded within the Concrete Barrier

When the rebar is exposed to moisture and water, possibly because of inadequate cover or surface irregularity, a chemical reaction takes place, resulting in the formation of iron oxide (rust) on the rebar surface. Due to the production of iron oxide, the rebar volumetrically expands by up to six times its original volume. This increase in volume imposes significant expansive forces on the surrounding concrete, which can cause a chunk of the concrete to spall and break off. Spalling increases access of air and water to the rebar embedded within the barrier and creates a cycle of corrosion, exacerbating the process with each subsequent cycle (2). Figure 3 shows an example of a barrier with a corroded rebar and spalled concrete.

Figure 3. Corrosion of Reinforcing Bar Embedded in the Toe of the Concrete Barrier.

2.1.2.3 Use of Non-Air-Entrained Concrete Mix

Air-entrained concrete uses a chemical admixture to produce a system of small voids during the mixing process. This admixture stabilizes the voids and keeps them suspended in the hardened concrete paste. During a freeze event, air voids provide pressure relief sites, allowing the water inside the concrete to freeze without inducing large internal stresses. The air voids also provide relief against the buildup of salt concentrations and the pressures that result due to concentration gradients. Having non-air-entrained concrete mix instead weakens the resistance against the freeze-thaw cycle, sulfates and alkali-silica reactivity which causes the concrete to flake or spall off (3).

2.1.2.4. Inadequate Curing

The curing of concrete is the process of maintaining moisture inside the concrete body during early life and beyond to develop the desired properties in terms of strength and durability. A good practice of curing involves keeping the concrete damp until it reaches the desirable strength (4). Insufficient curing leads to a weak surface skin susceptible to spall off if exposed to freezing and thawing in the presence of moisture and deicing salts (5).

2.1.2.5. Fire Damage

During fires, concrete can suffer extensive damage from temperature shock. When concrete is subjected to extreme heat, its outer layers expand more quickly than the inner sections. This differential expansion causes the concrete layers to separate and eventually break away (6).

2.1.2.6. Impact/Crash Loading

Vehicles crashing against the barrier during road accidents result in portions of the concrete breaking away (Figure 4). Depending on the vehicle type, impact speed, and angle, the extent of spalling may vary.

Figure 4. Spalling at the Toe of Barrier E due to a Vehicle Crashing into the Joint between Barriers A and E.

2.1.3. Effects on the performance of PCBs

2.1.3.1. Potential Snag Points

A snag point is a projection or depression that is of such magnitude that it can impart a strong longitudinal force to an impacting vehicle. If the vehicle snags, the strong force can cause high rates of deceleration and potential injuries to the occupants. If the strong force acts on a corner of the vehicle, the force can cause the vehicle to yaw, resulting in a potential rollover. The snagged element might also get deformed and penetrate the passenger compartment.

The effect of a snag point differs according to the type of vehicle. If a small vehicle hits the barrier, the vehicle can lean and get exposed to a snag point on the top of the barrier. If a large vehicle hits the barrier, the vehicle can cause the barrier to tilt, lift the toe, and snag strong elements low on the vehicle. Snag points can be created at

different locations, such as the top, edge, or toe. Depending on where the snag point is present, post-impact barrier performance and vehicle trajectory are affected differently. For example:

1. If the top edge is broken out at the lift point, the vehicle could get snagged to either the left or right. The snag point can catch the leading part of a door frame and crush it towards the passenger sitting in the vehicle.

2. If the snag point is at the toe, the barrier leans when it is strongly impacted. Areas broken out of the toe may be lifted above the bottom of the tire rims. At this height, they can snag other elements of the vehicle (6).

2.1.3.2. Increased Risk of Corrosion of Reinforcement Bars

Spalling exposes the embedded steel rebar to both water and air which cause it to rust. Iron from the steel rebar reacts with water and air to produce iron oxide (rust). Rust is up to six times more massive than the steel on which it deposits. The increase in rust mass creates a tensile stress that causes the surrounding concrete to crack and spall more. Spalling increases access of air and water to the reinforcing steel within a member which creates a cycle of corrosion, exacerbating the process with each subsequent cycle (2, 7).

2.1.3.3. Increased Deflection of the Concrete Barrier

Spalling leads to a reduced cross-sectional area of the concrete member and decreases its ability to safely carry imposed loads. The reduced cross-sectional area causes a significant reduction in the moment of inertia, which causes the deflection of the barrier to increase.

2.2. Cracking

2.2.1. Description

Cracks in concrete are complete or incomplete separation of the material into two or more parts through breaking or fracturing. Figure 5 shows cracks of varying extent at different locations of PCBs.

Figure 5. Cracking in Portable Concrete Barriers (8). Reprinted from Temporary Barrier Guidelines-Cracked Sections, NYSDOT.

2.2.2. Causes

2.2.2.1. Tight Clamping of Lifting Devices

The excessively tightened grip of lifting devices may lead to clustered horizontal cracks in the upper portion of the barrier stem. Figure 6 shows an example of clustered horizontal cracks.

Figure 6. Clustered Horizontal Cracks due to the Tight Clamping of Lifting Devices (10). Reprinted from Temporary Barrier Guidelines-Longitudinal Cracks, NYSDOT.

2.2.2.2. Mishandling during Lifting, Stacking and Transportation

Figure 7 shows the various stages of the transportation of PCBs: stacking, lifting, and loading. At any of these stages, pre-cast reinforced concrete barriers may be subject to stresses that overload them. If these stresses are encountered in the concrete's early life, the stresses may lead to permanent cracks in the barrier (11). Precast concrete barrier units should be lifted after the concrete has gained the required strength. Lifting

before the development of the desired strength causes the concrete to crack. Insufficient capacity of the lifting devices also causes damage to the barrier.

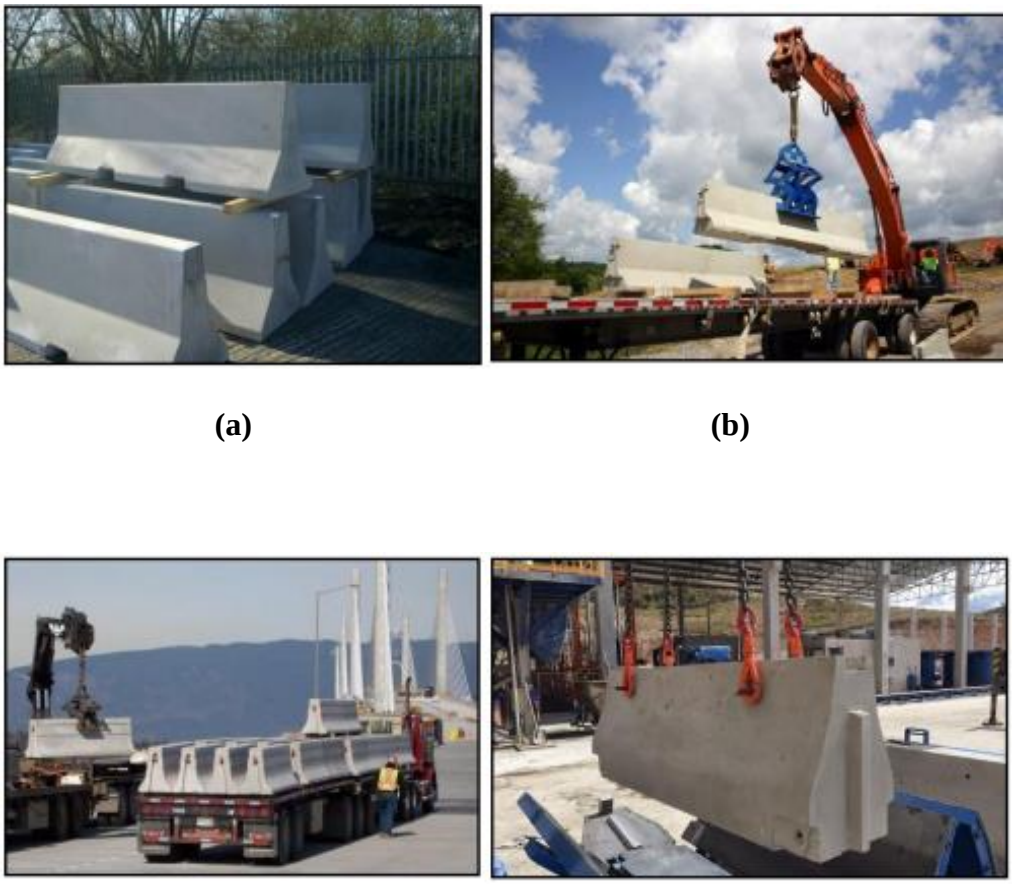

(a) **(b)**

(c) **(d)**

Figure 7. Various Stages in the Transportation of PCBs: (a) Stacking (12). Reprinted from externalworksindex.co.uk (b) Single-Point Lifting (13). Reprinted from kenco.com (c) Loading (14). Reprinted from eaglewestcranes.com (d) Two-Point Lifting (15). Reprinted from moldtechsl.es

2.2.2.3. Errors in Design and Detailing

One important aspect of design is ensuring sufficient and properly detailed reinforcement to withstand the bending stresses during lifting. Depending on the way the barrier is lifted, it could behave either as a cantilever beam (Figure 7b) or as a continuous beam (Figure 7d). The design engineer must have the correct sense of these support conditions to design the reinforcement area. Otherwise, the barrier is bound to crack on the tension side.

2.2.2.4. Shrinkage

Water more than the required amount is added to concrete mix to provide adequate workability for its placement and consolidation. Loss of some of this excess water from the concrete matrix as it hardens results in a volume reduction, which is known as shrinkage. If the volume reduction occurs before the concrete has hardened, it is called plastic shrinkage. It occurs via two modes: evaporation and absorption. Evaporation, being the predominant mode, depends on a combination of factors: wind speed, relative humidity, and temperature. The higher the wind speed, the lower the relative humidity and the higher the ambient temperature, rate of water evaporation increases. If the loss of moisture from an exposed surface exceeds the rate at which bleed water reaches the surface, the plastic shrinkage mechanism sets in. The volume reduction that occurs due to moisture loss after the concrete has hardened is called drying shrinkage. It occurs via complex mechanisms, but in general it involves the loss of adsorbed water from the hydrated cement paste. When concrete is initially exposed to a drying condition in which there is a difference between the relative humidity of the environment and that of the concrete, it first loses free water. In larger capillary pores,

this leads to little or no shrinkage, whereas in the finer water-filled capillary pores (2.5 to 50 nm), due to the loss of moisture, menisci (the curved upper surface of a liquid in a tube) are formed, and the surface tension of water pulls the walls of the pores. Internal negative pressure developed due to the formation of menisci in the capillary pores results in a compressive force that leads to concrete shrinkage. The thickness of the adsorbed water layer is reported to increase with increasing humidity. Therefore, a higher water content leads to a thicker layer of adsorbed water and more drying shrinkage. When the shrinkage movement is opposed by external or internal restraint, stresses develop. When these stresses exceed the tensile capacity of the concrete, cracks develop. Therefore, shrinkage should be considered at the design stage with appropriate detailing of reinforcement to minimize cracking. Usually, it takes several months to four years after casting for these cracks to form, depending on the rate of drying. Concrete near the corners and edges is vulnerable to cracking because loss of moisture takes place from the adjacent surfaces. There is no typical pattern that drying shrinkage cracking follows because the cracks form at any location where there is a restraint to shrinkage movement. Shrinkage cracks usually develop approximately at right angles to the direction of restraint (16, 17). Figure 8 shows examples of shrinkage cracks.

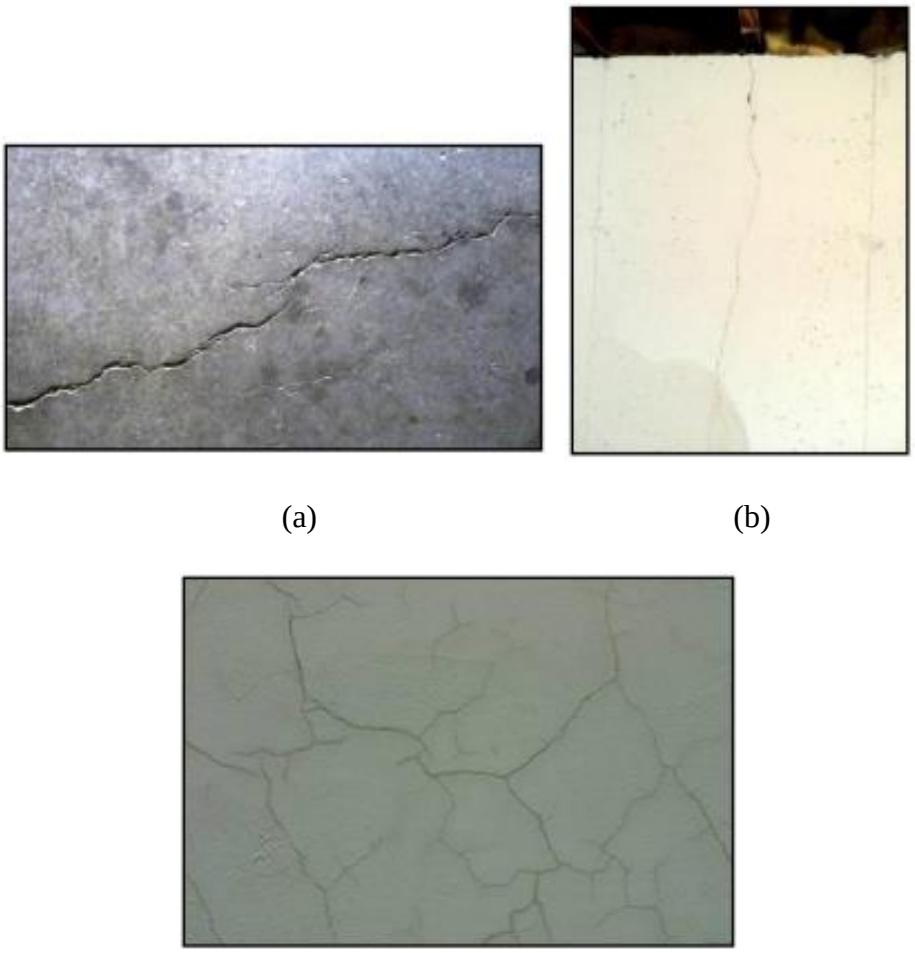

(a) (b)

(c)

Figure 8. Shrinkage Cracks (18,19,20) Note. Figure 8(a) Reprinted from "What are shrinkage cracks in concrete" by Gopal Mishra. Figure 8(b) Reprinted from "Structural vs Non-Structural foundation cracks" by Rachel Wood. Figure 8(c) Reprinted from "Types and Remedies of Cracks in Concrete" by Hasan Shirazi.

2.2.2.5. Chemical Reactions

Chemical reactions can be due to the materials used in the concrete mix taken to cast the barrier and due to the materials, the concrete mix may have encountered.

Cracking is caused by the expansive reactions that take place between the aggregate and

alkalis in the cement paste. The chemical reaction taking place between active silica and alkalis produces an alkali-silica gel as a byproduct (Figure 9). This gel forms around the aggregate surface, increasing its volume and putting pressure on the surrounding concrete. The increase in pressure can cause the tensile stresses to increase beyond the concrete's tensile strength, leading to cracks in concrete (21) (Figure 10).

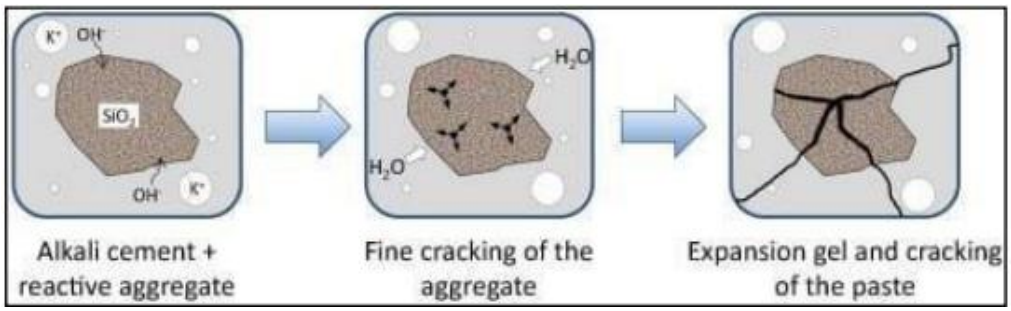

Figure 9. Cracking Mechanism due to Alkali-Silica Gel Formation (21). Reprinted from waterstopsolutions.com

Figure 10. Crack due to the Formation of More Voluminous Products (22). Reprinted from gharpedia.com

2.2.2.6. Corrosion of Steel Reinforcement

Three conditions that must be present to initiate corrosion are oxygen, moisture, and electron flow within steel. Elimination or limitation of any of these conditions reduces the corrosion of the steel reinforcement embedded in the concrete member, reducing the risk of cracking. Concrete provides a passive protection to the steel by forming a protective oxide coating around it in an alkaline environment. But as carbonation alters the concrete's levels of alkalinity, corrosion may take place. Iron oxides and hydroxides are formed as byproducts during the corrosive reaction. As these byproducts form on the surface of the steel reinforcement, volume of the rebar increases. This increase in volume increases the pressure on the concrete and causes radial cracking in the member because the tensile stresses developed in the concrete exceed the tensile strength (Figure 11). Repairing these cracks at the initial stage is important because as they become larger, oxygen and water have a greater chance to penetrate the concrete and accelerate the corrosion of the reinforcement (23).

Figure 11. Crack due to the Corrosion of Reinforcement (24). Reprinted from concrete.org.uk

2.2.2.7. Poor Construction Practices

Numerous poor construction practices, such as increasing the cement content to offset a decrease in strength from the addition of water, inadequate curing, etc. can lead to cracking in concrete (12) (Figure 12).

Figure 12. Crack-Like Formation due to the Lack of Mixing of Two Batches of Concrete during the Pour (21). Reprinted from waterstopsolutions.com

2.2.3. Effects on the performance of PCBs

2.2.3.1. Separation of Concrete into Loose Debris and Reduced Ability to Redirect Vehicles

Multiple closely spaced horizontal cracks caused due to the tightened grip of lifting devices weaken the strength of the stem. During an impact, these cracks reduce the ability of the barrier to redirect the vehicle and cause the concrete to separate in layers, flying off as debris that is detrimental to the safety of workers and incoming traffic (10).

2.2.3.2. Corrosion of Embedded Reinforcement

Cracks have a considerable impact on the durability of the barrier. Cracks enable the entry of foreign matter and aggressive substances into the concrete thickness. Studies have found that the eventual development of corrosion is independent of the crack width, whereas the time required for corrosion to start is a function of crack width. Corrosion of the embedded reinforcement starts as soon as an electrolytic cell is established. This occurs when the carbonization of concrete reaches the steel or when the chlorides penetrate the concrete thickness and make their way to the bar surface. The time taken for this cell to establish depends not only on the presence of a crack, the crack width, and the surrounding environment, but also on the thickness of cover and concrete permeability. After 5 to 10 years, the amount of corrosion is essentially independent of crack width (25). In addition to chlorides, relative humidity and ambient temperatures have a significant role to play in initiating corrosion. Corrosion is most probable to occur if the relative humidity exceeds 60 percent. Alternate wetting and drying of the concrete at the level of steel increase the chances of corrosion as well. High ambient temperature acts as a catalyst for the chemical reaction that is responsible for the corrosion action (25).

2.2.3.3. Increase in Deflection

When a reinforced concrete barrier section cracks, its moment of inertia decreases, leading to a decrease in its stiffness. When the barrier is further impacted, cracking increases, which causes a further reduction in stiffness. Eventually, the reinforcement yields at the impact point, leading to a large increase in deflection with minor change in load. Therefore, more impact loads lead to more cracking, which causes

a progressive reduction of stiffness, which ultimately results in increased deflection. Increased deflection of a PCB because of damage has some serious safety consequences, such as (26):

1. PCB may slide farther than expected into the construction zone, making the workers prone to serious injuries.
2. PCB may fall from an elevated structure into traffic, causing a fatal accident.
3. More deflection of the barrier may lead to the redirection of the impacting vehicle away from the barrier at a very high angle, potentially into incoming traffic.
4. PCB may fall into an excavation, injuring a worker or damaging a utility.

2.3. Damage to JJ Hook Connections

2.3.1. Description

F-shape and single-slope PCBs are connected via JJ hook connections, which consist of two identical J-shaped steel hooks, each of which is welded to an angle plate and multiple steel rebars (Figure 13a). This assembly provides a self-aligning continuous steel connection throughout the barrier installation. The connection automatically hooks into place without requiring workers to place their hands between the barrier units to make the connection. The major advantage of using JJ hooks to connect the barrier segments is that they are easy to install since the hooks are identical on both ends of the barrier. Since barriers can be vertically lifted, a single barrier unit can be removed without having to disturb the adjacent barrier units. There is no concern of lost or stolen hardware (bolts and pins) since this system is integrated in nature (27).

(a) **(b)**

Figure 13. JJ Hook Connections: (a) Isometric View of the JJ Hook Connection between Barrier Units; (b) Top View of a JJ Hook Connection between Barrier Units.

2.3.2. Causes

2.3.2.1. Manufacturing Flaws or Insufficient Material Properties

Any material discontinuity produced during the manufacturing of the JJ hook or plate may propagate to a bigger size because of repeated loading or corrosion, leading to the failure of the plate by brittle fracture (i.e., the plate fails at a stress well below the yield stress, and there is no or very little plastic deformation of the material, implying the full tensile capacity is not used). The fracture toughness of the steel used to make the JJ hook and plate may be low because the steel may have had non-uniform properties, because of improper heat treatment. If the barriers are used at a low service temperature (less than or equal to – 20°F), the material of the JJ hook plate may become brittle because its operating temperature is near its transition temperature.

2.3.2.2. Improper Transportation, Handling, and Placement

Just as initial discontinuities during manufacturing can later propagate to a bigger size because of fatigue or corrosion and lead to brittle fracture, cracks caused by improper transportation and handling have the same effect on the JJ hook. In addition, the hooks may get deformed, bent, or rotated if they are inadvertently impacted during transportation or handling.

2.3.2.3. Impact during Vehicular Collisions

Impact by vehicles during accidents transfers to JJ hooks, which in turn get deformed/rotated or suffer brittle failure. Rapid collision of the vehicle with the barrier assembly leads to an increase in the plate's tendency to fail by brittle fracture, owing to the resulting low fracture toughness.

2.3.3. Effects on the performance of PCBs

Deformation or rotation of the JJ hook leads to the opening of the connection between the two barrier segments. Repeated vehicle collisions with the barrier assembly reduce its ability to redirect the vehicle and cause the eventual separation of the segments.

2.4. References

1. Dobrovolny Chiara Silvestri, Shi Shengyi, Brennan Andrew, Bligh Roger, Sheikh Nauman, Synthesis of the Performance of Portable Concrete Barrier Systems, National Cooperative Highway Research Program Transportation Research Board of The National Academies of Sciences, Engineering, and Medicine, March 2019 http://onlinepubs.trb.org/onlinepubs/nchrp/docs/NCHRP22-36DraftReport-2019- 03-08.pdf

2. Concrete Spalling-Expert Article, Robson Forensic-The Experts, Last Accessed on May 28, 2021. https://www.robsonforensic.com/articles/concrete-spalling-expert-article/#:~:text=A%20spall%20is%20defined%20as,within%20the%20concrete%20member%20rusts.&text=These%20expansive%20forces%20can%20cause,%2C%20spall%2C%20and%20break%20off.

3. Finishing Air-Entrained Concrete, PCA America's Cement Manufacturers, Last Accessed on May 28, 2021. https://www.cement.org/learn/concretetechnology/concrete-construction/finishing-air-entrained-concrete

4. What Happens if Concrete is Not Cured Properly, Civil Site Visit, Last Accessed on May 28, 2021. https://civilsitevisit.com/what-happens-if-concrete-is-not-cured-properly

5. Scaling Concrete Surfaces-What, Why & How, Nevada Ready Mix, Last Accessed on May 28, 2021. https://www.nevadareadymix.com/concrete-tips/scaling-concrete-surfaces/

6. Benpeetz, Effects of Fire on Concrete Structures, Fire EMS, Last Accessed on May 28, 2021. http://notjustanotherfire.net/2017/03/31/effects-of-fire-on-concrete-structures/#gref

7. Concrete Surface Prep Part 1: Unsound Concrete, Graco Contractor, Last Accessed on May 28, 2021. https://www.graco.com/us/en/contractor/solutions/articles/concrete-surface-preppart-1-unsound-concrete.html

8. Temporary Barrier Guidelines- Cracked Sections, New York State Department of Transportation, Last Accessed on May 28, 2021.

https://www.dot.ny.gov/divisions/engineering/design/dqab/tcbacceptability/cracked_sections

9. Cracking in Concrete, American Concrete Institute (ACI), Last Accessed on May 28, 2021. https://www.concrete.org/topicsinconcrete/topicdetail/Cracking%20in%20Concrete?search=Cracking%20in%20Concrete

10. Temporary Barrier Guidelines- Longitudinal Cracks, New York State Department of Transportation, Last Accessed on May 28, 2021. https://www.dot.ny.gov/divisions/engineering/design/dqab/tcbacceptability/longitudinal_cracks

11. Evaluating Cracking in Concrete: Procedures, Giatec Scientific Inc., Last Accessed on May 28, 2021. https://www.giatecscientific.com/education/cracking-in-concrete-procedures/

12. Jersey Interlocking Concrete Safety/Security Barriers, External Works, Last Accessed on May 28, 2021. https://www.externalworksindex.co.uk/entry/115169/Elite-Precast-Concrete/Jersey-interlocking-concrete-safety-security-barriers/

13. Kenco Barrier Lift, Kenco, Last Accessed on May 28, 2021. https://kenco.com/products/barrier-lift/

14. Concrete Barrier Save Lives, Eagle West Cranes, Last Accessed on May 28, 2021. https://www.eaglewestcranes.com/concrete-barriers-save-lives/

15. Mold Tech, Last Accessed on May 28, 2021. https://www.moldtechsl.es/media/k2/galleries/238/MOLDTECH-MOLDE-DE-

BARRERAS-NEW-JERSEY-Y-PRETILES-Moulds-for-New-Jersey-barriersand-parapets-08.jpg

16. Nmai Charles, Bury Mark, Daczko Joseph, Shrinkage of Concrete: Minimizing/Eliminating the Potential for Cracking, Tilt-Up Today, Last 29 Accessed on May 28, 2021. https://tilt-up.org/tilt-uptoday/2018/01/27/shrinkage-of-concrete-minimizingeliminating-the-potential-for-cracking/

17. Drying Shrinkage Cracks, Concrete @ Your Fingertips, Last accessed on May 28, 2021. http://www.concrete.org.uk/fingertipsnuggets.asp?cmd=display&id=22#:~:text=Cracks%20formed%20by%20restraint %20to, in%20a%20reduction%20in%20volume

18. Gopal Mishra, What are Shrinkage Cracks in Concrete? – Types and Causes of Shrinkage Cracks, The Constructor-Building Ideas, Last Accessed on May 28, 2021. https://theconstructor.org/concrete/shrinkage-cracks-in-concrete-types-causes/9016/

19. Wood Rachel, Structural vs. Non-Structural Foundation Cracks, Quality Waterproofing-A Second Mile Service Company, Last Accessed on May 28, 2021. https://www.qualitywaterproofing.com/about-us/learning-center/structural-vs-non-structural-foundation-cracks

20. Hasan Shirazi PE, Types and Remedies of Cracks in Concrete, Prontubeam, Last Accessed on October 27, 2021. https://www.prontubeam.com/articles/2019-01- 28-Types-and-Remedies-of-Cracks-in-Concrete

21. Defects in Concrete Structures- With Focus on Identifying Concrete Cracks & How to Fix Them, Waterstop Solutions-Quality Service Quality Solutions, Last Accessed on

May 28, 2021. https://waterstopsolutions.com.au/identifying-concrete-cracks-how-to-fix-them/

22. Gharpedia, Last Accessed on May 28, 2021. https://gharpedia.com/wp-content/uploads/2018/08/0707020001-06-Cracks-due-to-Chemical-Reaction-_29567640_xxl-1024x683.jpg

23. Boullenois Eric, Why Does Concrete Crack? Part 2-The Impact of Cracks, Master Builders Solutions, Last Accessed on May 28, 2021. https://blog.masterbuilders-solutions.com/en/the-impact-of-cracks#:~:text=In%20general%2C%20a%20crack%20makes, and%20may%20lead%20to%20collapse

24. Cracks Due to Reinforcement Corrosion, Concrete @ Your Fingertips, Last Accessed on May 28, 2021. http://www.concrete.org.uk/fingertips-nuggets.asp?cmd=display&id=192

25. Wight, James K., and James G. MacGregor. Reinforced Concrete—Mechanics and Design. Fifth Edition, 2008.

26. Temporary Barrier Guidelines- Deflection Concerns, New York State Department of Transportation, Last Accessed on October 27, 2021. https://www.dot.ny.gov/divisions/engineering/design/dqab/tcbacceptability/deflection_concerns

27. Why JJ Hook Barrier, Concrete Safety Systems- JJ Hooks Concrete Barrier Rental, Last Accessed on May 28, 2021. https://concretesafetysystems.com/why-j-j-hooks-barrier/

3. OBSERVATIONS FROM THE BOGIE TEST SERIES

3.1 Introduction

3.1.1. Test Objective

Researchers at Texas A&M Transportation Institute constructed test installations for portable concrete barriers (PCB) as per the component testing plan and conducted bogie test on these installations to assess the baseline strength/deflection capacities of new barrier segments as well as corresponding residual capacities of damaged barrier segments. Impact speed of the bogie vehicle was determined in such a way that the impact severity equaled the bending capacity of the barrier about the vertical axis.

Various destructive tests were performed by crashing a 5000 lb. bogie vehicle perpendicularly into the barrier. Testing conditions, qualitative and quantitative characteristics of post impact damages seen in the barrier (namely, cracks, spalls, exposure of rebar, connection deformation) along with the resulting values of barrier deflection have been summarized in the next section.

3.2. Test Result Summary

Test Article Assembly: DEAB

Impact Point: Between Single Slope Barriers E and A (Joint E2-A1)

Table 1. Component Crash Test for Connection Capacity of JJ Hooks- Summary of Results

Test	Nominal Speed(mph)	Actual Speed (mph)	Percentage of Impact Severity	Condition of connection prior to impact	Max. Deflection (inches)
B-2	18	17.94	50	New	15.25
B-9	23	23.18	75	Damaged	31.6
B-7	26	26.00	100	Damaged	45.5
B-10	26	26.32	100	Damaged	49.5

Test Article Assembly: ABCDE

Impact Point: Middle of Single Slope Barrier C

Table 2. Component Crash Test for Single Slope Barrier Strength- Summary of Results

Test	**Nominal Speed (mph)**	**Actual Speed (mph)**	**Percentage of Impact Severity**	**Condition of connection prior to impact**	**Max. Deflection (inches)**	**Max. Crack Width (inches)**
B-1	**26**	**27.07**	**100**	**New**	**16.4**	**0.25**
B-8	**26**	**27.02**	**100**	**Damaged**	**19.7**	**1.5**

3.3. Post Impact Damages Observed in Single Slope Barriers

3.3.1. E2|A1 Joint- Impact Side

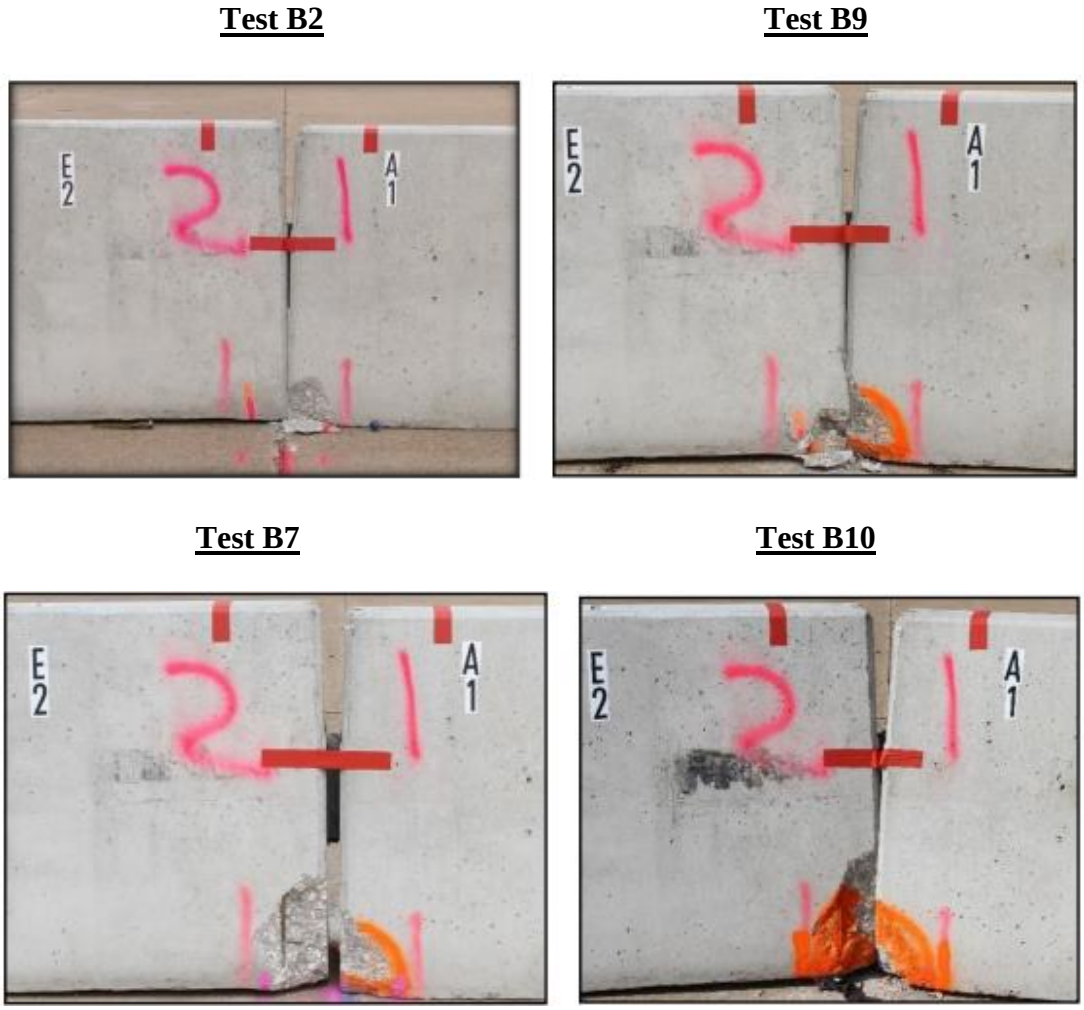

Figure 14. Damages observed in single slope barriers after the component testing performed to evaluate the connection capacity of JJ hooks.

In Test B2, bogie hit the joint between the single slope barriers E2 and A1 perpendicularly at a speed of 18 mph. As a result, concrete spalled off from the toe of the barrier A1. In Test B9, speed of the bogie increased to 23 mph due to which spall on the toe of barrier A1 increased in size and concrete from the toe of barrier E2 also got spalled. In Test B7, speed of the bogie increased to 26 mph. As a result, more concrete spalled off from the toe of barrier E2 exposing the embedded rebars. In Test B10, bogie hit the same joint at the speed of 26 mph because of which barrier E2 rotated more with an increase in the size of the spall.

3.3.2. JJ Connection at E2|A1 Joint

Test B2

Test B9

Test B7

Test B10

Figure 15. Stages of deformation of the joint between the single slope barriers E and A.

Rotation of the connection between the JJ hooks of the barriers E2 and A1 increased as the speed of the bogie increased from 18 mph (Test B2) to 26 mph (Test B10). Also, the JJ hooks successively opened more as the impact speed increased from 18 mph to 26 mph.

3.3.3. Single Slope Barrier C-Impact Side

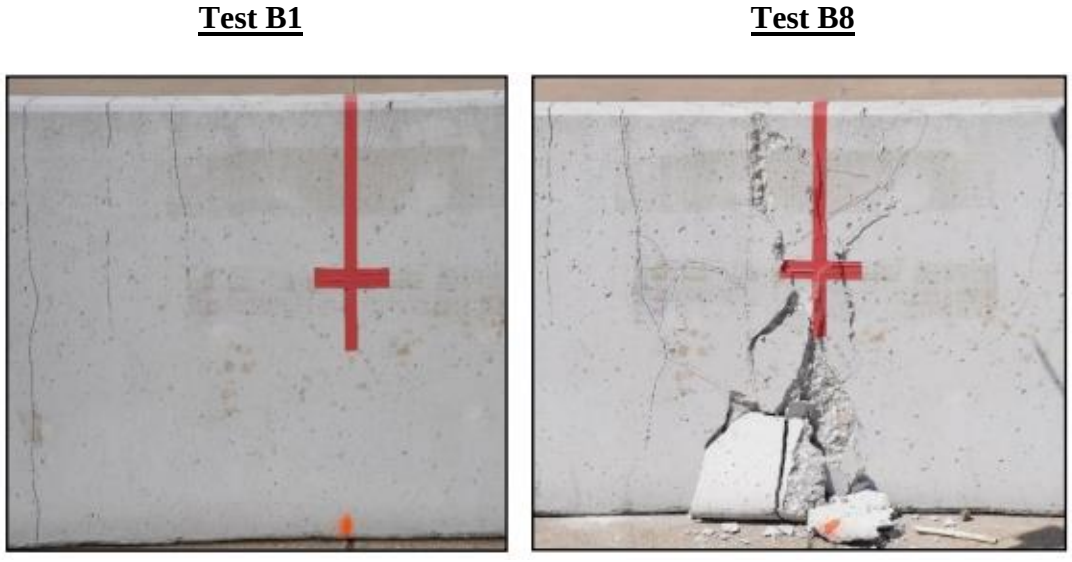

Figure 16. Damage observed on the impact side the single slope barrier after the component testing performed to evaluate the barrier strength.

In Test B1, bogie hit the single slope barrier C perpendicularly at a speed of 26 mph, few transverse cracks developed on the compression side of the barrier. On hitting the damaged barrier again at a speed of 26 mph, a major portion of concrete got crushed on the compression side of the barrier.

3.3.4. Single Slope Barrier C- Back side

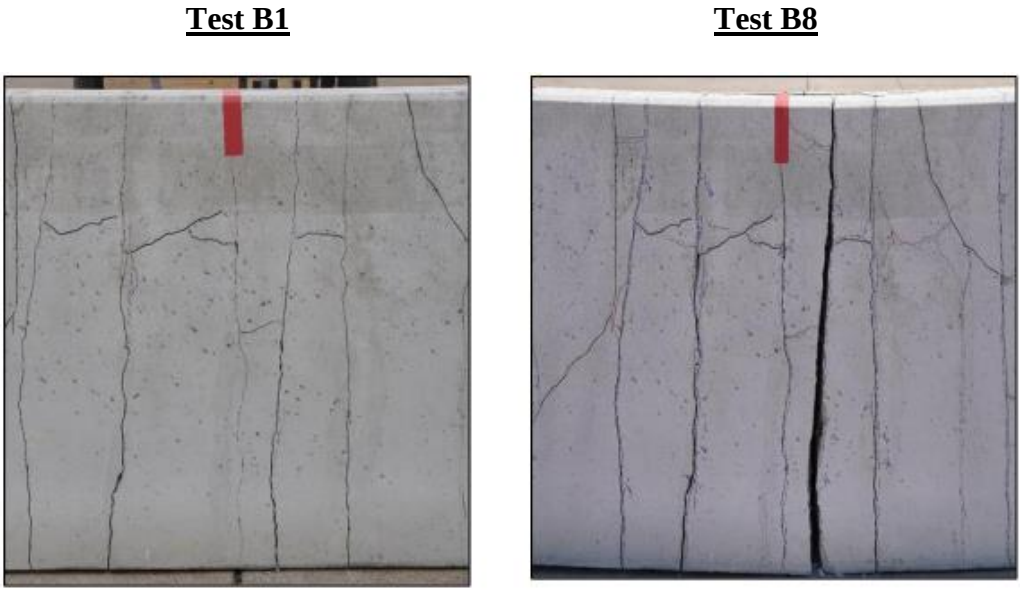

Figure 17. Damage observed on the back side the single slope barrier after the component testing performed to evaluate the barrier strength.

In Test B1, multiple transverse cracks developed on the tension side of single slope barrier C. Further in Test B8, when the damaged barrier was hit again at a speed of

26 mph, one of the transverse cracks on the tension side split open rendering the barrier completely unacceptable.

3.3.5. C|D Joint- Impact Side

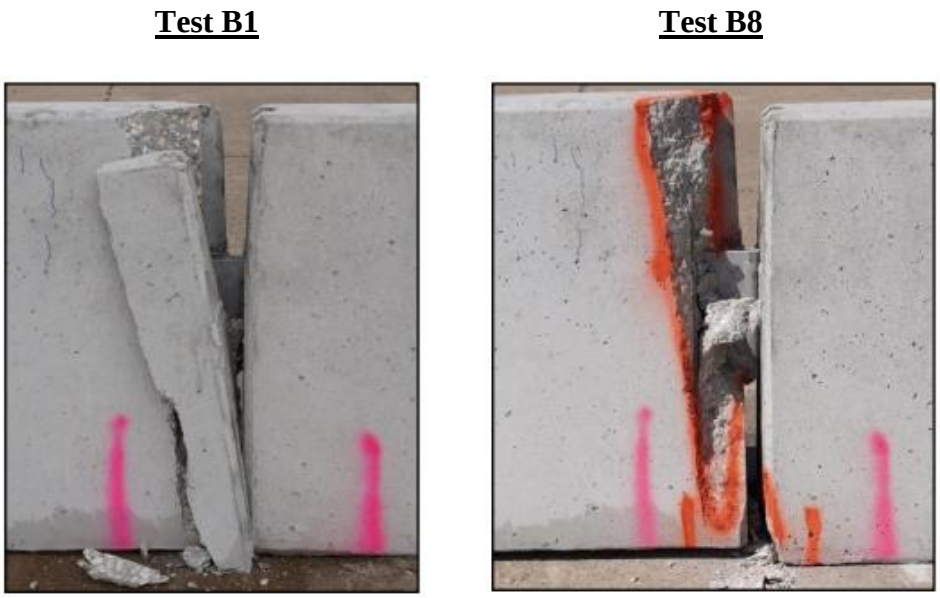

Figure 18. Damage observed near the joint between the single slope barriers C and D after the component testing performed to evaluate the barrier strength.

In Test B1, a large portion of concrete broke from the compression side of barrier C near the joint towards barrier D. As a result of this, rebars were exposed. Further, in Test B8, more concrete loss took place from the compression side of barrier C near the joint towards barrier D as the damaged barrier was hit again at a speed of 26 mph.

4. NON-DESTRUCTIVE EVALUATION OF SELECTED BARRIERS

4.1. Introduction

4.1.1. Description

Non-destructive testing (NDT) techniques are used to evaluate the structural condition of objects without causing damage to them. NDT gives real time results and provides the possibility to repeat the tests. It also enables the person on field to test a large portion of the barrier with no significant increase in the cost.

Non-destructive testing was conducted on select portions of portable concrete barriers damaged during bogie testing using two types of devices – Ultrasonic Low-Frequency Tomograph and Ground Penetrating Radar (GPR). Results from these devices were processed in the software, Ideal Viewer and RADAN 7, respectively.

4.1.2. Test Object

Up to two damaged specimens of single slope concrete barriers were tested non-destructively with the help of the tomography device.

Barrier Letter Code: E

Barrier Type: Single slope

Last bogie test conducted on the barrier: B-10.

Two regions of damaged barrier E were chosen to draw the 2 in. by 2 in. test grid

<u>Region 1</u>

Region 1 was chosen somewhere in the middle of Barrier E, above and near the scupper. This region had multiple transverse cracks gradually increasing in width as one moved from left to right along the longitudinal direction of the barrier. These cracks resulted from the series of destructive tests (B2, B9, B7, B10).

Figure 19. Region 1 with transverse cracks gradually increasing in width (left to right), Barrier E.

Region 2

Region 2 was located towards the barrier end, near the joint which was previously impacted four times during the series of destructive tests-B2, B9, B7, B10. The region had a spall on the right corner with exposed reinforcement.

Figure 20. Region 2 at the extreme end of Barrier E. Right corner has a spall with exposed reinforcement.

Similar regions were selected on Barrier A to check the reliability of results obtained for Barrier E.

Barrier Letter Code: A

Barrier Type: Single slope

Last bogie test conducted on the barrier: B-10

Region 3

Region 3 was chosen on Barrier A, like the way Region 1 was chosen on Barrier E.

Figure 21. Region 3 on Barrier A, encompassing cracks gradually increasing in their width.

Region 4

Region 4 was chosen on Barrier A, like the way Region 2 was chosen on Barrier E.

Figure 22. Region 4 towards the end of Barrier A. Part of the base at the left end has a spall with no exposed reinforcement.

4.2. Materials and Methods

4.2.1. Ultrasonic Low-Frequency Tomograph

4.2.1.1 Description

The device, Tomograph A1040 MIRA looks like a mono block with the provision of a demountable handle which includes the built-in computer and antenna array. The tomograph is a completely autonomous measurement unit for collecting and processing the data obtained. It consists of a matrix antenna array from 48 (12 blocks, each containing 4 elements) low frequency broad banded transducers of shear waves, facilitated with dry point contact and ceramic wear resistant tips, which can work with rough surfaces for a long time. Each transducer has an in-built independent spring suspension, which allows inspection on the uneven surfaces. Nominal frequency of the array is 50 kHz. Inspection with dry point contact transducers does not require any liquid. The interface of device allows working with laser beams projected on a surface of the testing object, which help the operator in maintaining a swift step of the antenna array during a complete technical diagnostic of the testing object. The inspection is carried out in steps which mainly comprise of sounding the testing object with data combination and reconstruction of volume over the whole scanned surface of the testing object (1).

4.2.1.2 Purpose

This device is used with the purpose of evaluating the consistency of construction, search for foreign inclusions, cavities, voids, delamination, leaks, cracks and for measuring thickness of the object under inspection (1).

A quick and effective survey of the internal structure can be achieved with the application of this device. The data collected is further processed and converted to 3D image in the software -Ideal Viewer. With the help of the 3D image and reconstructed volume, operator can easily understand the configuration of the internal structure of the testing object. Ultrasonic tomograph is also used to estimate the thickness of the concrete cover and depth/spacing of reinforcement.

The device is operated under a temperature range of -10 to 50 degree Celsius (1).

4.2.1.3. Technical Specification

For technical specifications of the device, the reader is directed to Table 1 on Page 6 of the operation Manual of "ACS Low Frequency Ultrasonic Tomograph 1040 MIRA".

4.2.1.4. Data collection

Region 1, Barrier E

Following settings were kept for taking the scans:

Table 3: Settings used for scanning Region 1, Barrier E.

Setting	Selected value
Color gain, dB	10

Table 3. Continued.

Setting	Selected value
Analog gain, dB	50
Number periods	1.0
Pause between the emission pulses	Off
Operating frequency, kHz	50
Using the measured velocity	On
Velocity, m/s	2590*
Delay, microseconds	20
Image quality	Average
The depth of the map	500
Horizontal step, mm	50
Vertical step, mm	50
Horizontal size of the map	50
Vertical size of the map	50

*Calibration of velocity: Velocity was calibrated by taking three readings over different patches in region 1. The readings were averaged to give a single value which was fed into the tomograph device as the measured velocity.

The device took three types of scans of the barrier: C scan, B scan and D scan.

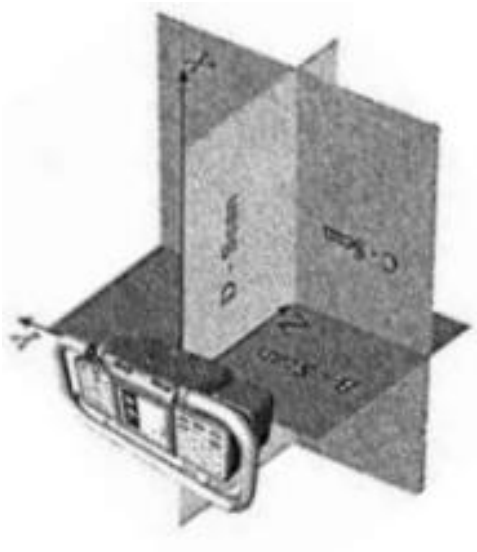

Figure 23. Orientation of three types of scans (1). Reprinted from A1040 MIRA Operation Manual.

From Figure 23, following can be concluded

Axis Y is directed lengthways of the barrier surface along the long part of tomograph. The right direction is a direction from left to right. The zero is in the middle of the antenna array.

Axis Z is directed in depth of the barrier, it is perpendicular to the barrier's surface. The right direction is a direction into the depth of the barrier (where the transducers look). The zero is located on a surface of the barrier.

B-scan – any section of the barrier, perpendicular to axis X. (Top-view)

C-scan – any section of the barrier, perpendicular to axis Z. (Front view)

D-scan - any section of the barrier, perpendicular to axis Y. (Side-view)

The collected data set was transferred to the external PC for advanced processing via special software, IDEAL viewer. Configuration of the internal structure of the barrier

can be conveniently understood from tomograms as well as 3D images generated by the software after it reads data from the instrument.

Region 2, Barrier E

Following settings were kept for taking the scans:

Table 4. Settings used for scanning Region 2, Barrier E.

Setting	Selected value
Color gain, dB	10
Analog gain, dB	50
Number periods	1.0
Pause between the emission pulses	Off
Operating frequency, kHz	50
Using the measured velocity	On
Velocity, m/s	2630*
Delay, microseconds	20
Image quality	Average
The depth of the map	500
Horizontal step, mm	50
Vertical step, mm	50
Horizontal size of the map	50
Vertical size of the map	50

*Calibration of velocity: Velocity was calibrated by taking three readings over different patches in region 2. The readings were averaged to give a single value which was fed into the tomograph device as the measured velocity.

Region 3, Barrier A

Following settings were kept for taking the scans:

Table 5. Settings used for scanning Region 3, Barrier A.

Setting	Selected value
Color gain, dB	10
Analog gain, dB	50
Number periods	1.0
Pause between the emission pulses	Off
Operating frequency, kHz	50
Using the measured velocity	On
Velocity, m/s	2593*
Delay, microseconds	20
Image quality	Average
The depth of the map	500
Horizontal step, mm	50
Vertical step, mm	50
Horizontal size of the map	50

Table 5. Continued

Setting	Selected value
Vertical size of the map	50

*Calibration of velocity: Velocity was calibrated by taking three readings over different patches in region 3. The readings were averaged to give a single value which was fed into the tomograph device as the measured velocity.

Region 4, Barrier A

Following settings were kept for taking the scans:

Table 6. Settings used for scanning Region 4, Barrier A

Setting	Selected value
Color gain, dB	10
Analog gain, dB	50
Number periods	1.0
Pause between the emission pulses	Off
Operating frequency, kHz	50
Using the measured velocity	On
Velocity, m/s	2833*
Delay, microseconds	20
Image quality	Average

Table 6. Continued.

Setting	Selected value
The depth of the map	500
Horizontal step, mm	50
Vertical step, mm	50
Horizontal size of the map	50
Vertical size of the map	50

*Calibration of velocity: Velocity was calibrated by taking three readings over different patches in region 4. The readings were averaged to give a single value which was fed into the tomograph device as the measured velocity.

Like region 1, collected data for regions 2, 3 & 4 was also transferred to the external PC for further processing in the software. Through this test, a definite conclusion was drawn regarding the reinforcement layout and some important clue was obtained with regards to a possible defect present in the barriers.

4.2.2. Ground Penetrating Radar (GPR)

4.2.2.1 Description

Ground Penetrating Radar (GPR) transmits electromagnetic waves (in the range of 10 ~ 1000 Hz) into the probed material and receives the reflected pulses as they encounter discontinuities. A boundary or an interface between materials with different dielectrics or a subsurface object such as a delamination acts as a discontinuity. The amplitudes of the received echoes and their corresponding times of arrival are used to

determine the nature and location of the discontinuity (3). A series of pulses over a single area result into a scan. As antennae move along the survey line, a series of traces are collected at specific points along the line. The scans are then positioned side by side to form a profile of the area. Apart from the GPR energy pulse, which is reflected to the antenna, a part of energy also keeps travelling through the material until it either dissipates (attenuates) or the GPR control unit has closed its time window. The rate of signal attenuation depends on the properties of the material through which the pulse is passing. GPR mainly comprises of a waveform generator, a single transducer consisting of an emitting and receiving antenna, a signal processor, and a data storage/display unit. Data collected by the device is processed in a specialized software, RADAN. A simple line scan format is used to mark the approximate area of the target on the survey surface whereas for a detailed subsurface map, 3D mode of data collection shall be required. The software also applies mathematical functions to the data to remove background interference, migrate hyperbolas, calculate accurate depth, etc. (4).

4.2.2.2. Purpose

Ground penetrating radar (GPR) is a mature technology which has been used on all kinds of engineering structures including bridges and tunnels. GPR signals compute surface layer dielectrics which by limited coring are calibrated to in place density. With these calibrations, density profiles are developed for the entire project. With the help of GPR technology, one can identify section breaks and detect subsurface defects such as voids and water-based deteriorations. The most common applications of GPR are

locating spacing and depth for reinforcing steel, post-tensioning cables or anchors, measuring rebar covers and mapping voids.

4.2.2.3 Technical Specification

For technical specifications of the device, the reader is directed to "Appendix C: Technical Specifications" on page 51 of GSSI Structure Scan Mini XT Manual. The quality and quantitative characteristics of scans taken from the GPR device depend upon the values of various parameters such as dielectric constant, scan density, auto target, display, auto depth, auto gain, depth, grid type, contrast, and migration type. These parameters have been explained in detail in GSSI Structure Scan Mini XT Manual and GSSI Structure Scan Mini Quick Start Guide, the reader is encouraged to refer to the same.

4.2.2.4 Data collection

Following settings were used while taking the readings:

Table 7. Common settings used for scanning Regions 1-4.

Setting	Selected value
Depth	16 in.
Dielectric	7.5
Auto Target	Off
Display	B
Scan Density	Normal

Table 7. Continued.

Setting	Selected value
Migration Type	Max
Grid Type	2 x 2
Setting	Selected value
Auto Depth	Off
Auto Gain	On
Contrast	Low

4.3. Results and Discussion

4.3.1. Ultrasonic Low-Frequency Tomograph

Region 1, Barrier E

Figure 24 shows the rebars present within the barrier spaced 11.8 in. apart. As per the standard drawings issued by TxDOT, spacing between the vertical rebars is 12 in. Figure 25 shows the reinforcement spacing for the tested region (Region 1) as shown in TxDOT standard drawing of the single slope barrier. Figure 26 shows the position of C scan in the 3D volumetric view of the barrier.

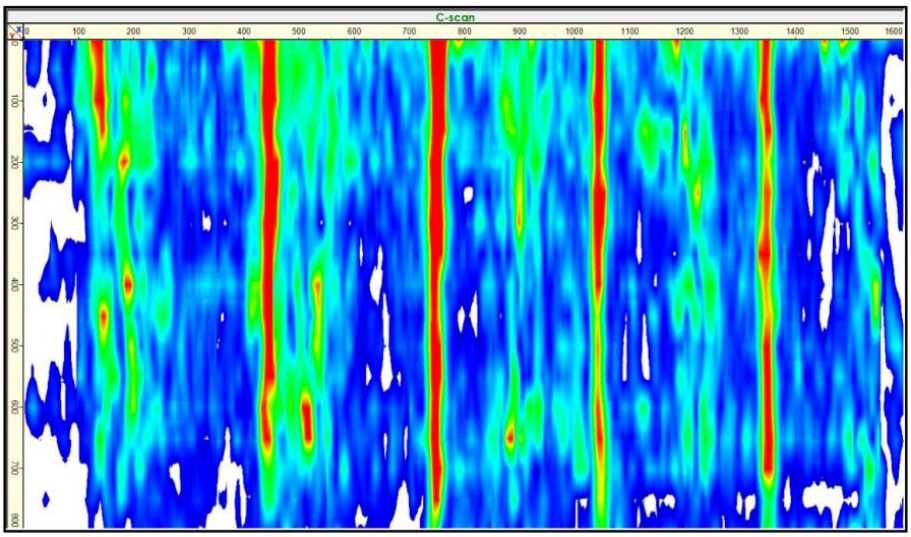

Figure 24. C scan showing vertical rebars in the barrier spaced at 11.8 in.

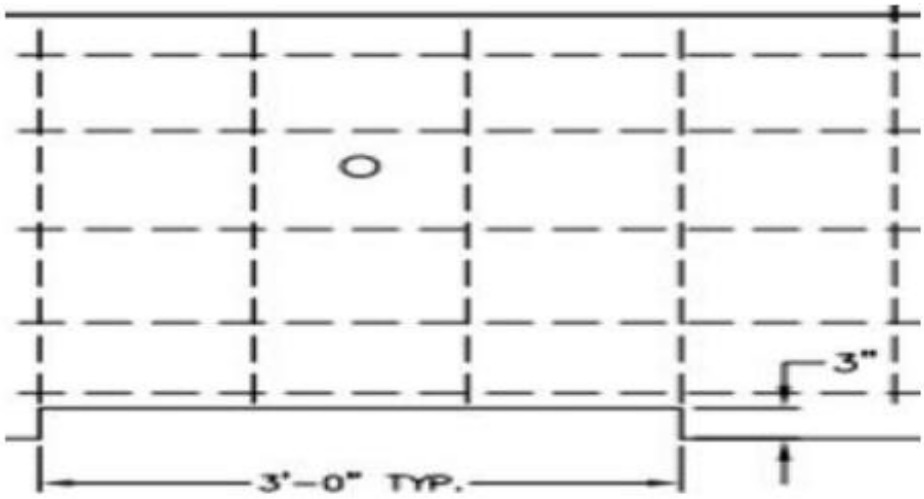

Figure 25. Elevation view of vertical reinforcement in region 1 spaced at 12 in.

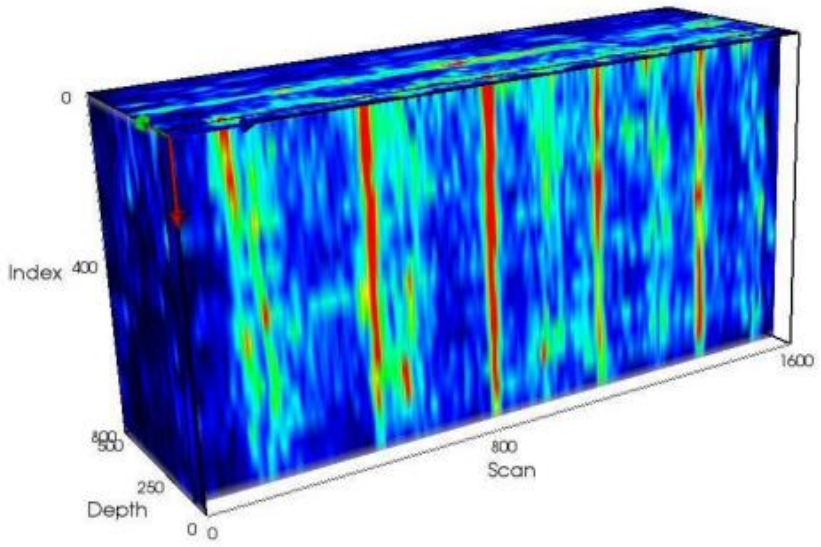

Figure 26. 3D volumetric view of the barrier with C scan in the front.

Figures 27(a) – 27(c) show the C-scans depicting different layers of horizontal reinforcement in the barrier (left) and the corresponding 3D volumetric view (right).

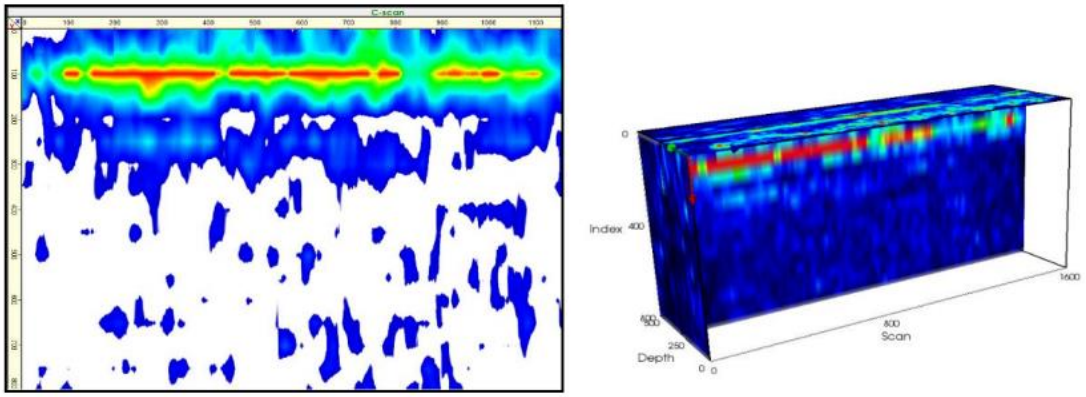

Figure 27 (a). First horizontal layer of reinforcement, C scan (left) and 3D volume (right).

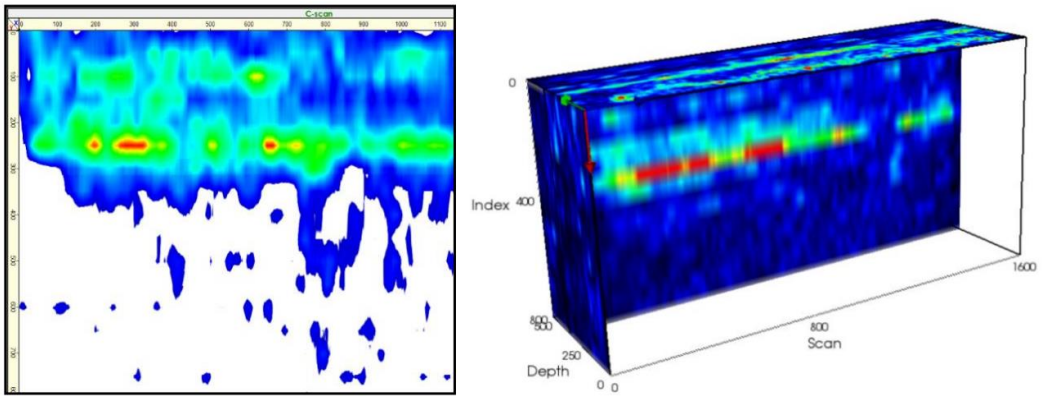

Figure 27 (b). Second horizontal layer of reinforcement, C scan (left) and 3 D volume (right)

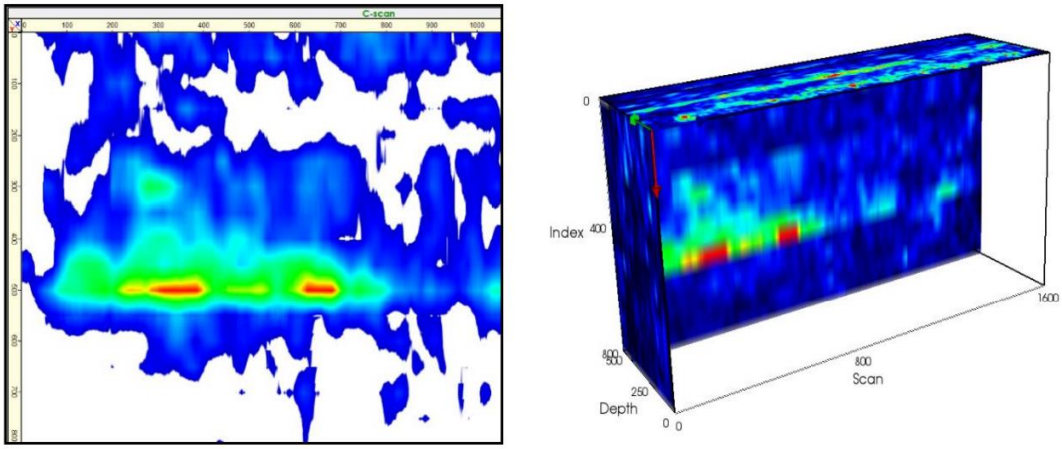

Figure 27(c). Third horizontal layer of reinforcement, C scan (left) and 3D volume (right).

From figures 27(a)-27(c), we see that the first layer is seen at 3.9 in. below the top edge of the barrier. The spacing between the consecutive layers of horizontal reinforcement shows as 5.9 in. and 9.8 in. respectively. Figure 28 shows the actual spacing between different layers of horizontal rebars as given in the standard TxDOT drawings.

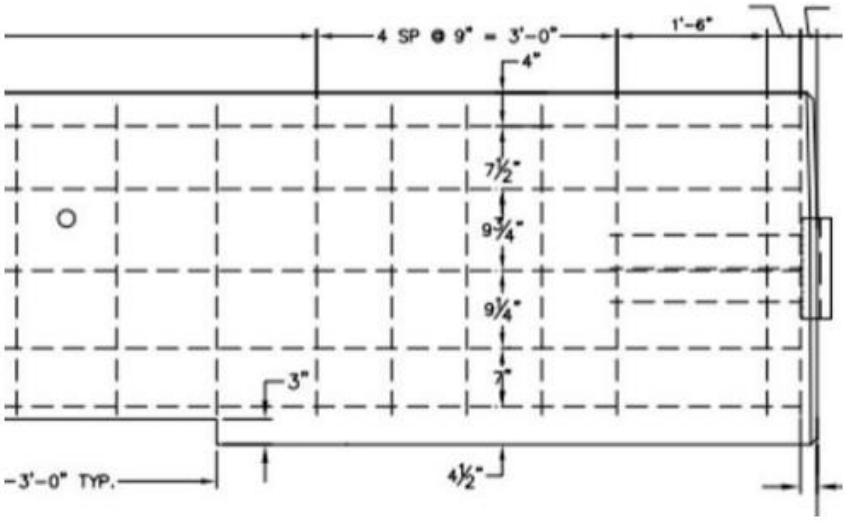

Figure 28. Spacing between horizontal layers of reinforcement in region 1. With respect to the top edge of the barrier, the first three spacings are 4 in., 7.5 in., and 9.75 in.

B scans in figures 29(a)-29(b) show a large red region in the barrier between depths 9.8 in. to 13.8 in.:

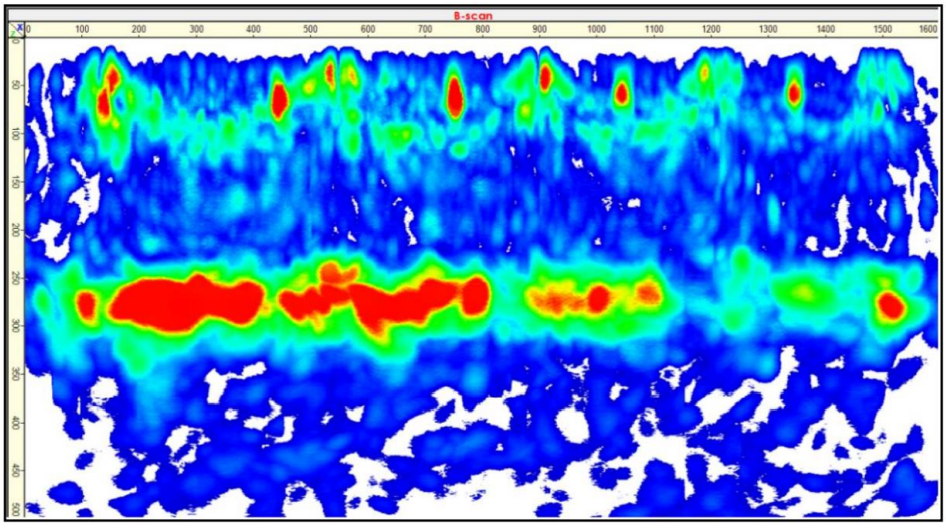

Figure 29(a). B scan, red region between depths Z=9.8 in. and Z=11.8 in.

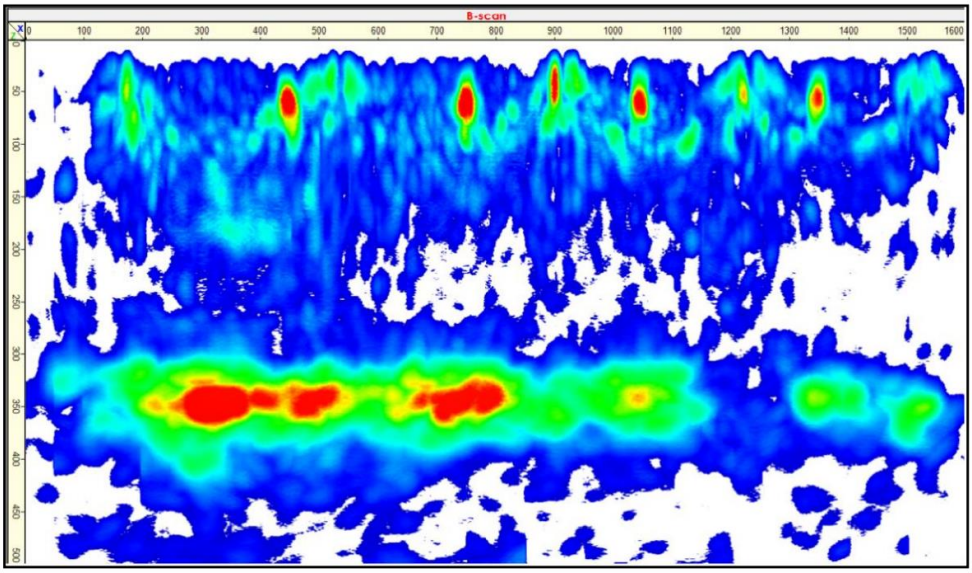

Figure 29(b). B scan, red region at depth Z=13.8 in.

Significance of these red regions needs to be further investigated. Red spots are found at X=5.9 in., 17.7 in., 29.5 in., 41.3 in., and 53.1 in. As per the drawing, rebars are located at the above-mentioned positions, which suggests that these spots possibly give the top view of the rebars.

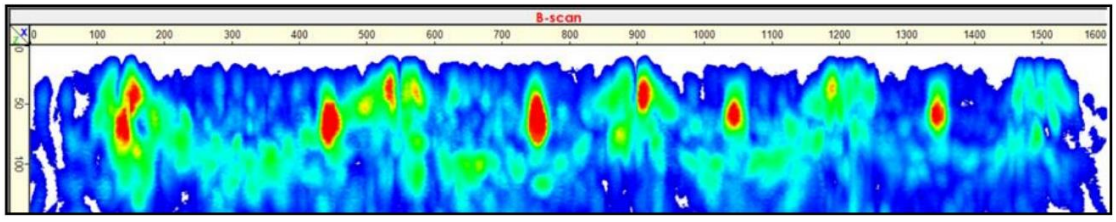

Figure 29(c). Magnified view of red spots at X= 5.9 in., 17.7 in., 29.5 in., 41.3 in., 53.1 in. (left to right)

Region 2, Barrier E

Like region 1, collected data for region 2 was transferred to the external PC for further processing in the software. Figure 30 shows the rebar positions at X= 13.8 in., and 17.8 in. (from left to right). As per the standard TxDOT drawing shown in Figure 18, first rebar is located 14 in. away from the reference line XX whereas the second rebar is located at 18 in. away. Three more red lines are observed at X = 2 in., 7.9 in., and 21.7 in., which are possibly also rebars. This observation is verified with the help of Ground Penetrating Radar (GPR), as will be shown later.

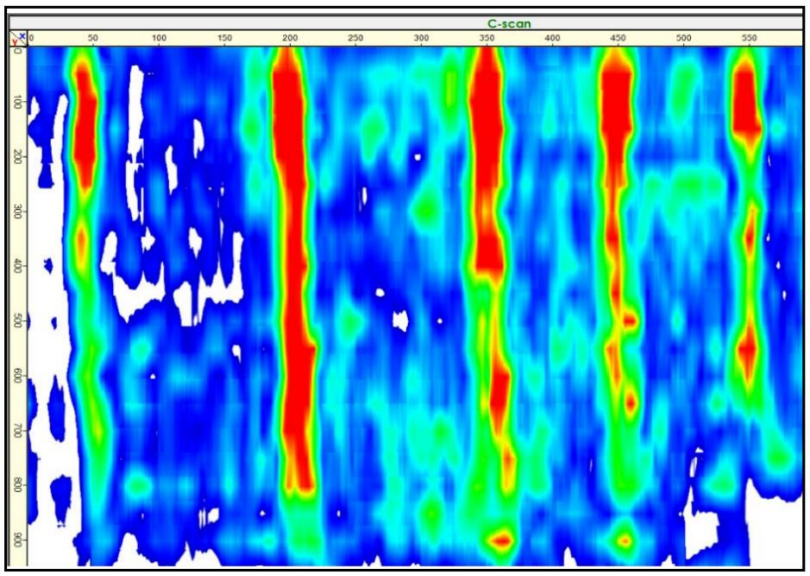

Figure 30. C scan showing vertical rebars at X=2 in., 7.9 in., 13.8 in., 17.8 in., 21.7 in.

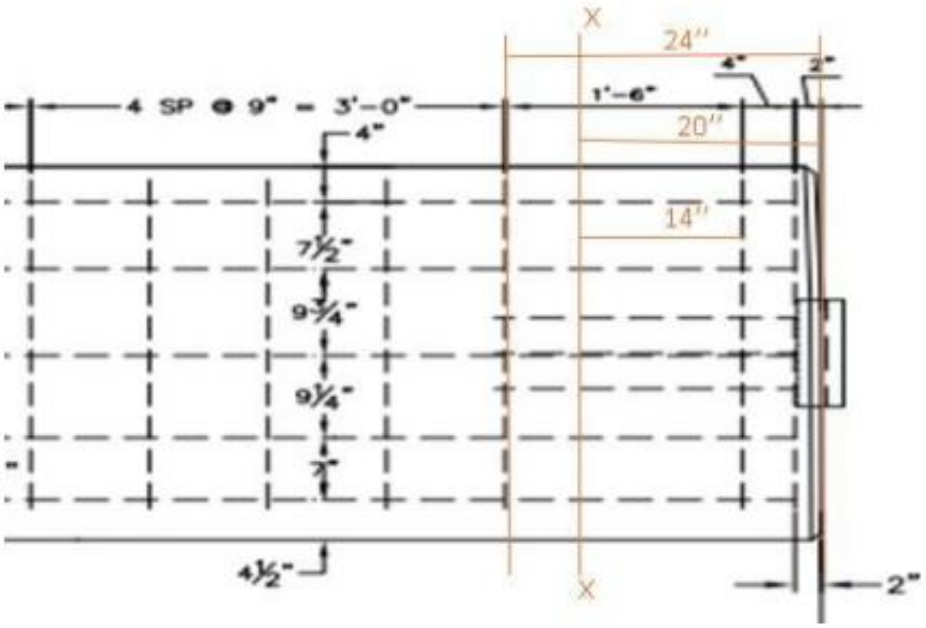

Figure 31. Grid ends at 20 in. measured from the extreme right end towards left. With line XX as the reference, first rebar is placed at X=14 in., and the second rebar is placed at X= 18 in.

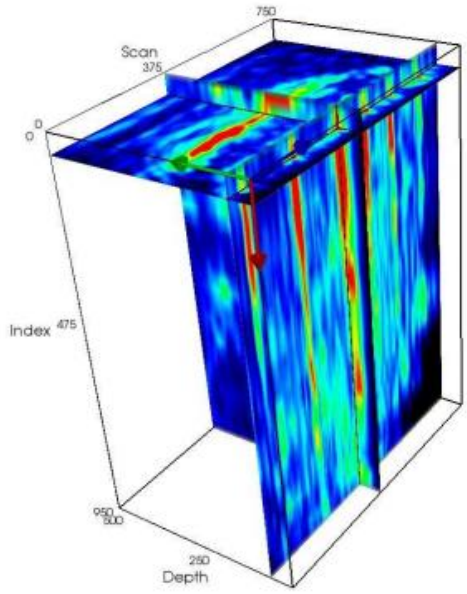

Figure 32. 3D volumetric view of the barrier with C scan in the front.

Figures 33(a)-(b) show the C-scans depicting different layers of horizontal reinforcement in the barrier and the corresponding 3D volumetric view.

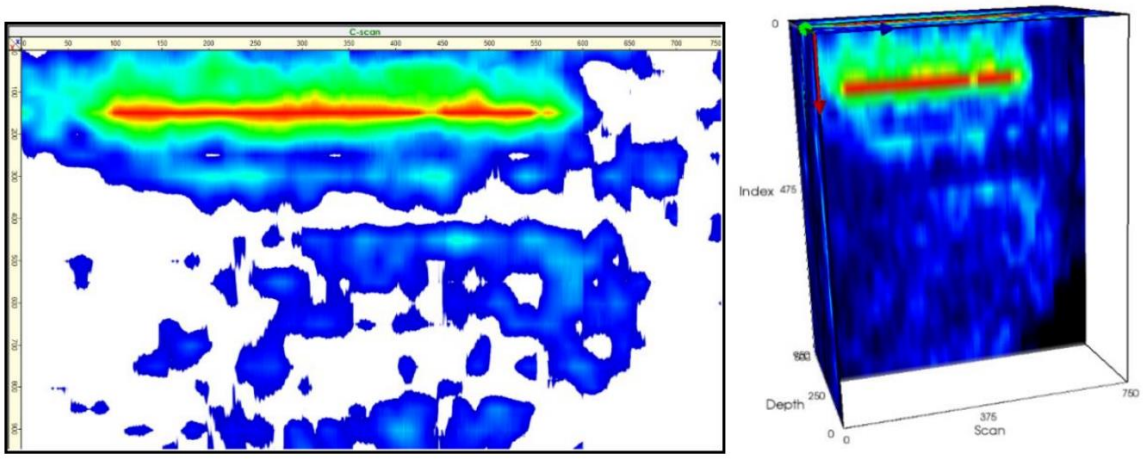

Figure 33 (a). First horizontal layer of reinforcement, C scan (left) and 3D volume (right)

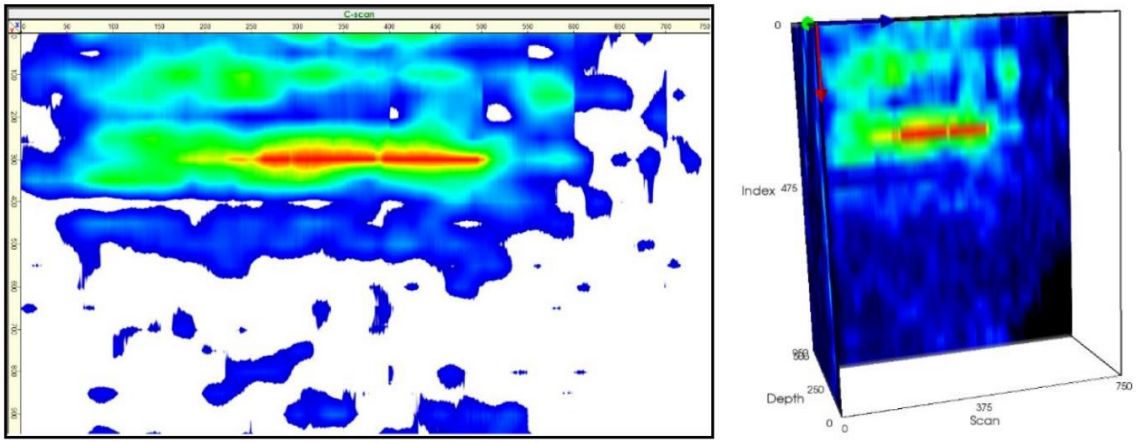

Figure 33 (b). Second horizontal layer of reinforcement, C scan (left) and 3 D volume (right)

In the above figures, we see that the first layer is located at 5.9 in. below the top edge of the barrier, the second layer appears at 11.8 in. below the top edge of the barrier. As per the standard TxDOT drawing shown in Figure 31, the first layer is located at 4 in. below the top edge of the barrier and the second layer is located at 11.5 in. below the top edge. B scans below show a large red region in the barrier between the depths Z=7.9 in. and Z=11.8 in. In the X direction, the same region stretches from X=2.0 in. to X=21.7 in.

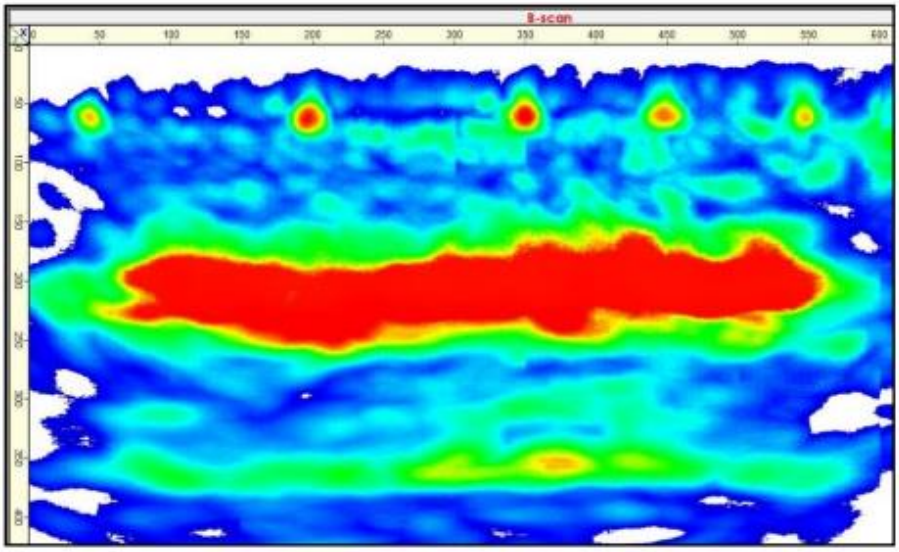

Figure 34(a). B scan, red region between Z=7.9 in. and Z=9.8 in.

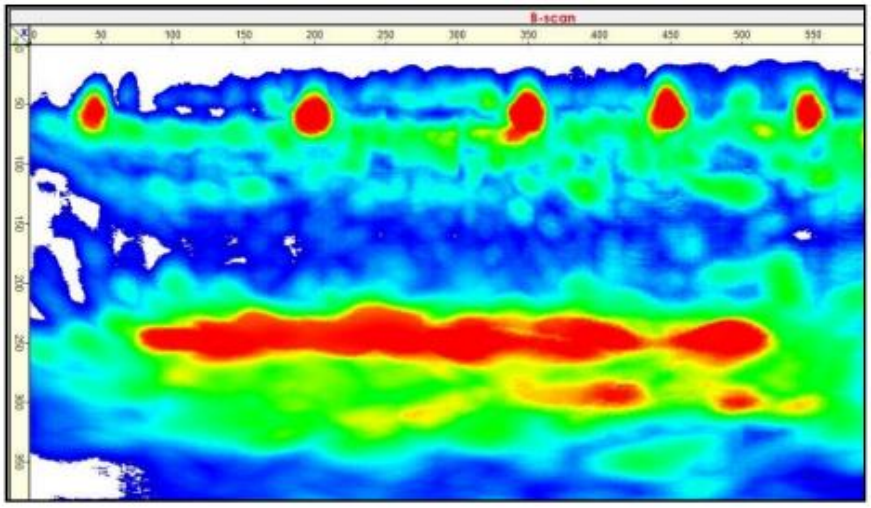

Figure 34(b). B scan, red region around Z=9.8 in.

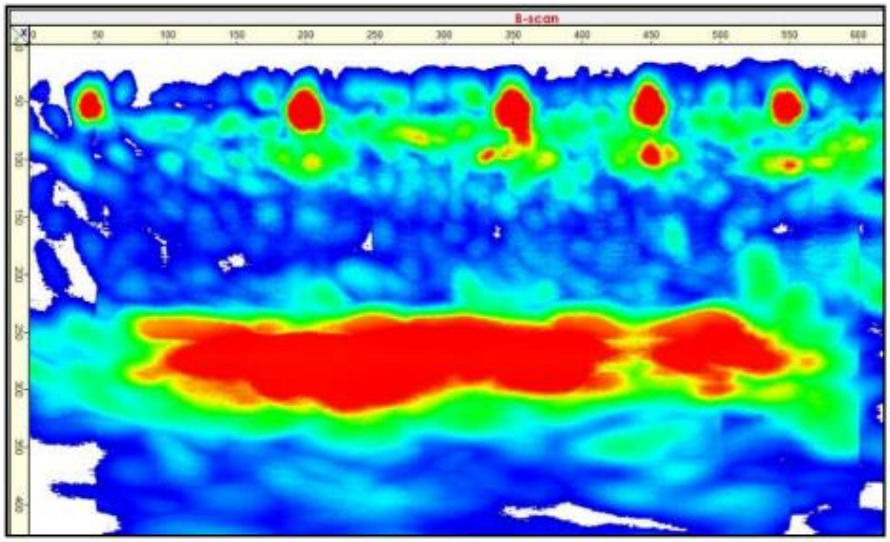

Figure 34(c). B scan, red region between Z=9.8 in. and Z=11.8 in.

Red spots are found at X = 2 in., 7.9 in., 13.8 in., 17.8 in., 21.7 in. As per the drawings, rebars are located at the positions X = 13.8 in., 7.9 in. which suggest that the red spots at these locations possibly give the top view of rebars. Occurrence of red spots at X = 2 in.,

7.9 in. and 21.7 in. are also indicative of the presence of rebars. This observation is also verified with the help of Ground Penetrating Radar (GPR), as will be shown later.

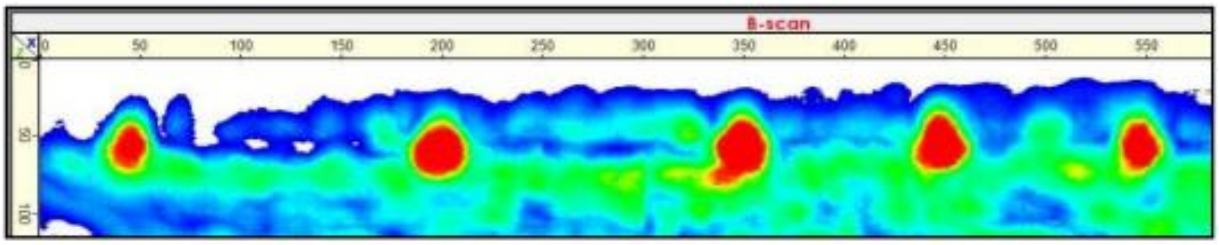

Figure 34(d). Magnified view of red spots at X= 2 in., 7.9 in., 13.8 in., 17.7 in., 21.7 in. (left to right)

Region 3, Barrier A

Figure 35 shows rebar positions at X= 4.9 in., 16.7 in., 29.5 in., 41.3 in., 53.1 in. As per the standard TxDOT drawing shown in Figure 25, vertical rebars are spaced at 12 in.

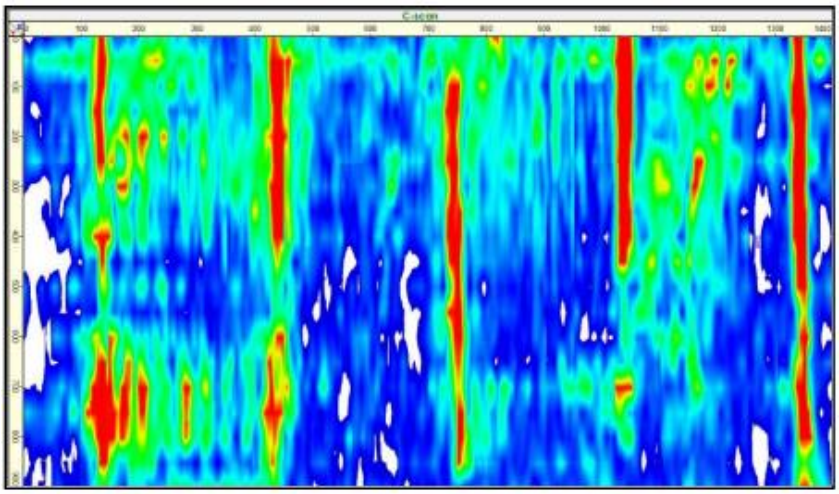

Figure 35. C scan showing vertical rebars in the barrier at X= 4.9 in., 16.7 in., 29.5 in., 41.3 in., 53.1 in.

C scan shown in Figure 35 suggests that the rebars are approx. 11.8 in. apart.

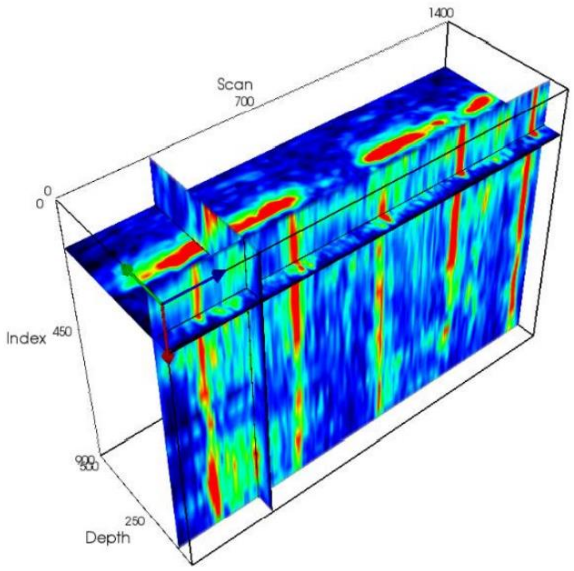

Figure 36. 3D volumetric view of the barrier with C scan in the front.

Figures 37(a)-(b) show the C-scans depicting different layers of horizontal reinforcement in the barrier and the corresponding 3D volumetric view.

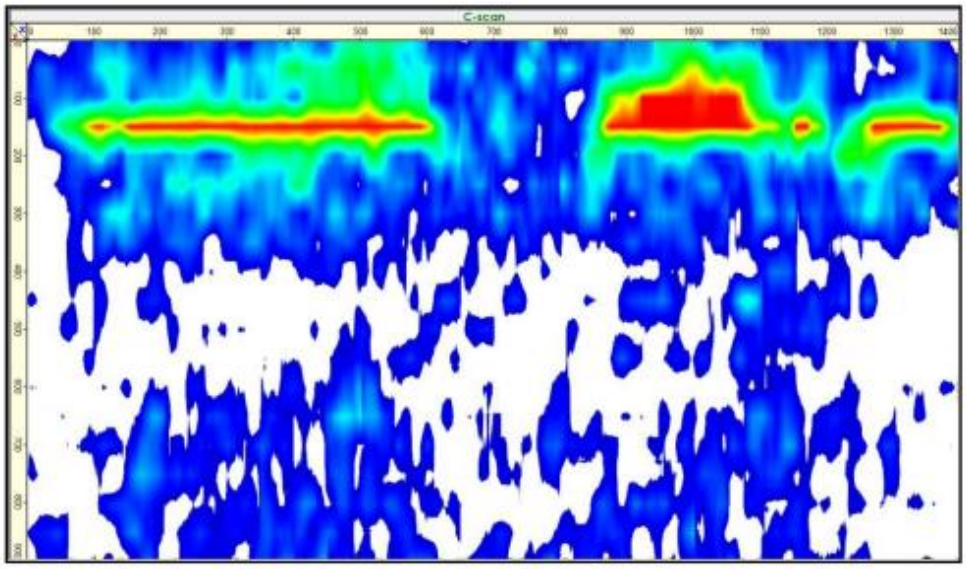

Figure 37 (a). First horizontal layer of reinforcement, C scan.

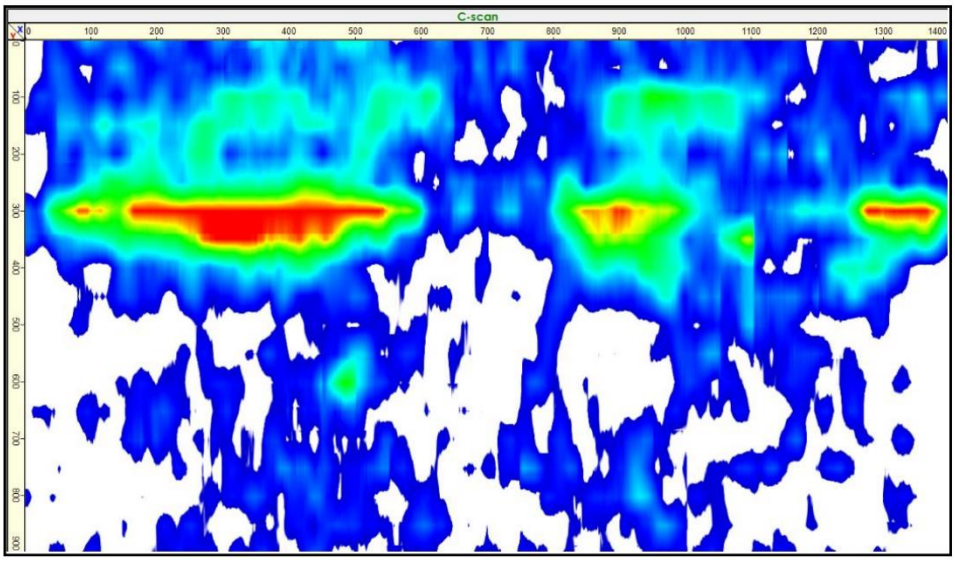

Figure 37(b). Second horizontal layer of reinforcement, C scan.

In the above figures, we see that the first layer is located at 5.9 in. below the barrier edge and the second layer is located at 11.8 in. Figure 28 shows first horizontal layer of rebars

67 at 4 in. from the top edge and second horizontal layer of rebars at 11.5 in. away from the top edge.

B scans in figures 38(a)-38(c) show a large red region in the barrier between the depths Z=7.9 in. and Z=15.7 in.:

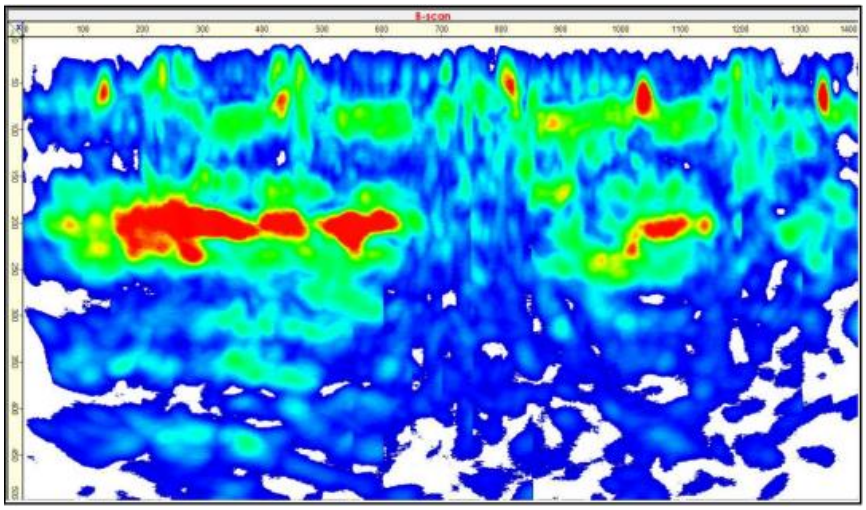

Figure 38(a). B scan, red region between Z=7.9 in. and Z=9.8 in.

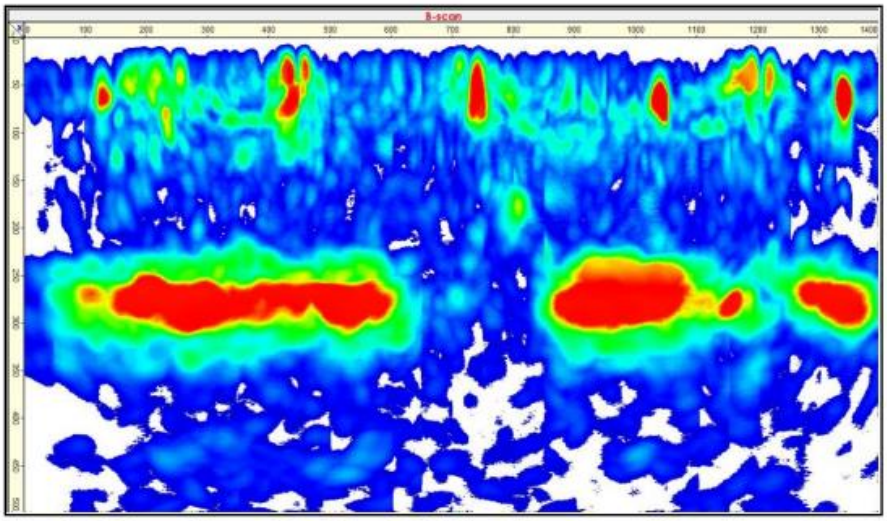

Figure 38(b). B scan, red region between Z=9.8 in. and Z=11.8 in.

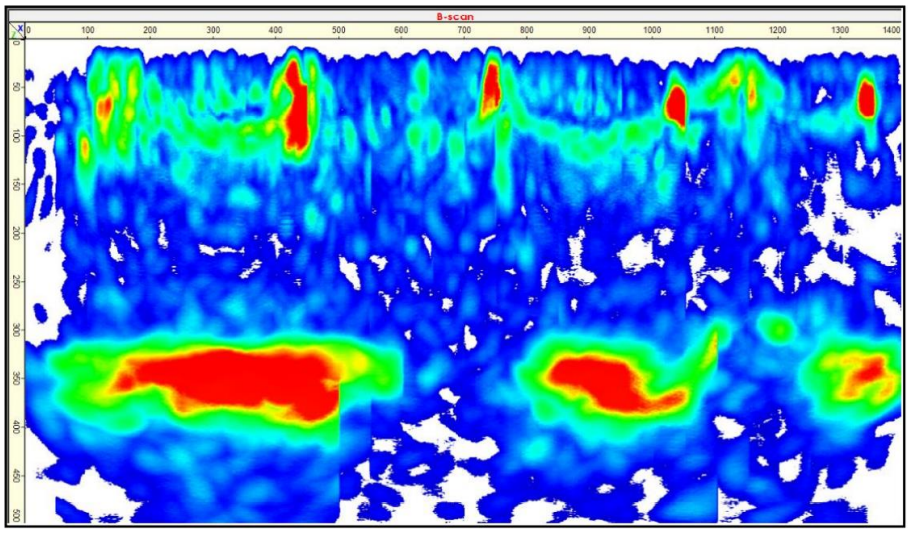

Figure 38(c). B scan, red region around Z=13.8 in.

The red region seen in figures 38(a)-(c) is a possible indication of a defect which needs to be further investigated. In figure 38(d), red spots are found at X=4.9 in., 16.7 in., 29.5 in., 41.3 in., and 53.1 in. As per the drawing, rebars are located at the above-mentioned positions, which suggests that these spots possibly give the top view of rebars.

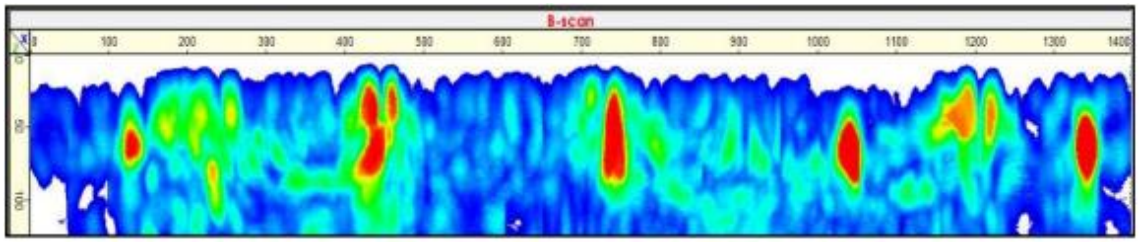

Figure 38(d). Magnified view of red spots at X=4.9 in., 16.7 in., 29.5 in., 41.3 in., and 53.1 in. (left to right).

Region 4, Barrier A

The data collected was further processed in the software, IDEAL viewer. Figure 39 shows the C scan with vertical red lines appearing at X=8.9 in., 12.8 in., 16.7 in., 21.7 in., 28.5 in., and 40.4 in. in region 4. Readings were taken from the extreme left end while moving the instrument towards right. As per the standard TxDOT drawing shown in Figure 40, starting from line XX, rebars are located at X=2 in., 6 in., and 24 in. In figures 39-40, we see that the spacing of vertical lines in the C scan and spacing of rebars in the drawing are not in conformance. This is further verified with the help of Ground Penetrating Radar (GPR), as will be shown later.

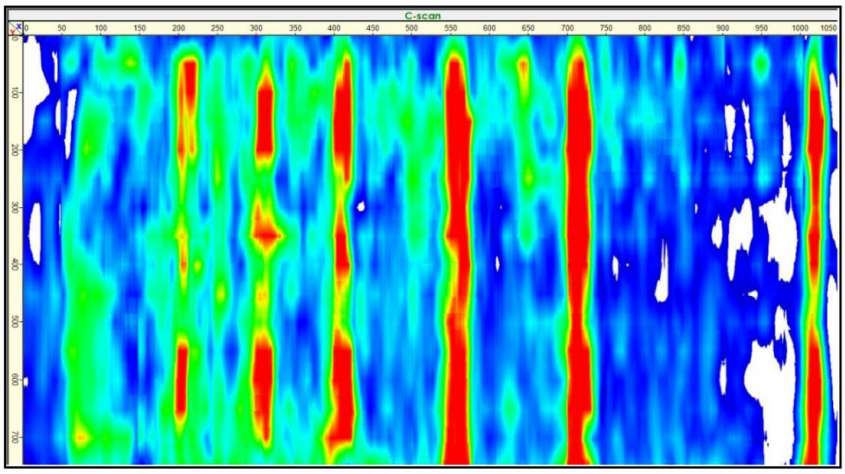

Figure 39. C scan showing vertical rebars in region 4.

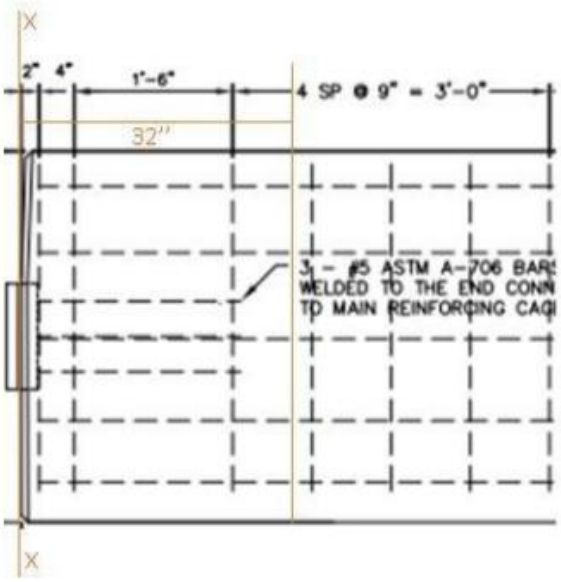

Figure 40. Grid ends at 32 in. measured from the extreme end towards right. With line XX as the reference, first rebar is placed at X=2 in., second rebar is placed at X=6 in., and third rebar is placed at X=24 in.

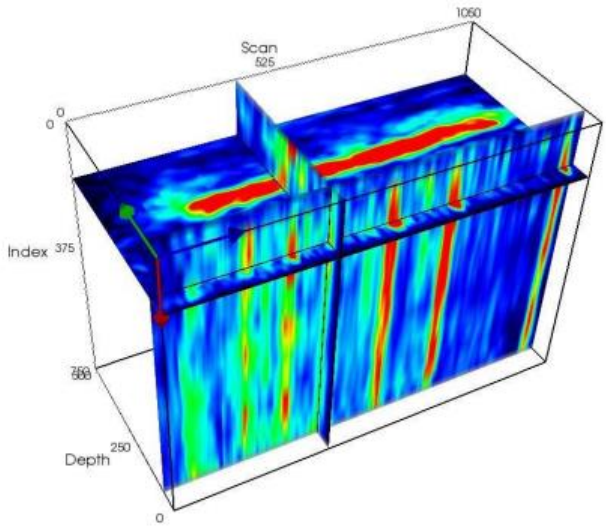

Figure 41. 3D volumetric view of the barrier with C scan in the front.

Figures 42(a)-(b) show the C-scans depicting different layers of horizontal reinforcement in the barrier.

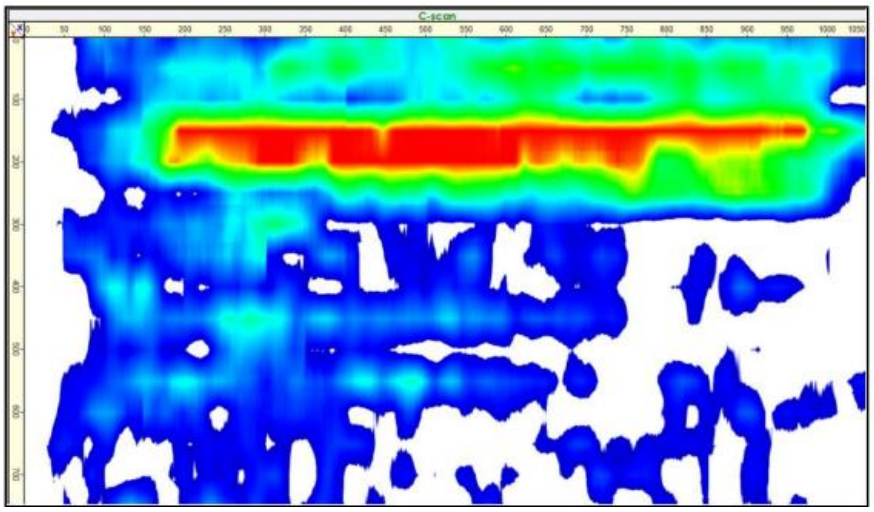

Figure 42 (a). First horizontal layer of reinforcement, C scan

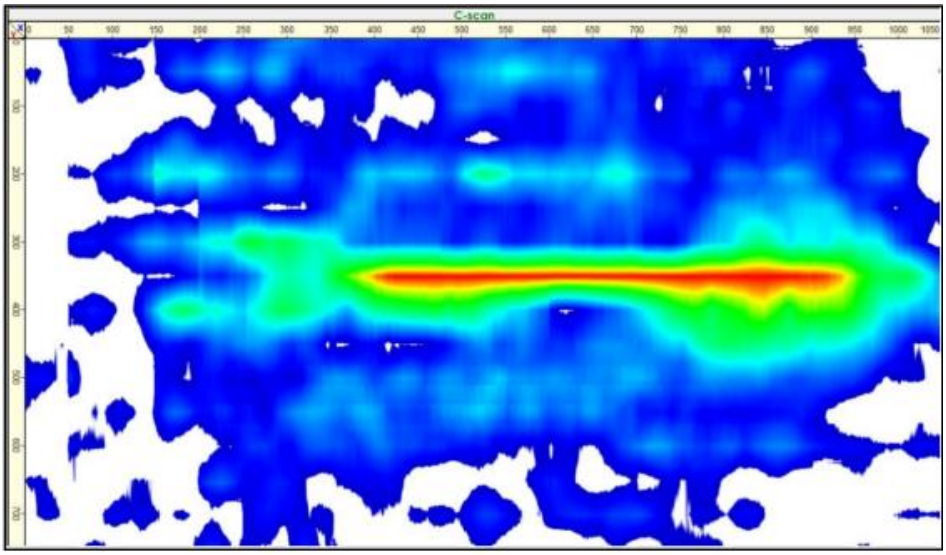

Figure 42 (b): Second horizontal layer of reinforcement, C scan

In figures 42(a)-(b), we see that the first layer is located at 5.9 in. below the top edge of the barrier, the second layer is located at 13.8 in. below the top edge of the barrier. As per the standard TxDOT drawing shown in figure 31, the first layer is located at 4 in. below the top edge of the barrier and the second layer is located at 11.5 in. below the top edge. B scans below show a large red region in the barrier between the depths Z=7.9 in. and Z=17.7 in.:

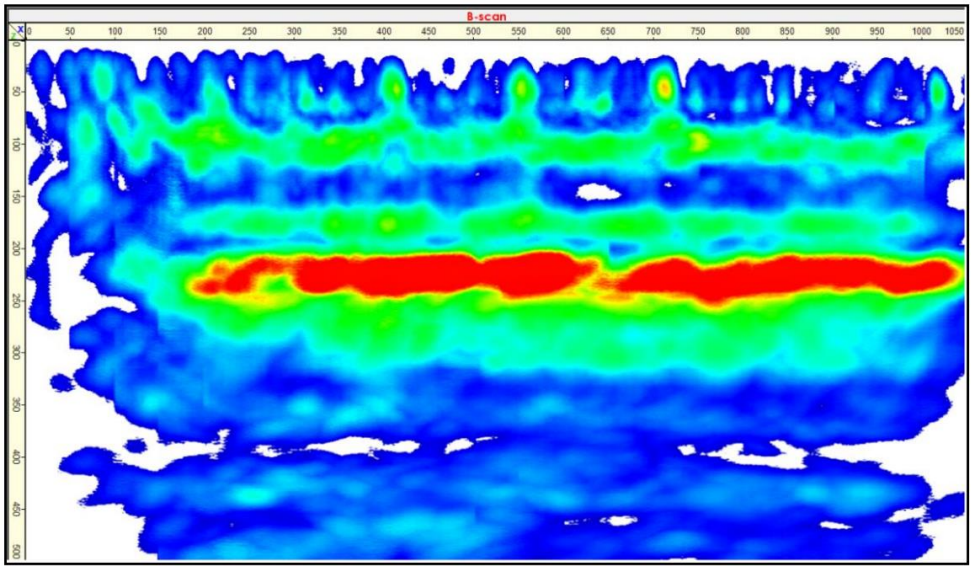

Figure 43 (a). B scan, red region between Z=7.9 in. and Z=9.8 in.

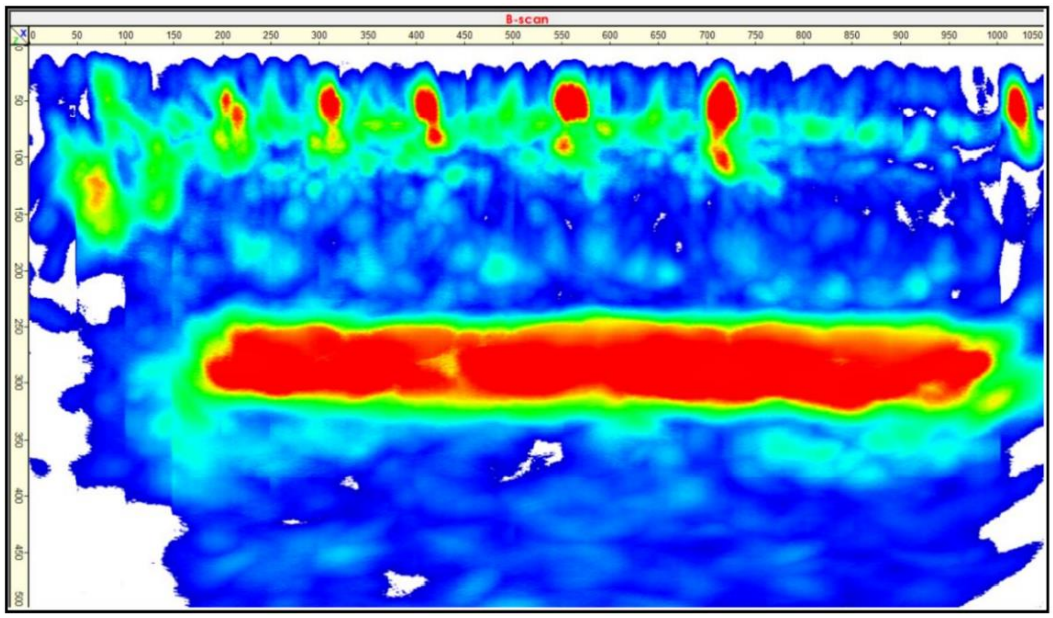

Figure 43 (b). B scan, red region between Z=9.8 in. and Z=11.8 in.

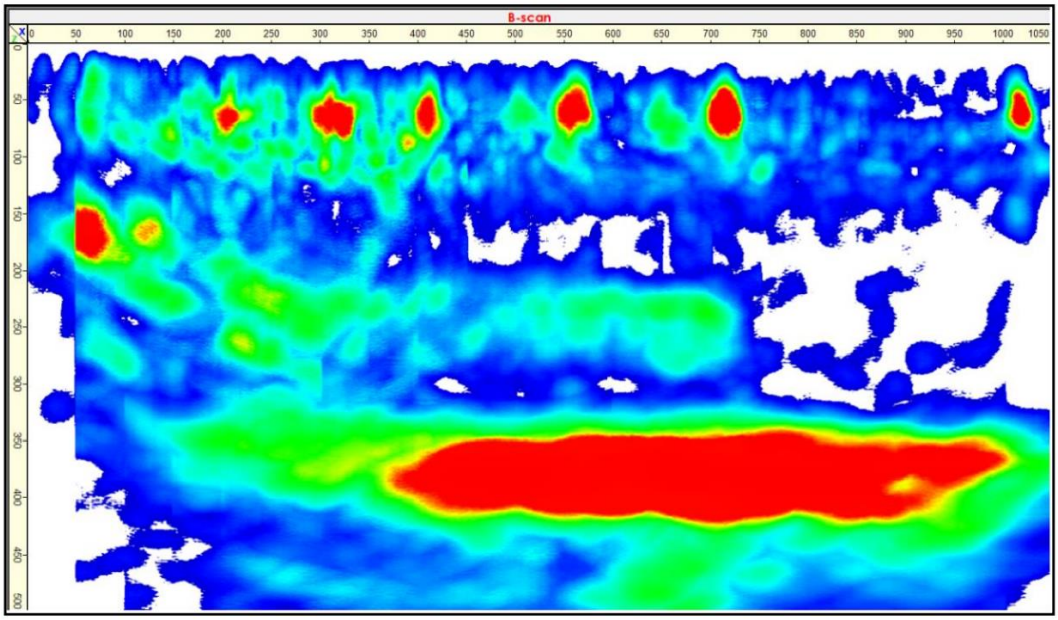

Figure 43 (c). B scan, red region between Z=13.8 in. and Z=17.7 in.

The red region seen in figures 43(a)-(c) is a possible indication of a defect which needs to be further investigated.

In figure 43 (d), red spots are found at X=8.9 in., 12.8 in., 16.7 in.,21.7 in., 28.5 in., and 40.4 in. These positions do not conform to the spacings between vertical rebars shown in the drawing. This observation is verified with the help of Ground Penetrating Radar (GPR), as will be shown later.

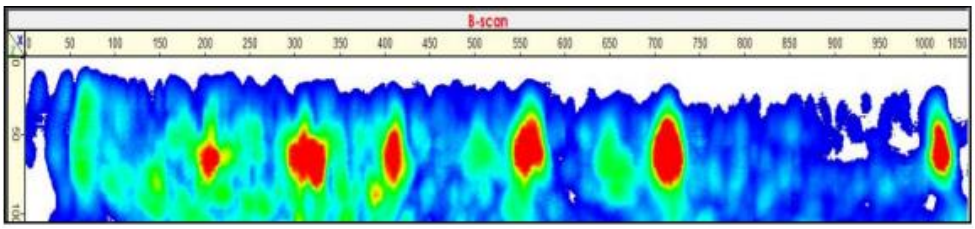

Figure 43 (d): Magnified view of red spots at X=8.9 in., 12.8 in., 16.7 in., 21.7 in., 28.5 in., and 40.4 in.

4.3.2. Ground Penetrating Radar

Region 1, Barrier E Data collected by the device (in 2D mode) was transferred to the computer and processed further in the software RADAN 7. Images obtained consist of hyperbola peaks which indicate the positions of vertical rebars. Distance between the peaks suggests the actual distance between the vertical rebars of the barrier (5). Any black band cutting through the hyperbolas with white positive peaks suggests a potential void present in the barrier. As the signal travels from a material of higher value dielectric (concrete) to a material of lower value of dielectric (air), the region appears black in the scan (4). Figure 44 shows two images representative of region 1 of Barrier E.

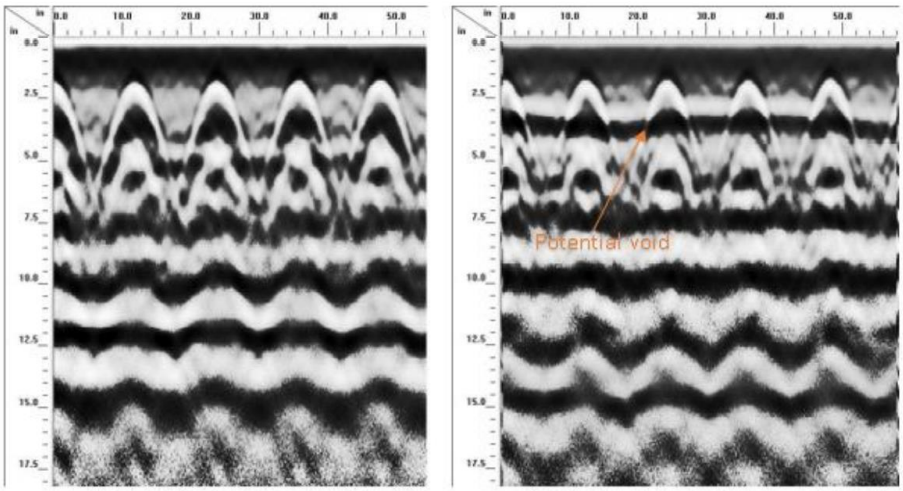

Figure 44. Image (left) depicts rebar spacing, image (right) depicts potential void.

From the above images, we observe that the distance between the two positive peaks is 12 inches. The peaks occur at a constant depth of around 1.5 inches which is the cover depth of reinforcement in single slope barriers. The black band in the image on the right suggests the presence of a potential void in the barrier.

Rebar spacing concluded from the images captured with the GPR device are found to be consistent with the rebar spacing earlier concluded from the C scan (Figure 24).

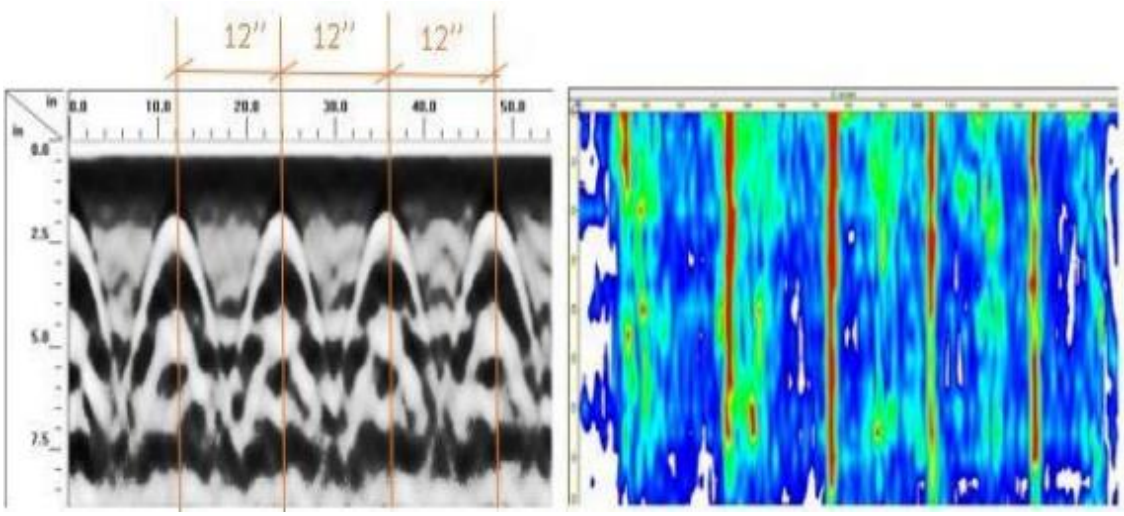

Figure 45. Comparison of GPR scan and C scan of region 1 showing vertical rebar spacing of 304.8 mm (12 in.)

This spacing is also seen consistent with the layout shown in standard TxDOT drawings (Figure 25).

Region 2, Barrier E

Figure 46 shows an image representative of region 2, Barrier E.

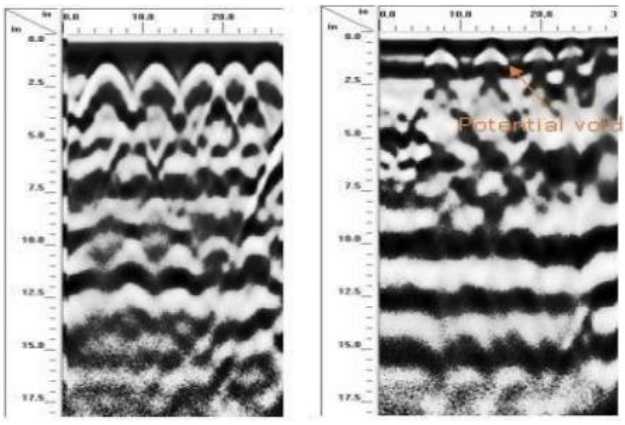

Figure 46. Image (left) depicts rebar spacing, image (right) depicts presence of a potential void.

In figure 46, on referring to image on the right, we see a black band cutting through the hyperbolas. This suggests the presence of a potential void inside the barrier.

On looking into the image shown on the left, starting from the right, we see three positive peaks separated by the spacing of vertical rebars which is 4 inches (as also depicted in the TxDOT drawing). In addition to these peaks, we also see that there are extra hyperbola peaks in the image spaced 6 inches apart.

Inspecting the C scan of the region again, we can also see that apart from those at X=13.8 in. and X=17.7 in., there are extra vertical red lines (Figure 47). This suggests that the actual reinforcement layout might be different than what is illustrated in the standard drawings. Possibly in reality, within 20 in. distance from the extreme right end, starting from left, we have three bars at a spacing of 6 in. and another two bars at a gap of 4 in. each. Whereas in the drawing, within 20 in. from the extreme right end, there are only two bars spaced 4 in. apart with one of the bars placed at 2 in. from the right end.

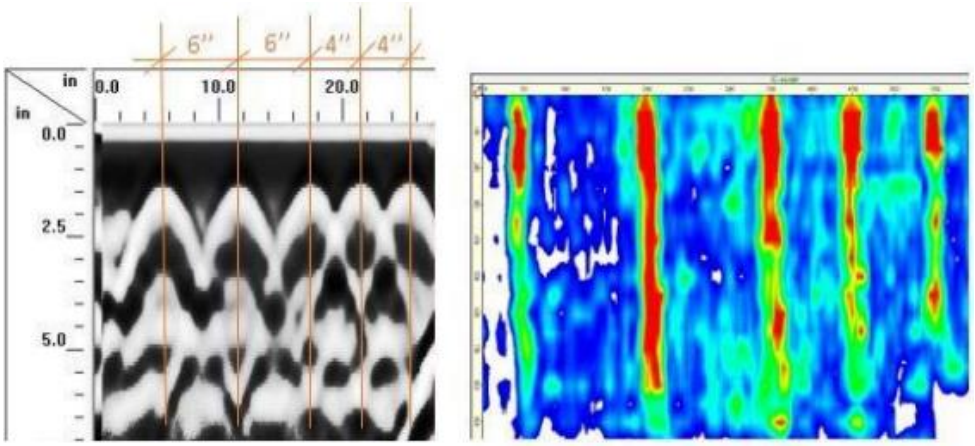

Figure 47. Comparison of GPR scan and C scan of region 2 showing the layout of vertical rebars.

Region 3, Barrier A

Figure 48 shows an image representative of region 3, Barrier A.

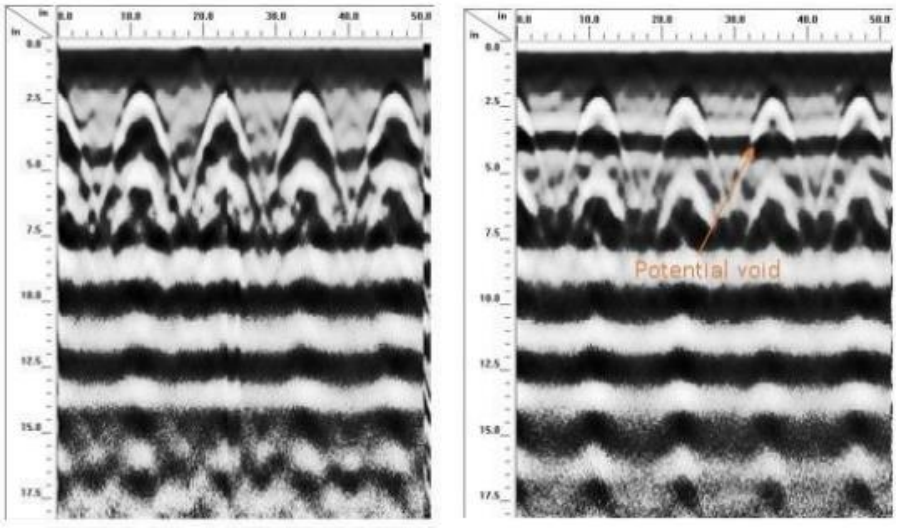

Figure 48. Image (left) depicts rebar spacing, image (right) depicts presence of a potential void.

Like Region 1 of Barrier E, this region also has consecutive positive peaks spaced at 12 in. which suggests the vertical rebars are placed at the same distance as depicted in the standard drawing. Black band seen in between the hyperbolas suggests the presence of a potential void.

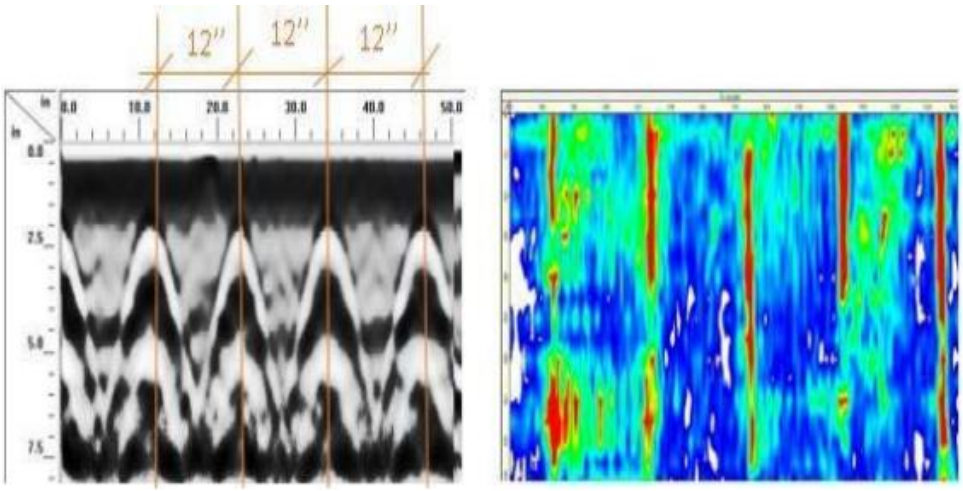

Figure 49. Comparison of GPR scan and C scan of region 3 showing the vertical rebar spacing of 12 in.

Region 4, Barrier A

Figure 50 shows an image representative of region 4, Barrier A.

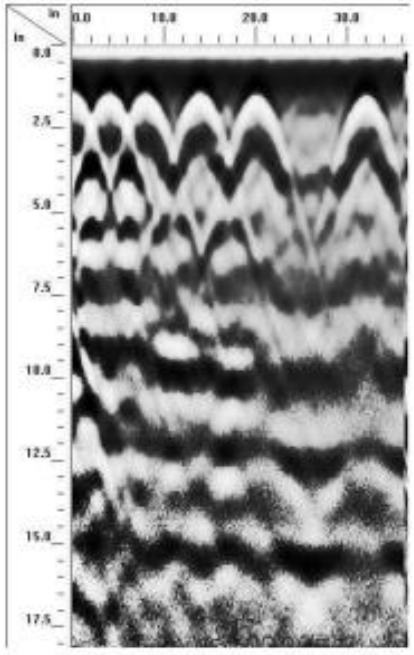

Figure 50. Image depicts vertical rebar spacing.

Like Region 2 of Barrier E, this region shows extra hyperbola peaks. Also, in the corresponding C scan of this region, extra red vertical lines were seen (Figure 51). This suggests the possible presence of extra reinforcement other than what is shown in the TxDOT drawing.

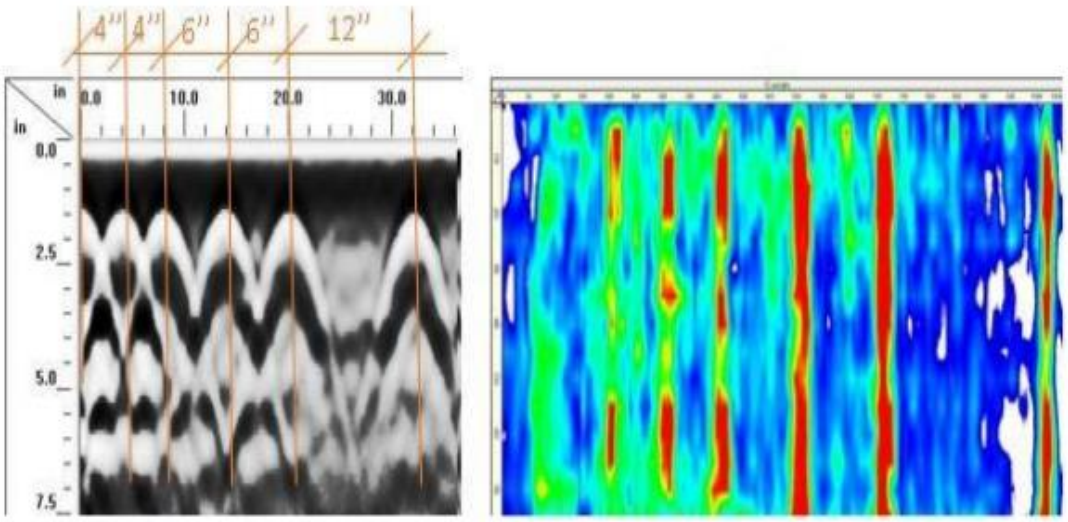

Figure 51. Comparison of GPR scan and C scan of region 3 showing the vertical rebar-layout.

Processing of GPR data collected in 3D mode

Data collected from the GPR device in 3D mode was processed in the RADAN software to obtain the reinforcement layout of vertical and horizontal rebars. Figure 52 (a) shows the reinforcement layout obtained for a cracked region of a portable concrete barrier. It is similar to the reinforcement plot obtained for a new or undamaged barrier shown in Figure 52 (b).

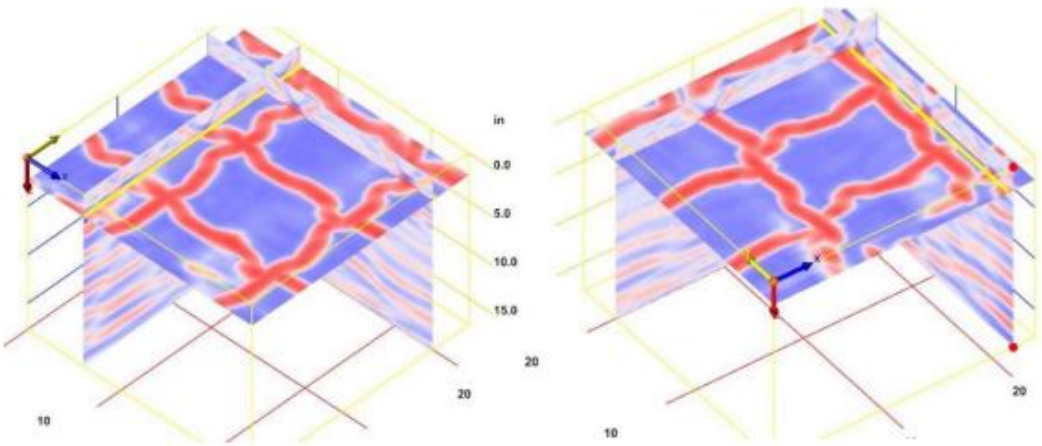

Figure 52. (a) Rebar layout for undamaged or new portable concrete barrier (b) Rebar layout for a cracked region of a portable concrete barrier.

The depth slices shown in figure 52 (a) & (b) are taken at 2.27 inches. Cracks in the barrier were caused due to the impact by the bogie vehicle and not due to an inherent factor like corrosion, thus there seems to be no change in the internal structure of the barrier in undamaged and damaged states.

4.4. Conclusion

Non-destructive testing (NDT) is performed to find out defects and damages in the object without having to cause changes to the object. Two kinds of non-destructive testing devices were used to evaluate the internal structure of the barriers: (I) Low Frequency Ultrasonic Tomograph and (II) Ground Penetrating Radar. Two regions were selected on each barrier. The first region encompassed cracks of gradually increasing width and the second region was the area around the spall. With the help of Low

Frequency Ultrasonic Tomograph technique, we saw the actual reinforcement spacing. However, this evaluation did not suggest any change in the internal structure corresponding to the cracks seen on the barrier surface (Region 1, Region 3) or spall on the toe (Region 2, Region 4). There were some large red bands observed in the C scans, a definite conclusion on these bands could not be drawn. It is recommended to further investigate the significance of these regions. Ground Penetrating Radar (GPR) additionally gave information on the cover depth and potential voids that might be present inside the barrier(s). Reinforcement layout found through the results from both the devices were compared with each other as well as compared with the standard TxDOT drawings. For the middle region of the barriers, the reinforcement arrangement was found consistent throughout the results of tests done using both the devices and matched with the reinforcement arrangement shown in the standard drawings as well. However, for the end region near the joint, the vertical rebar arrangement was found different from the one shown in the drawings. GPR data collected in 3D mode for cracked region of a portable concrete barrier and new/undamaged barrier was processed to obtain the respective vertical and horizontal rebar layouts. Since the crack in the damaged barrier was a result of the bogie impact and not an inherent factor like corrosion, rebar layout for undamaged and damaged barriers looked similar suggesting no change in the internal structure.

4.5. References

1. Ultrasonic Low-Frequency Tomograph A1040 MIRA Operation Manual

2. Y. Dong, F. Ansari, Non-destructive testing, and evaluation (NDT/NDE) of civil structures rehabilitated using fiber reinforced polymer (FRP) composites, Woodhead Publishing Series in Civil and Structural Engineering, Pages 193-222, 2011.

3. <https://www.geophysical.com/whatisgpr>

4. Structure Scan Mini XT Manual, Geophysical Survey Systems Inc.

5. Structure Scan Mini Quick Start Guide, Geophysical Survey Systems Inc.

5. EVALUATION GUIDELINES GIVEN BY OTHER STATE DOTS

5.1. Introduction

5.1.1. Description

Over the time, different transportation agencies such as State Departments of Transportation (DOTs), American Association of State Highway and Transportation Officials (AASHTO), Federal Highway Administration (FHWA), American Traffic Safety Services Association (ATSSA) have come up with their own set of guidelines to help the engineer on site determine the suitability of the PCB. These evaluation guidelines are given for the different damages observed in the PCBs such as spalling, cracking and damages to the JJ hook connection.

5.2. Guidelines to Evaluate Spalling

Different DOTs suggest checking the different aspects of pre-existing spall such as the spall location, number of spalls and length/width/depth of spall. Their recommendations for the acceptability criteria also differ. Table 8 summarizes the acceptability criteria laid down by some of the DOTs:

Table 8. DOT Guidelines on Spalls Found in PCBs (1).

DOT Name	Acceptability criteria for PCB
New York	For spalls on the middle of the PCB base: Acceptable – Less than 12 inches in length/width/depth (2). For spalls on the corner of the PCB (toe): Acceptable – Less than 3 inches in depth (2).
Florida	Acceptable- Less than 1.5 inches in depth with no rebar exposure (3).
New Jersey	Acceptable- Spalled area less than 3 inches by 3 inches (4).
South Carolina	Spalls entirely or partially within the boundary of end connection areas and drainage slot areas: Acceptable- Spalled area less than 1 inch by 1 inch (5). Spalls beyond end connection areas: Acceptable – Spalled area less than 4 inches by 4 inches (5).
Ohio	Acceptable- Up to 3 spalls with each of them having a surface dimension less than 12 inches and a depth less than 1.5 inch (6).

Table 8. Continued

DOT Name	Acceptability Criteria for PCB
Virginia	Acceptable- Concrete intact along the top/bottom/sides or end section (7).
Illinois State Toll Highway	Acceptable- Concrete spall depth less than 1.5 in. Horizontal/vertical/diagonal spall length less than 4 in. (8)
Indiana/Oregon/Washington	Acceptable- Few minor blemishes. Spalls and chipped concrete pose no threat of damaging or snagging tires (9), (10), (11).
Kansas	Acceptable- Minimal spalls and chipped concrete or exposed rebar (12).
Wisconsin	Acceptable- Spalling or chipping that does not compromise the overall profile of the barrier. Spalling that does not cause a potential snag point. Spalling or chipping that is not greater than 4 in. in width and abrupt in character (13).
Iowa	Acceptable- Less than 5 sq. foot-corner breaks/bottom spalls including base (14).

From the above table, we see that not only different DOTs quantify pre-existing spall differently (area/width/depth) but also the threshold limits are different in different DOT documents depending on the location of the spall. DOTs of states such as Virginia, Indiana, Oregon, Washington, and Wisconsin do not give out any critical sizes of pre-existing concrete spall, rather their guidelines are qualitative in nature.

5.3. Guidelines to Evaluate Cracking

Assessment of cracks is done by inspecting parameters such as direction of propagation (whether transverse or longitudinal), size (wide enough to expose rebar or hairline), length and number/density (whether single or multiple). Table 9 summarizes the acceptability criteria for cracks, laid down by some of the DOTs:

Table 9. DOT Guidelines on Cracks found in PCBs (1).

DOT Name	Acceptability criteria for PCB
New York	Acceptable – Single longitudinal crack of less than 4-ft. length (2).
Florida	Acceptable - There must not be any transverse (flexural) crack or shear crack (3).
New Jersey	Acceptable- There must not be multiple transverse cracks (4).
South Carolina	Acceptable- Any crack must not be wide enough to expose rebars (5).

Table 9. Continued.

DOT Name	Acceptability criteria for PCB
Ohio	Acceptable- Smooth, flat surfaces with few minor blemishes (6).
Virginia	Acceptable -There must not be a through crack. Hairline cracks are acceptable (7).
Illinois State Toll Highway	Acceptable- Cracks are tightly compressed, exhibiting no displacement and do not compromise the structural integrity of the wall (8).
Indiana/Oregon /Washington	Acceptable- Few minor blemishes (9), (10), (11).
Kansas	Acceptable- Superficial gouges or minor cracks (12).
Wisconsin	Acceptable- Cracks that are being tightly compressed by the barrier's reinforcement. There is no other damage e.g., anchor hole damage, end section loss or loop damage (13).
Iowa	Does not talk about cracks (14).

From the above table, we see that except New York DOT, all the other DOTs instruct to inspect cracks on a qualitative basis only. Multiple open transverse cracks are considered as unacceptable by all the DOTs, whereas multiple hairline cracks are considered as either acceptable or marginal.

5.4. Guidelines to Evaluate the Condition of the Connection

In general, all the DOTs suggest rejecting the PCB in case the connection components are bent/rotated/damaged. A PCB is considered acceptable only when the connection components are in a good, sound, and functioning condition. Table 10 summarizes the acceptability criteria for connection components, laid down by some of the DOTs:

Table 10. DOT Guidelines on Connections Between PCB Segments (1).

DOT Name	Acceptability criteria for PCB
Florida	Acceptable- Connection should must not be bent/rotated/deformed/broken (3).
New Jersey	Acceptable- Anchor bolt holes and rod holes must be in a functioning condition (4).
South Carolina	Does not talk about connections (5).
Ohio	Acceptable- All the connecting loops should be sound and in place with no broken strands (6).
Virginia	Does not talk about connections (7).

Table 10. Continued

DOT Name	Acceptability criteria
Illinois State Toll Highway	Acceptable- The connecting loop bars are in place and in good condition (8).
Indiana/Oregon /Washington	Acceptable- The connecting system is all sound and in place with no broken parts (9), (10), (11).
Kansas	Acceptable- Loop and pins are all intact, fixed in their positions (12).
Wisconsin	Acceptable- Steel loops are aligned and firmly connected to the concrete barrier (13).
Iowa	Acceptable-Undeformed connection (14).

All these DOTs instruct to inspect the connections on a qualitative basis only i.e., if the connection is bent, deformed, or rotated, PCB is rejected.

It may be concluded that the evaluation guidelines suggested by different DOTs lay down different quantitative criteria for acceptance and in parts, are very subjective to the knowledge of the inspector evaluating the PCB. Wherever the DOTs have suggested some critical sizes/areas/volumes of pre-existing concrete damage, the numbers are found to be different in different guidelines and when compared, these sizes/areas/volumes are not even close to each other. It is very difficult to comprehend which recommendation would be most practical without running an engineering analysis

or an actual crash test. Running an actual crash test is a costly affair, it would be impractical to run a crash test to evaluate the crashworthiness of the barrier system based on every other DOT guideline thus, making it imperative to first run an engineering analysis with MASH TL-3 impact conditions to predict the most critical pre-existing damage or a combination of pre-existing damages and then run an actual crash test for a barrier arrangement with the same pre-existing damage, to verify the result predicted by the engineering analysis.

5.5. Guidelines on the Repair of PCBs

In the survey conducted by the TTI researchers, only 16% DOTs said that they had repair guidance. These DOTs were that of the states Florida, New Jersey, South Carolina, Pennsylvania, and Utah (1). With reference to "102-9.6.2.4 Temporary Concrete Barrier Repair", Florida DOT has given the following repair procedure:

1. Remove all laitance, loose material, and any other deleterious matter to sound concrete or a minimum depth of 1 inch.

2. When reinforcing bars, inserts or weldments are exposed, remove the concrete to provide a minimum one-inch clearance all around.

3. Fill the repair area with an approved high-performance concrete repair material in accordance with 930-5 and the manufacturer's recommendations.

4. Restore surfaces and edges to the original dimensions and shape of the barrier (1), (3).

South Carolina DOT uses guidelines from “Standard Specifications for Highway Construction, SCDOT, 2007, Section 605.2.3.2 Temporary Concrete Barrier”. These specifications prohibit the repair of the barrier in the following cases:

1. A barrier has exposed reinforcing steel rebar.
2. A spall area of 6 inches or more in all three dimensions (depth, width, and height).

For repair of spalling areas less than 6 inches in all dimensions that do not expose steel reinforcement, the specifications suggest carrying out repair with a premanufactured patching material specifically fabricated for patching structural concrete (1), (5). A similar survey was also conducted by the TTI researchers within the state of Texas. It was found that districts Lufkin, Pharr and Waco had formal repair guidance. Lufkin and Pharr referred to the TxDOT Concrete Repair Manual (1). In the TxDOT Concrete Repair Manual 2021, Section 1 of Chapter 2 deals with definitions of concrete spalls based on severity. Spalls can be categorized as minor, intermediate, or major. Detailed explanations are further given for each of the spall categories. Depending upon the location to be repaired and volume of work, repair procedures are suggested. Sections 1 to 3 of Chapter 3 exclusively cover the repair materials and the repair procedures for the different spall categories.

Sections 5 to 7 of Chapter 3 cover the different repair procedures for cracks and associated crack repair materials. Section 5 recommends the use of pressure-injected epoxy for sealing cracks as narrow as 0.002 inches. Associated repair materials are TxDOT Type IX low-viscosity epoxy resin and TxDOT Type V or VII concrete

epoxy adhesive. It is further added that epoxies and adhesives are covered in DMS 6110 and MPL. Section 7 talks about the procedure to only seal cracks to prevent the infiltration of water, chlorides, and other contaminants. Two methods are explained under this category: Routing-and-sealing, surface sealing. For routing and sealing, Class 4 low modulus silicone meeting the requirements of DMS 6310 and Joint Sealants and Fillers/Type V adhesive meeting the requirements of DMS 6100 are recommended. For surface sealing, Type VIII or Type X epoxy meeting the requirements of DMS 6100, Epoxies and Adhesives is suggested (1), (15).

5.6. References

1. Dobrovolny Chiara Silvestri, Bligh Roger, Hurlebaus Stefan, Aldahlki Husain, Agarwal Hemangi, Moran Sana, Technical Memorandum 2 for TxDOT Project 0-7059, “Develop Guidelines for Inspection, Repair and Use of Portable Concrete Barrier”.

2. NYSDOT “Acceptance Criteria for Damaged Temporary Concrete Barrier (TCB)”.

3. FDOT (2019). “FDOT Evaluation Guide – Temporary Concrete Barrier.” Florida Department of Transportation, Tallahassee, Florida.

4. NJDOT (2019). “Standard Specifications for Road and Bridge Construction.” New Jersey Department of Transportation, Ewing Township, New Jersey.

5. SCDOT (2007). “Standard Specifications for Highway Construction.” South Carolina Department of Transportation, Columbia, South Carolina.

6. ODOT (2020). “Quality Standards for Temporary Traffic Control Devices and Acceptable Delineation Methods for Vehicles” Ohio Department of Transportation, Columbus, Ohio.

7. VDOT (2016). “Road and Bridge Specifications.” Virginia Department of Transportation, Richmond, Virginia.

8. IDOT (2016). “Traffic Control Field Manual- Quality Standard for Temporary Concrete Barrier.” Illinois Department of Transportation, Springfield, Illinois.

9. INDOT (2020). “Standard specifications.” Indiana Department of Transportation, Indianapolis, Indiana.

10. ORDOT (2018). “Oregon Standard Specifications for Construction.” Oregon Department of Transportation, Salem, Oregon.

11. WSDOT (2020). “Standard Specifications for Road, Bridge, and Municipal Construction.” Washington State Department of Transportation, Olympia, Washington State.

12. KDOT (2017). “Guidelines for Temporary pre-cast Concrete Safety Barrier Condition Inspection.” Kansas Department of transportation, Topeka, Kansas.

13. WisDOT (2019). “Construction and Materials Manual.” Wisconsin Department of Transportation, Madison, Wisconsin.

14. IADOT (2020). “Standard Specifications for Highway and Bridge Construction.” Iowa Department of transportation, Ames, Iowa.

15. TxDOT Concrete Repair Manual 2021

6. PRELIMINARY EVALUATION AND REPAIR GUIDANCE

6.1. Introduction

6.1.1. Description

This guide discusses the different criteria to classify PCBs into three categories:

• Acceptable.

• Acceptable with repair.

• Unacceptable.

Examples of acceptable, acceptable with repair, and unacceptable barriers have been illustrated to assist the engineer in charge in categorizing PCBs. A PCB can be classified as unacceptable if it meets at least one of the following conditions. PCBs that are acceptable with repair are also discussed.

6.2. Evaluation Criteria for the Classification of PCBs

6.2.1. Depth of Spall beyond Outer Layer of Rebar

A PCB is unacceptable if the depth of spalling at any location of the barrier is beyond the outer layer of the rebar (Figure 53). Spalling beyond the outer layer of reinforcement not only exposes it but may make it protrude from the barrier. The protruded rebar becomes prone to corrosion and may act as a snagging hazard to incoming vehicles. A PCB is acceptable with repair if the spalled region does not have rebars protruding to act as a snagging hazard (Figure 54).

Figure 53. Unacceptable Barrier—Spalling beyond the Outer Layer of Rebar Embedded within the Barrier, Exposing It and Making It Protrude.

Figure 54. Barrier which is Acceptable with Repair—Spalled Region Where Reinforcement May Have Some Exposure but Does Not Protrude

6.2.2. Unsound Concrete Vulnerable to Break Off If Further Impacted

A PCB is unacceptable if it has a large block of unsound concrete partially hanging and susceptible to break off if further impacted (Figure 55). (A possible size of the spall has been suggested based on the findings of the predictive FEA simulations discussed in Chapter 7). This poses a risk to the stability of the vehicle because of higher chances of the barrier to deflect more, thus making the barrier unacceptable. Provided the reinforcement is not exposed and the unsound concrete is small, PCB can be considered acceptable without being necessarily having to be repaired (Figure 56).

Figure 55. Unacceptable Barrier—Large Chunk of Partially Broken Concrete Piece from the Toe Susceptible to Break Off When Further Impacted.

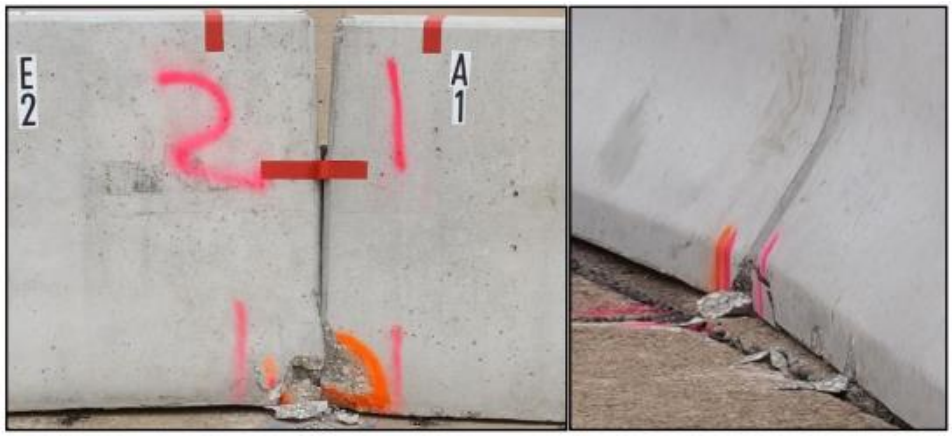

Figure 56. Barrier which is Acceptable—Small Chunk of Partially Broken Concrete (no exposed rebars) from the Toe Likely to Break Off When Further Impacted.

6.2.3. Spall over Toe Greater than 12 inches.

A PCB is unacceptable if it has a spall over the toe with a dimension in any surface direction equal to or exceeding 12 inches and a spalled depth less than or equal to the cover depth (reinforcement is not exposed) (Figure 57). The threshold dimension of 12 inches is being suggested based on the extensive review of the guidelines (concerning spalling) laid down by other DOTs.

A PCB is acceptable if the spalled dimension is less than 12 inches, and the spall depth is less than the cover depth (reinforcement is not exposed) (Figure 58). This guideline has been reviewed again after discussing the findings of the predictive FEA simulations in Chapter 7.

Figure 57. Unacceptable Barrier—Spalled Dimension Equal to 12 Inches and Spall Depth Less than the Cover; Reinforcement Is Not Exposed.

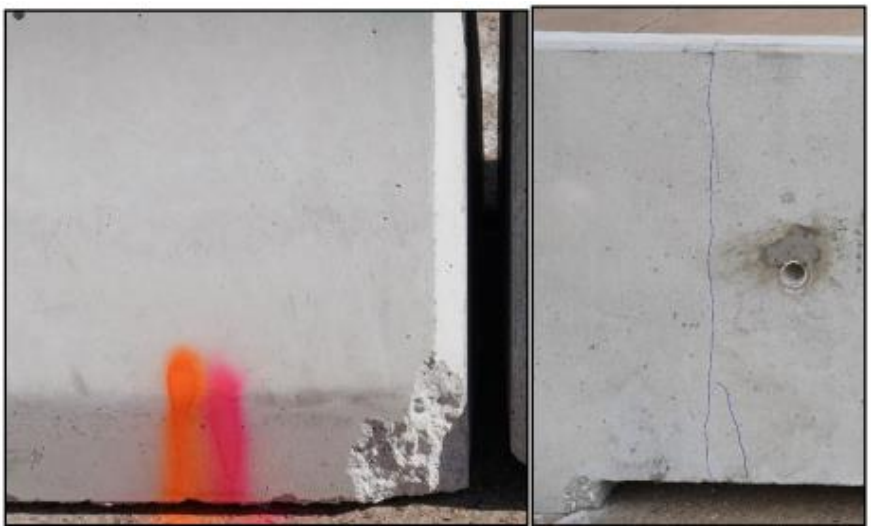

Figure 58. Acceptable Barrier— Spalled Dimension Less than 12 Inches and Spall Depth Less than the Cover; Reinforcement Is Not Exposed.

6.2.4. Spall over Base has a Surface Projecting towards Traffic by More Than 30 Degrees and that is Exposed to a Depth Exceeding 1.75 Inches for Traffic Approaching the Barrier at 25 Degrees.

A PCB is unacceptable if it has a spall over the base with a surface that projects toward traffic by more than 30 degrees and that is exposed to a depth exceeding 1.75 inches for traffic approaching the barrier at 25 degrees (1), as illustrated in Figure 59. Figure 60 shows an example of an unacceptable barrier. A PCB is acceptable if the spall projects toward s traffic by less than 30 degrees and the spall depth does not exceed 1.75 inches for traffic approaching the barrier at 25 degrees (Figure 61).

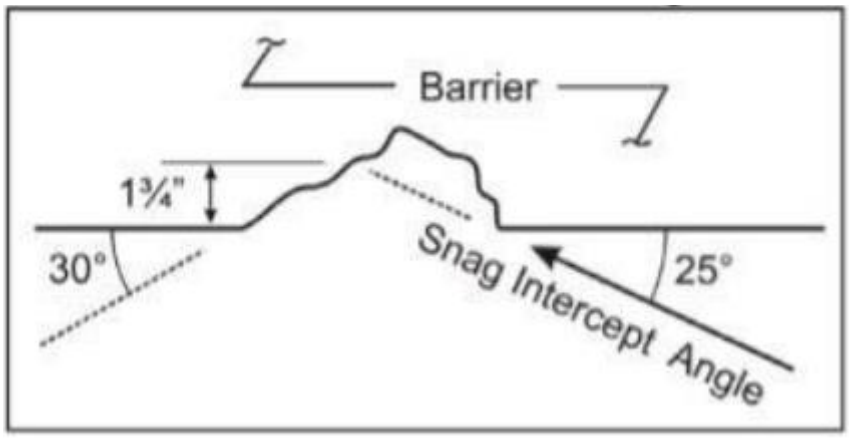

Figure 59. Threshold Criteria for Snag Point (1). Reprinted from Temporary Barrier Guidelines-Snag Points, NYSDOT.

Figure 60. Unacceptable Barrier—Spall Projects towards Traffic by More than 30 Degrees.

Figure 61. Acceptable Barrier—Spall Projects toward Traffic by Less than 30 Degrees.

WHAT IF?

WE HAVE A BARRIER WITH MULTIPLE SPALLS ON ONE SIDE AND NO SPALLS AT ALL ON THE OTHER SIDE. CAN IT BE FLIPPED

If the barrier is damaged on one side while the other side is undamaged, it is recommended to not to flip the barrier; it is suggested to either repair if there are minor spalls before continuing to use or replace the unit with new one if at least one of the spalls meets the unacceptability criteria discussed in 6.2.3 or 6.2.4.

6.2.5. Multiple Open Cracks Running in the Transverse Direction

A PCB is unacceptable if multiple open cracks (i.e., cracks having a measurable width) run in the transverse direction of the barrier section (Figure 62).

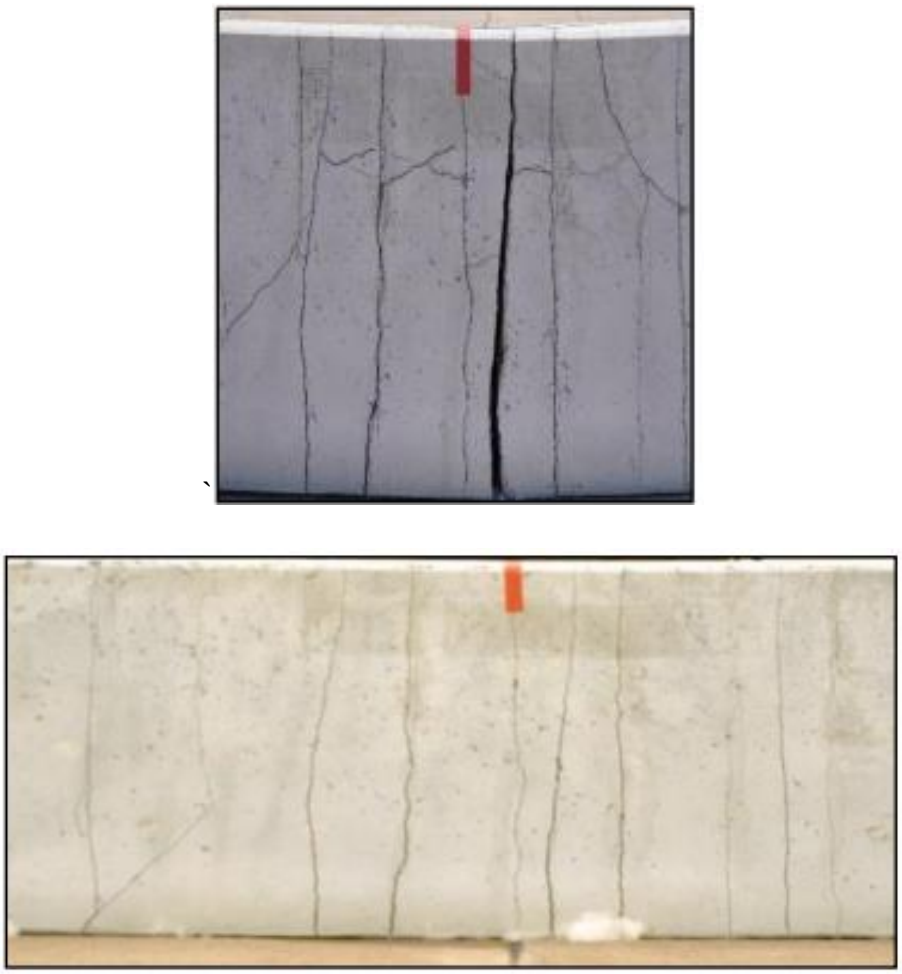

Figure 62. Unacceptable Barrier—Multiple Open Transverse Cracks.

However, if the cracks are not severe to the extent of being open and propagating on both sides of the barrier, repair could be considered. The durability of any repair method chosen to rectify cracks (in terms of number of years added to the present age of the barrier) is not standard and depends on several factors such as the present age of the barrier, the climatic conditions of the region where the barrier is installed, crack width,

etc. The decision to repair or replace is influenced by cost, safety levels, and the expected service life associated with repair or replacement.

The service lives associated with repair and replacement are different (the life of a new barrier is greater than the life of a repaired barrier). Therefore, the per-year cost of repair (which includes the costs of materials and labor) should be estimated based on the number of cracks present, average crack width, and length. This cost should be compared to the per-year cost (which includes the costs of materials, transportation, and installment) of a new barrier to arrive at a decision. Figure 63 provides a flowchart suggesting a methodology to choose the best alternative.

In some cases, instead of deciding immediately among structural repair and replacement, the barrier may be kept in service after closing the cracks with a surface sealant (to prevent the infiltration of contaminants and water). The barrier condition may be monitored periodically (within two years) to check how the cracks progress. A suitable structural repair or decision to replace could be taken later depending on the findings of the assessment period.

For example, consider the case in figure 64 where the transverse cracks are compressed. The barrier may be monitored for a certain time while keeping it in service to check if the cracks propagate further. Depending on the findings of the assessment period, further action could be taken.

A PCB is acceptable if it has hairline cracks (width is less than 1/16 in.), these cracks could be sealed using a surface sealant to prevent infiltration of water and contaminants (Figure 65).

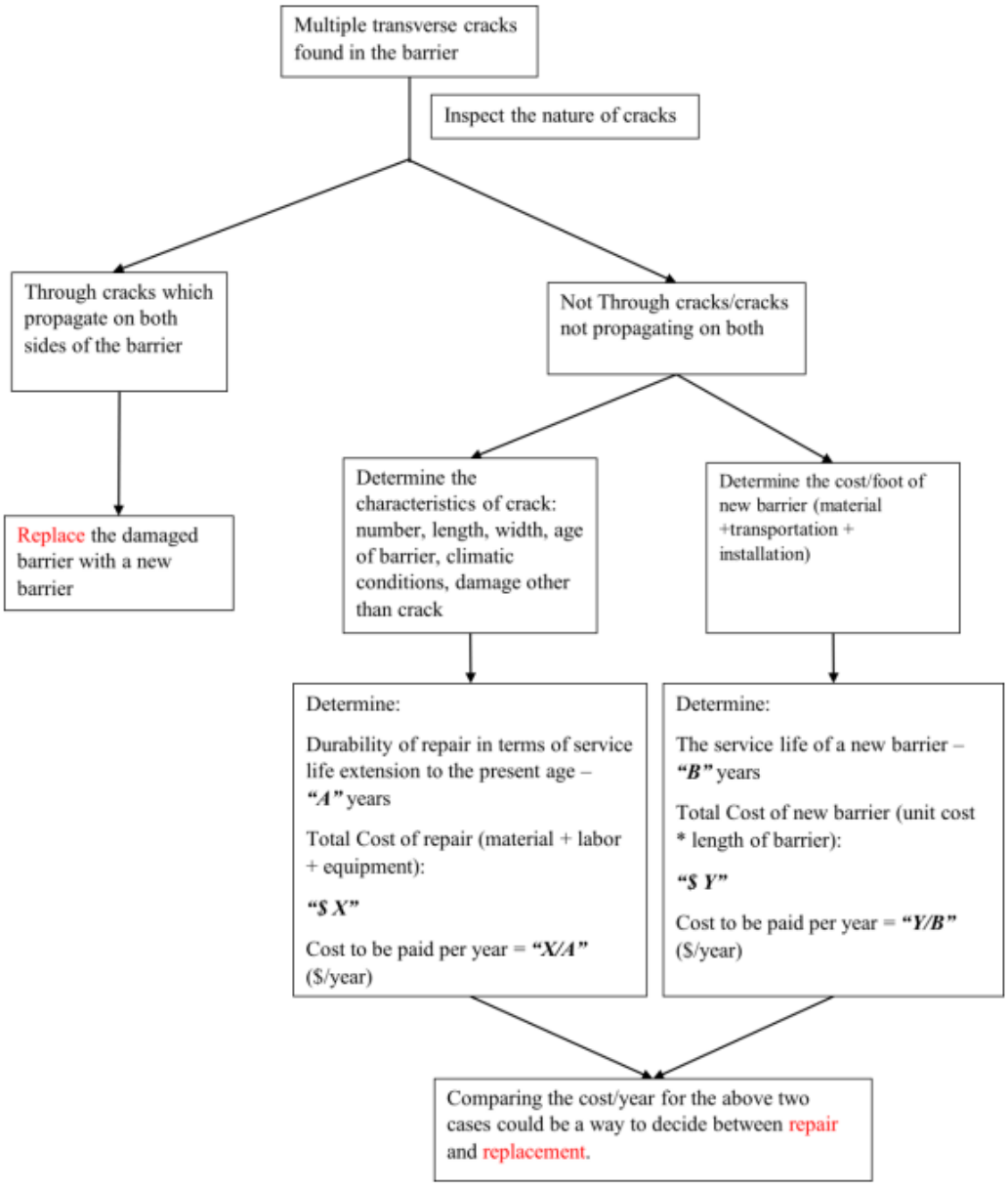

Figure 63. Decision Flowchart for Choosing the Best Alternative.

Figure 64. Compressed Transverse Cracks: A Decision May Not Be Made Immediately.

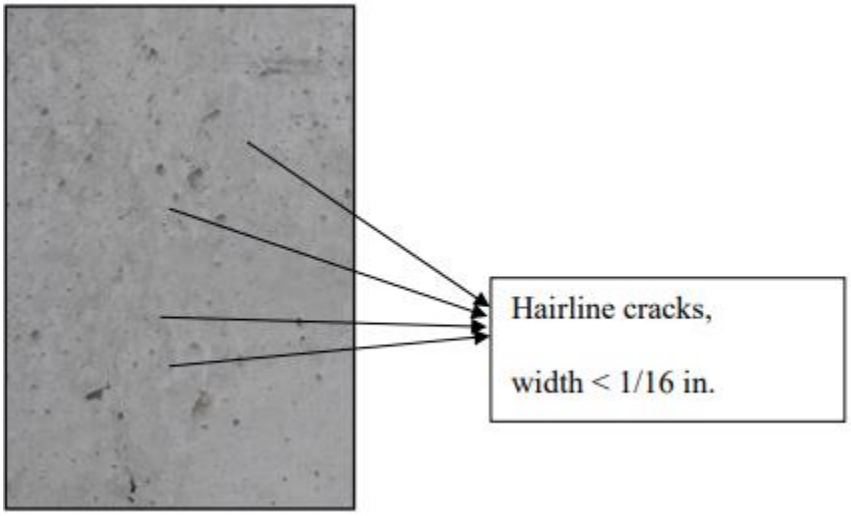

Figure 65. Acceptable Barrier—Hairline Cracks Could Be Sealed Using a Surface Sealant to Prevent Infiltration of Water and Contaminants.

6.2.6. Longitudinal Open Crack in the Upper Half of the Barrier Stem

A PCB is unacceptable if it has a longitudinal open crack (measurable width) in the upper half of the barrier stem (50 percent of the total height, starting from the top edge) with or without the evidence of rusting (Figure 66). However, a PCB with a compressed longitudinal crack in the lower portion of the stem that does not show any evidence of rusting maybe deemed acceptable (2) (Figure 67). To decide if a repair is necessary on a later date, this barrier may be observed for two years while keeping it in service to see if the longitudinal crack (temporarily closed with a surface sealant) propagates further.

(a) (b)

Figure 66. Unacceptable Barrier—(a) Clustered Longitudinal Cracks in the Upper Half of the Barrier Stem; (b) Open Longitudinal Crack More than 4 ft in Length (2). Reprinted from Temporary Barrier Guidelines-Longitudinal Cracks, NYSDOT.

Figure 67. Acceptable Barrier—Compressed Longitudinal Crack in the Lower Half of the Barrier Stem (Bottom 50 Percent of the Total Height) (2). Reprinted from Temporary Barrier Guidelines-Longitudinal Cracks, NYSDOT.

As far as repair is concerned, all longitudinal cracks are not repairable. For example, as shown in Figure 68, transverse cracks intersect longitudinal cracks at intermediate locations. In this case, the damaged barrier should not be repaired but be immediately replaced with a new barrier.

Figure 68. Unacceptable Barrier—Longitudinal Cracks Intersected by Transverse Cracks at Intermediate Locations (2). Reprinted from Temporary Barrier Guidelines-Longitudinal Cracks, NYSDOT.

6.2.7. Single Transverse Crack Running throughout the Section with Corrosion

A PCB is unacceptable if it has a single transverse crack running throughout the section with evident corrosion of the rebar. Figure 69 shows a barrier with a single transverse crack with no evidence of corrosion found on visual inspection, this barrier may be deemed acceptable with repair. In case, it is not obvious through visual inspection (e.g., a rust stain on the crack surface) whether the rebar is corroding, a sophisticated nondestructive technology may be adopted to determine the same. For example, Proceq, a Swiss-based nondestructive testing company, has patented Profometer Corrosion, Resipod, and Torrent instruments, which are designed and manufactured to assess the durability of concrete structures by measuring corrosion potential, concrete resistivity, and permeability. The reader is encouraged to read the instrument descriptions on the website, https://www.proceq.com.

Figure 69. Barrier which is Acceptable with Repair—Single Transverse Crack with No Evidence of Corrosion (3). Reprinted from Temporary Barrier Guidelines-Cracked Sections, NYSDOT.

6.2.8. High Crack Density or Erosion near Discontinuities

A PCB is unacceptable if it has high crack density or erosion near discontinuities (e.g., a pipe- drain hole or scupper) (Figure 70).

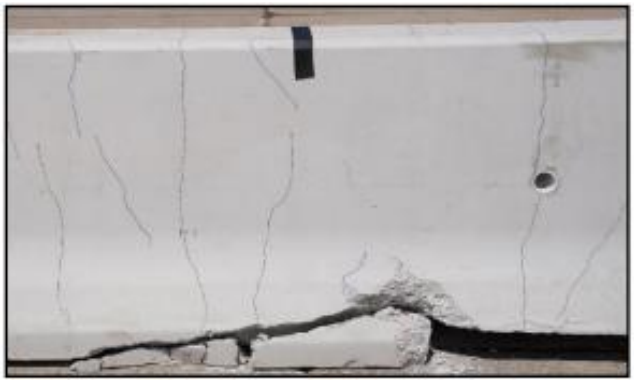

Figure 70. Unacceptable Barrier—Missing Section near the Edge of the Scupper.

6.2.9. Barrier Segment Having Bent, Rotated, Deformed, or Broken JJ Hook

A PCB is unacceptable if it has a bent, rotated, deformed, or broken JJ hook at either or both ends (Figure 71 through Figure 73). Segments with hooks rotated by different angles (or one segment with a straight hook along with another segment with a bent hook) do not properly align to make a continuous and sound connection when brought together. Even if connectors are rotated by the same degrees and if the connection is further rotated during an accident, the ability of redirecting the errant vehicle should be reduced. Effect of bent/rotated/deformed JJ hooks on the crashworthiness of the barrier system has been further investigated through predictive FEA simulations in Chapter 7.

Figure 71. Unacceptable Barrier—Rotated JJ Hooks Coming from Different Ends; The Ability of This Connection to Redirect an Errant Vehicle Will Be Reduced.

Figure 72. Unacceptable Barrier—Rotated JJ Hook at the End; a Connection Will Be Difficult to Form.

Figure 73. Unacceptable Barrier—JJ Hook Failure by Brittle Fracture.

Rotation of the hook can be quantified with the help of a scale and protractor. The opening size can be measured with the help of a scale and compared with the original diameter (opening) to see the increase (Figure 74). The tolerance of opening of

the hook, ‘d’ should be equal to thickness of the plate (0.4 inches). Bending/rotation in the hook can be gauged by measuring the angle ‘a’ with the help of a protractor. In Chapter 7, Section 7.4.4, different values of ‘d’ and ‘a’ have been used in the set of predictive FEA simulations carried out to check the effect of JJ hook deformations on the crashworthiness of the barrier system.

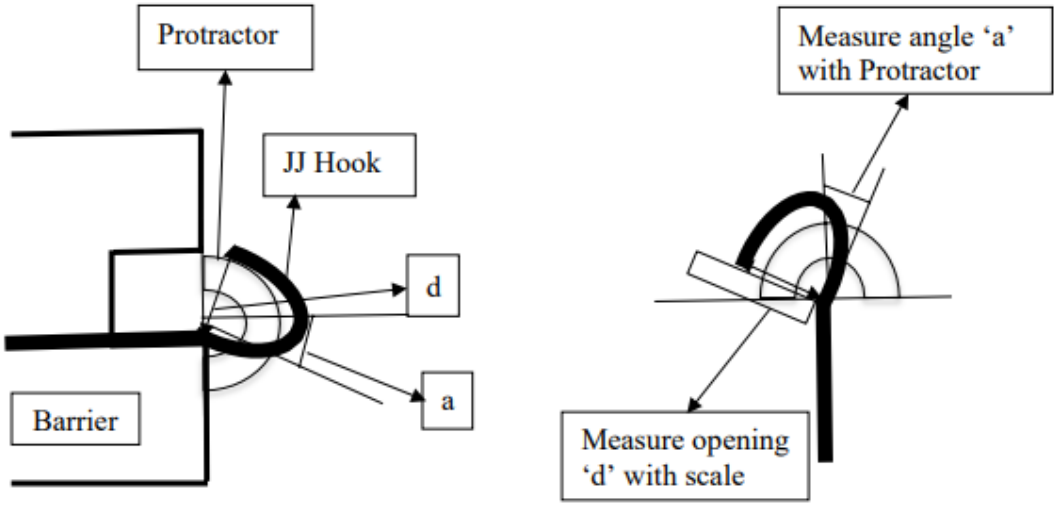

Figure 74. Quantification of the Rotation of the JJ Hook.

6.2.10. JJ Hook or Plate That is Corroded or Has Flaws

A PCB is unacceptable if it has a JJ hook or plate that is corroded or has a flaw in the form of a crack of any width, or a combination of both (Figure 75).

Figure 75. Unacceptable Barrier—Cracked JJ Hook.

6.3. Repair Guidelines for PCBs

The guidelines in this section have been drafted for repairing concrete related damage modes namely, spalling and cracking. Barriers with damaged JJ hooks must be replaced for there is no known repair method which could restore the connection capacity back to the original.

6.3.1. Spall Repair

6.3.1.1. Description

According to Section 1, Chapter 2 of the TxDOT Concrete Repair Manual, based on severity, spalls are categorized as minor, intermediate, and major. The severity is decided by assessing the spall depth, size (area) of the spall, causes, and configuration (horizontal, vertical, or overhead). The engineer in charge may define the severity of the

spall differently than the definitions outlined by the concrete repair manual on a case-by-case basis. The following are the spall category definitions:

Category 1: Minor Spall: The spall is less than 1 inch deep and covers an area less than 12 square inches. If more than 50 percent of a rebar circumference is exposed due to inadequate cover, then the spall is "intermediate" even if the spall is less than 1 inch deep.

Depending on the location and extent of the spall, the inspector may choose to designate patches that cover more than 12 square inches as "minor." A deeper spall of depth up to 2 inches can be categorized as "minor" if it does not progress beyond the outer layer of reinforcement.

Category 2: Intermediate Spall: More than 50 percent of the outer cage of the rebar is exposed, or the spall is deeper than 2 inches. The maximum depth of the spall is 6 inches.

Significant stresses are not likely to develop in or immediately around the repair material due to service loads.

Category 3: Major Spall: The spall extends well beyond the outer layer of reinforcement.

Significant stresses are likely to develop in or immediately around the repair material due to service loads.

Repair guidelines prescribed in this section are for correcting minor spalls. Researcher advises rejecting the barrier in the event of intermediate and major spalls and immediately replacing the damaged barrier with a new one.

6.3.1.2. Repair Materials

The contractor can use any prepackaged, fast-setting, DOT-approved concrete product to repair minor spalls. Manufacturers have different specifications and procedures for different variations of spalls or concrete erosion-related issues, namely missing corners, thin repair, aesthetic repair, and broken edges. The specific method statement with the exact ratios and quantities to be used should be that recommended by the selected manufacturer. However, the next section describes the general repair methodology.

6.3.1.3. Repair Procedure

The following is the general repair procedure for spalls:

1. Clean the surface of the damaged area (which needs repair) by removing any loose material such as dirt, oil, or grease, and unsound or flaking concrete.
2. Scrub and clean the surface of the area to be repaired with a stiff bristle brush.
3. Thoroughly rinse the repair area after cleaning.
4. Select a TxDOT-approved manufacturer of fast-setting repair material. Follow the specific method statement issued by the manufacturer to prepare the mixture or use a premixed combination of repair material and a liquid base to apply on the damage area.
5. Achieve the desired consistency of this mixture according to the method statement issued by the manufacturer. Apply the mixture on the dampened damaged area according to the method statement.
6. Level and match the rectifying layer with the surrounding concrete.

6.3.2. Crack Repair

6.3.2.1. Description

According to Sections 5, 6, and 7 of the TxDOT Concrete Repair Manual, cracks can be repaired by using pressure-injected epoxy, gravity-fed sealant, and surface sealant. While pressure-injected epoxy and gravity-fed sealant can restore the capacity of the cracked section, a surface sealant only seals the cracks at the outer surface of the concrete to prevent the infiltration of water, chlorides, and other contaminants. Therefore, it is not advisable to use the surface sealing technique where a significant crack displacement is anticipated. However, surface sealant can be used to close hairline cracks (nonstructural) to keep contaminants from reaching the reinforcement surface. Injecting epoxy resin is the best technique for filling cracks on a vertical surface such as a barrier wall.

Injection of epoxy resin can seal cracks as fine as 0.002 inches (0.05 mm) in width. Using an epoxy resin of low viscosity (less than 20 poise) enables the resin to penetrate the full depth of the crack at working pressure (4).

For injecting epoxy, entry ports must be installed. For small jobs, to avoid the installation of fittings, short gaps can be left at regular intervals in the seal over the crack, and epoxy resin can be injected through a caulking gun. The spacing between the entry ports or gaps should be sufficient to assure that liquid injected into one port flows through the full thickness of the member before flowing out of the next port or gap. For sealing vertical cracks, the operator injects epoxy into the lowest port until it emerges out of the port above. The operator then seals off the lower port or gap, starts injection

into the next port or gap, and continues until all cracks are filled. The fittings, if installed, are removed when the adhesive is cured.

The epoxy used should be able to develop 1400 psi strength in 14 days and used at a temperature less than 40°F or between 40°F and 60°F. Epoxy has a grease-like, non-sagging consistency and bonds even with moist concrete.

6.3.2.2. Repair Materials

According to Section 5 of the TxDOT Concrete Repair Manual, crack repair materials are specified according to their designated purposes as follows:

• **Structural repair**: Material selected for repair shall meet the requirements given in DMS 6110—Quality Monitoring Program for Epoxies and Adhesives. The Material Producer List (MPL) provides names of prequalified producers of epoxies and adhesives (Type II–X) that can be used for repairing cracks. Use the following materials for:

o **Injecting cracks**: TxDOT Type IX low-viscosity epoxy resin (ASTM C 881 Type IV, Grade 1), which typically consists of two liquid components that are combined automatically during the pressure injection process.

o **Sealing the surface of cracks**: TxDOT Type V or VII concrete epoxy adhesive.

• **Nonstructural repair**: Use the following materials for:

o **Routing and sealing cracks:** pre-approved Class 4 low-modulus silicone that meets the requirements of DMS 6310—Joints Sealants and Fillers or Type V adhesive

that meets the requirements of DMS 6100—Epoxies and Adhesives as specified in the plans (5).

o **Sealing the surface of cracks**: preapproved Type VIII or Type X epoxy that meets the requirements of DMS 6100—Epoxies and Adhesives (5).

6.3.2.3. Repair Procedure

6.3.2.3.1 Epoxy Injection for Structural Cracks

The following is the procedure to inject epoxy for structural cracks:

1. Depending on the size of the job and the manufacturer's specifications, drill holes at appropriate intervals to permit installation of the injection ports (Figure 76) or mount the ports on the surface.

2. Clean the interior of the vertical cracks from bottom to top and remove all the loose materials entrapped in the cracks.

- If compressed air is used to remove the loose materials from the cracks, ensure that the debris is not forced deeper into the crack.
- Consult the engineer if it appears that debris in the crack hinders proper injection of the epoxy resin.

Figure 76. Drilling Holes in the Concrete Member (6). Reprinted from "Concrete Repairing by Epoxy Injection", Design Consulting Services.

If debris is only near the surface, drill holes for the injection ports away from the exposed portion of the crack. The holes are to be drilled at an angle such that the injection ports intersect the crack beneath the surface away from the dust and debris (Figure 77).

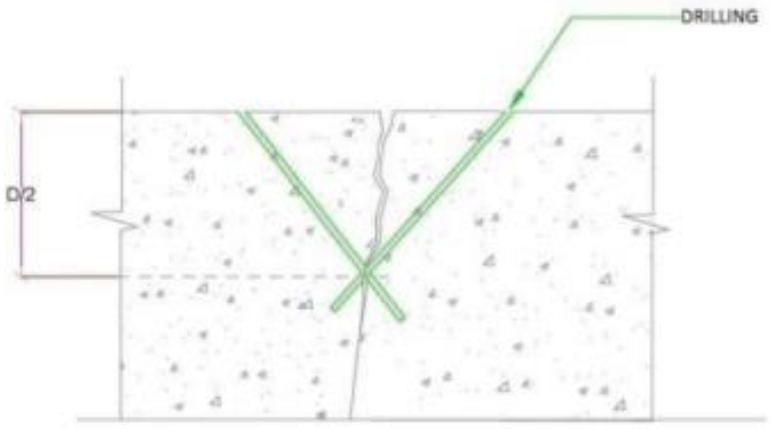

Figure 77. Section Showing Holes Drilled at an Angle (6). Reprinted from "Concrete Repairing by Epoxy Injection", Design Consulting Services.

3. After drilling, remove contaminants such as laitance, oil, dust, debris, and other foreign particles where the surface seal will be applied.

4. Unless the manufacturer or engineer mentions it, do not grind the concrete around the crack to remove contaminants or provide a V-shaped groove along the crack.

• Grinding can force dust into the crack and consequently hinder proper flow of the epoxy resin.

• If a V-shaped groove is cut along the crack, carefully remove the dust using compressed air and/or high-pressure water blasting. Do not commence the surface sealer application or injection work until the crack and concrete surface have dried.

5. As directed in the method statement issued by the manufacturer, mix the epoxy surface sealer. Use portable injection equipment capable of automatically mixing the liquid components at the proper proportion during the pressure injection operation.

6. Depending on the size of the job and the manufacturer's instructions given in the method statement, either install the injection ports (Figure 78) or leave short gaps at appropriate intervals. If installing ports:

• Place the ports directly on the crack or in drilled holes that intersect the crack.

• Install the injection ports at appropriate intervals along the crack.

o The port spacing should not exceed the depth of the crack. If the depth of the crack is not known, space the ports as recommended by the resin manufacturer.

o If the crack projects through the entire concrete section, the intervals between ports should not exceed the section depth.

• Ensure that the ports are placed in locations where the crack is not too narrow or clogged with debris to permit adequate flow of epoxy resin.

Figure 78. Installing Injection Ports (6). Reprinted from "Concrete Repairing by Epoxy Injection", Design Consulting Services.

• Anchor the injection ports, if used, and seal the surface of the crack between ports or gaps using a sealer as required by the resin manufacturer.

• Allow sufficient time for the sealer to cure before commencing the resin injection.

• The sealer must have adequate strength to hold the injection ports in place and withstand the pressure along the crack during the injection operations.

• Apply sealer over the crack surface on the backside if the crack extends completely through the concrete section.

• Begin pressure-injecting the epoxy resin into the crack through the ports (Figure 79).

• Use a positive displacement pump, air- or hand-actuated caulking gun, or paint pressure pot as recommended by the epoxy resin manufacturer and approved by the engineer. Small jobs which do not have fittings installed may involve the use of caulking gun to inject the epoxy resin into the cracks (4).

• On a vertical surface, start injecting at the lowest port and work upward.

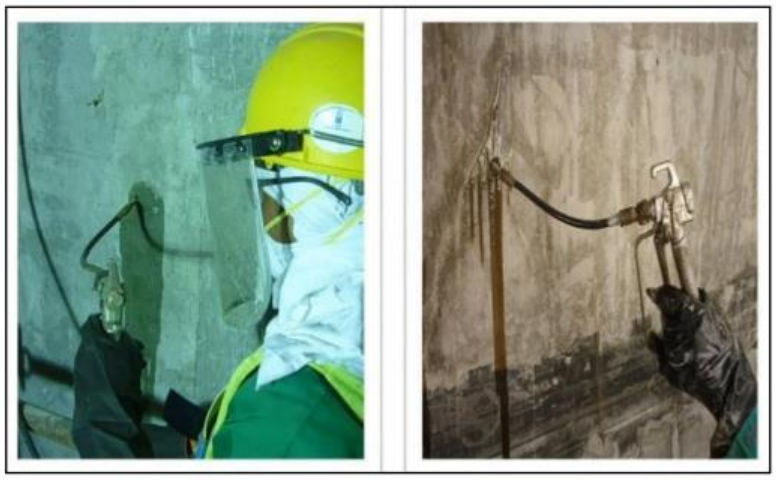

Figure 79. Injection of Epoxy Resin into the Holes (6). Reprinted from "Concrete Repairing by Epoxy Injection", Design Consulting Services.

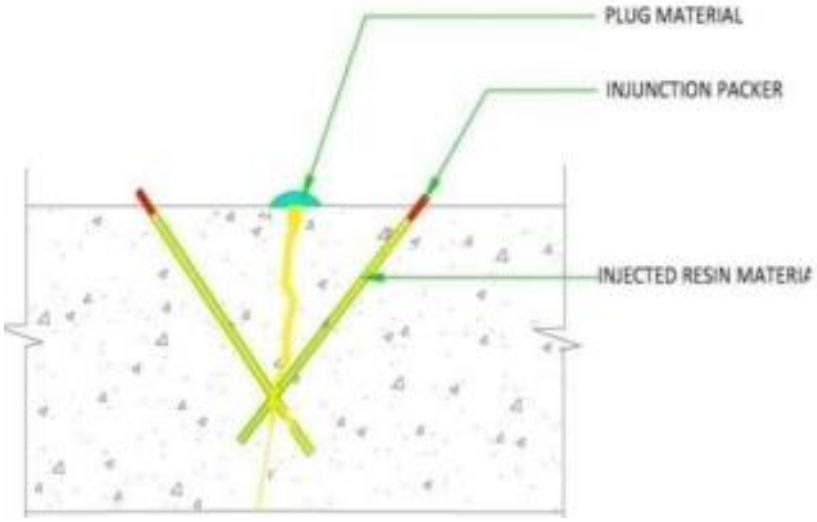

Figure 80. Injection of Epoxy: Section Showing Drilled Holes and a Crack Filled with Repair Material (6). Reprinted from "Concrete Repairing by Epoxy Injection", Design Consulting Services.

- Maintain adequate pressure until resin emerges from the adjacent port.

o If resin does not emerge from the adjacent port, stop the work, and reevaluate the crack.

o Ports may need to be placed more closely together or debris cleared from under the existing ports.

o Ports should be installed at an angle, so they intersect the crack at a deeper point if debris is clogging the crack near the concrete surface.

o Inadequate flow of the epoxy resin may be a sign that the crack is either too shallow or too narrow for pressure injection to serve its purpose.

• If the epoxy begins to flow out of a non-adjacent port or gap, temporarily plug that port or gap until the epoxy begins to flow out of the adjacent port or gap.

Figure 80 shows a cracked section filled with the resin material injected through the ports.

• Once the resin appears in an adjacent port, remove the injection nozzle, and seal the port.

• Move the equipment to the next adjacent port and proceed with the epoxy resin pressure injection.

• Remove the injection ports and surface sealer after the epoxy resin has been given adequate time to cure (Figure 81). Resin material should not flow from the crack after the surface sealer is removed.

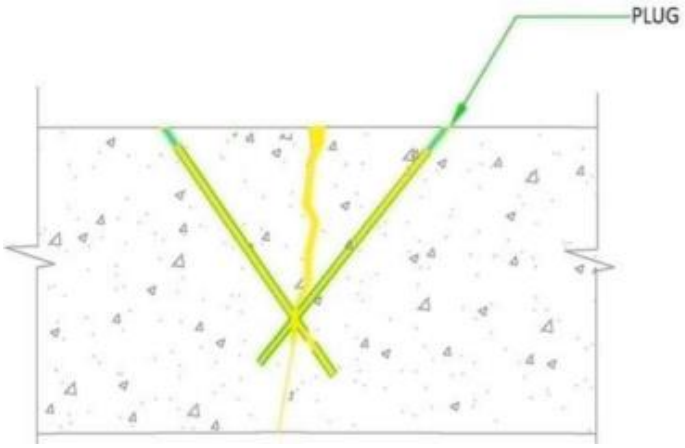

Figure 81. Removal of Surface Sealer and Installation Ports after the Resin Cures (6). Reprinted from "Concrete Repairing by Epoxy Injection", Design Consulting Services.

7. Grind away any epoxy resin or surface sealer residue that is left on the concrete surface after the injected material has had sufficient time to cure.

6.3.2.3.2. Routing and Sealing Cracks and Surface Sealing for Nonstructural Cracks

Routing and sealing can be used where a small amount of movement is anticipated due to service loads, thermal effects, or other causes. The following is the procedure to rout and seal nonstructural cracks:

1. Route the crack using a grinder to create a V-shaped groove, with the crack centered in the groove. Grooves are typically about 3/8 inches deep.
2. Ensure that the substrates are clean and sound by removing contaminants including laitance, oil, dust, debris, and other foreign particles.
3. Fill the groove using a preapproved Class 4 low-modulus silicone that meets the requirements of DMS 6310—Joints Sealants and Fillers or Type V adhesive that meets the requirements of DMS 6100—Epoxies and Adhesives as specified in the plans (5).

The following is the procedure to seal the surface:

1. Apply an adhesive directly over the crack to prevent the infiltration of contaminants. Use a preapproved Type VIII or Type X epoxy that meets the requirements of DMS 6100—Epoxies and Adhesives.
2. Work the epoxy into the crack.
3. Remove any excess epoxy from the surface before it sets (5).

6.4. References

1. Temporary Barrier Guidelines-Snag Points, New York State Department of Transportation. https://www.dot.ny.gov/divisions/engineering/design/dqab/tcbacceptability/snagpoints

2. Temporary Barrier Guidelines- Longitudinal Cracks, New York State Department of Transportation, Last Accessed on May 28, 2021. https://www.dot.ny.gov/divisions/engineering/design/dqab/tcbacceptability/longitudinal_cracks

3. Temporary Barrier Guidelines- Cracked Sections, New York State Department of Transportation, Last Accessed on May 28, 2021. https://www.dot.ny.gov/divisions/engineering/design/dqab/tcbacceptability/cracked_sections

4. Kuenning, William H. How to Repair Cracks by Grouting with Epoxy Resin. Concrete Construction, May 1, 1972. https://www.concreteconstruction.net/how-to/materials/how-to-repair-cracks-by-grouting-with-epoxy-resin_o

5. Texas Department of Transportation. Concrete Repair Manual. 2021.

6. Design Consulting Services. Concrete Repairing by Epoxy Injection. YouTube, Oct. 8, 2020. https://www.youtube.com/watch?v=tAYKBVW08d0.

7. ENGINEERING ANALYSIS

7.1. Introduction

7.1.1. Description

To further assess the crashworthiness of the barrier system based on the most critical considerations from the preliminary evaluation guidance, various FE models were developed in a non-linear dynamic analysis program, LS-DYNA. The scope of this engineering analysis is limited to the evaluation of the performance of the single slope barrier assembly having pre-existing damage in the form of spalls. The researcher carried out predictive simulations with damaged barrier models made in LS DYNA. Based on the observations from component testing (Chapter 3) and review of the guidelines given by other state DOTs (Chapter 5), spall size of 13 in. by 4 in. by 2 in. was selected and strategically placed once on the toe of one of the barriers and then on adjacent toes of two barriers. This location was chosen because the barrier was expected to deflect the most in such a situation thus, creating maximum threat for the stability of the vehicle. Further investigation was also carried out to study the effect of different JJ hook deformation levels on the crashworthiness of a much smaller and lighter weight barrier model, F shape barrier modelled by another Graduate Student Researcher, Aniruddha Zalani. Table 11 lists the guidelines which were evaluated in this engineering analysis:

Table 11. Top Critical Guidelines.

Sec. Ref. No.	Preliminary Guidelines (from Chapter 6)
6.2.1.	Depth of Spall beyond Outer Layer of Rebar.
6.2.3.	Spall over Toe Greater than 12 inches.
6.2.9.	Barrier Segment Having Bent, Rotated, Deformed, or Broken JJ Hook

Various components of the PCB assembly such as the concrete body of the barrier, reinforcement, JJ hooks were visualized individually and then combined through numerical modelling in LS-DYNA. Appropriate connections, constraints and contacts were used to make an integrated assembly of these components. The vehicle models used for the simulation were (i) 2018 Dodge RAM quad cab, 4 door, 0.5-ton truck model (ii) Toyota Yaris model which represented a 2420 lb. (1100 C) MASH small car test vehicle and (iii) 5000 lb. bogie model. The first two models of the pickup truck and passenger car were used in the simulations with MASH TL 3-11 and TL 3-10 impact conditions, respectively whereas the bogie model was used in the simulation of the component crash test conducted earlier at the TTI proving ground. Thus, the bogie simulation was used to validate the crash behavior of the 4-segment barrier assembly model (120 ft long) and the pickup truck/passenger car simulations were used to predict the behavior of the 7-segment barrier assembly (210 ft long) under MASH TL 3 impact

conditions. The crash data from LS-DYNA for the various simulations was processed further in the Test-Risk Assessment Program called TRAP, developed at TTI. Based on the results from TRAP, researcher has reviewed the earlier proposed guidelines on spalling/ deformed JJ hooks and has made recommendations for the actual crash test planned in the future.

7.2. Finite Element Modelling

7.2.1. Consistent Units

LS-DYNA requires consistent system of units as defined below:

1 force unit = 1 mass unit*1 acceleration unit

1 acceleration unit = 1 length unit/ (1 time unit) ^2

1 density unit = 1 mass unit/ (1 length unit) ^3

For the models developed for this project, Table 12 shows the consistent units which were considered in LS DYNA:

Table 12. Consistent Units.

Mass	Length	Time	Force	Stress	Energy
ton	mm	s	N	MPa	N-mm

To document the findings in this thesis, equivalent American units have been used.

7.2.2. Geometry, Elements and Mesh Size

7.2.2.1. Single Slope Barrier Body

Cross section of the single slope barrier was first developed in LS-DYNA using dimensions of the TxDOT compliant single slope barrier used in the component crash test. The cross section was meshed using “Auto Mesher”, thereby creating shell elements in the cross section. With the cross-section elements selected, solid elements were generated in the longitudinal direction using “Shell Drag”. Further, the leave out (for JJ hooks) was created in the solid barrier by deleting the required number of solid elements on both the ends. The shell cross section face was deleted at the end to avoid any potential error which could have abruptly stopped the simulation from running. 36 in. (length) by 3 in. (height) size scuppers were created in the solid barrier body by deleting the required number of elements.

In the 7-segment barrier assembly, each 1-foot-long portion towards the end had a mesh size of 1 in. by 1 in. by 1 in. whereas the rest of the barrier (28-foot-long) had a mesh size of 1.5 in. by 1 in. by 1 in.

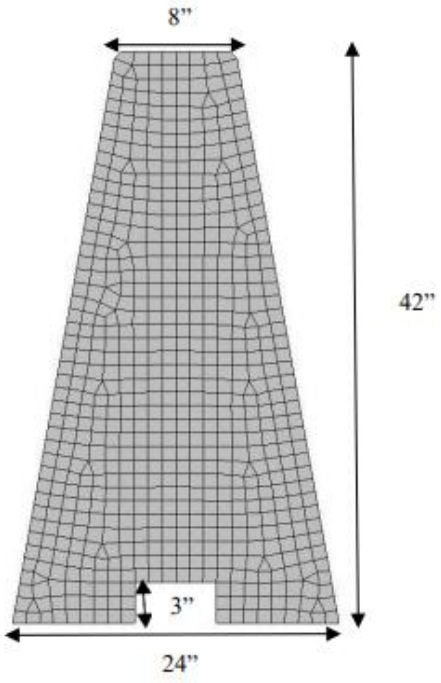

Figure 82. Cross-section of the Single Slope Barrier Model

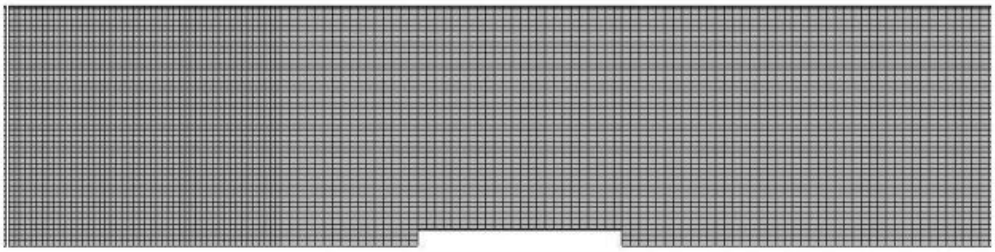

Figure 83. Half Elevation of the Single Slope Barrier Model

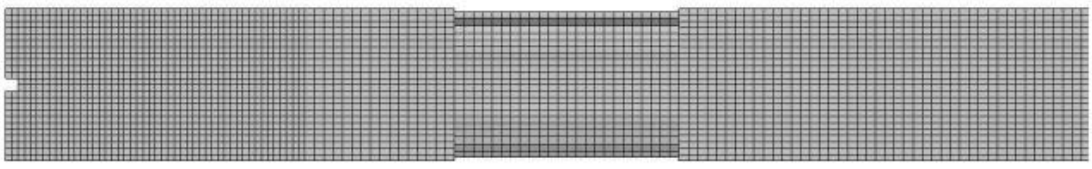

Figure 84. Half (Bottom) Plan of the Single Slope Barrier Model

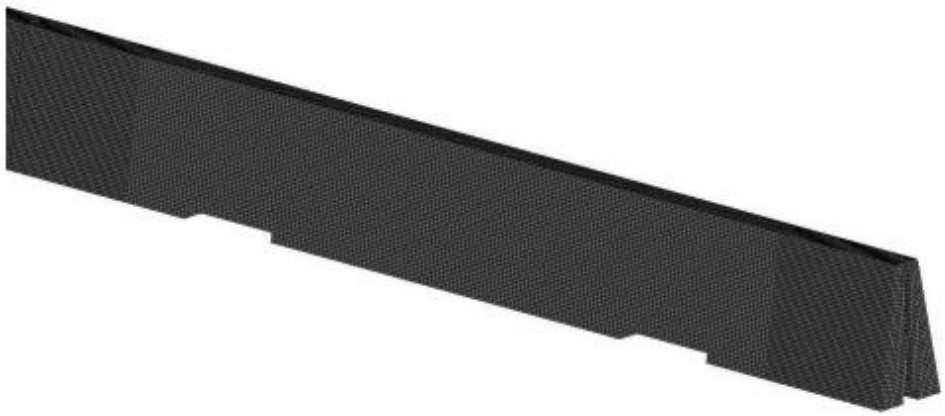

Figure 85. Isometric View of the Single Slope Barrier Model, Length=30 foot

7.2.2.2. Reinforcement

The rebars were modelled as beam elements. Each discretized beam element was kept about 0.8 in. long. The longitudinal reinforcement (#5 bar) was provided a cross section diameter of 0.625 in., whereas the stirrup (#4 bar) was provided a cross section diameter of 0.5 in. ELFORM was set to the default value of 1 for both cross-sections. While modelling the geometry, it was ensured that the stirrups and longitudinal rebars were kept under separate part ids 16 & 17, it was ensured that there was no initial penetration between these parts. Figure 86 and figure 87 show the elevation and isometric view of the reinforcement cage, respectively.

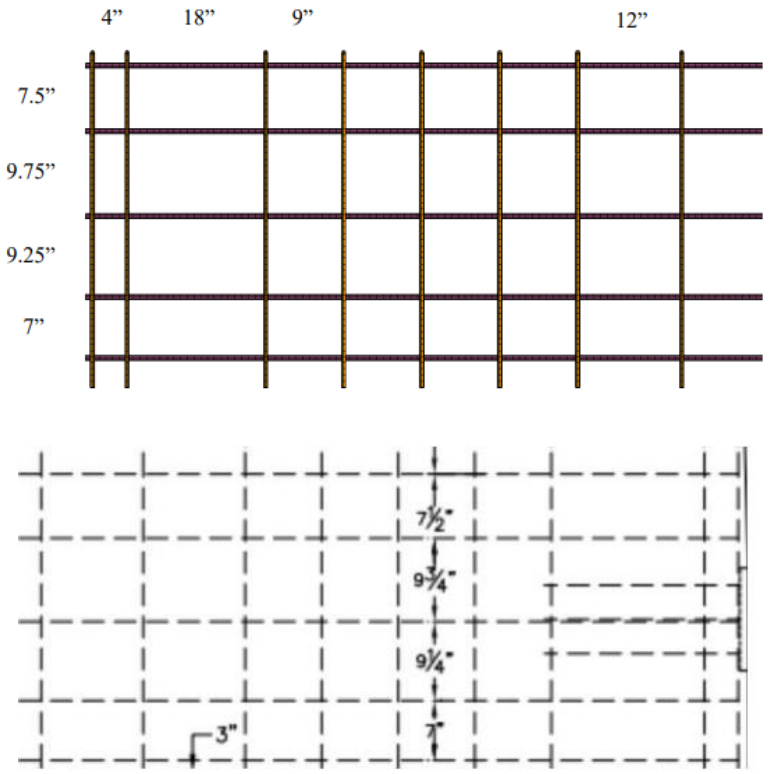

Figure 86. Partial Elevation of the Reinforcement Cage Consisting of Longitudinal Rebars and Stirrups

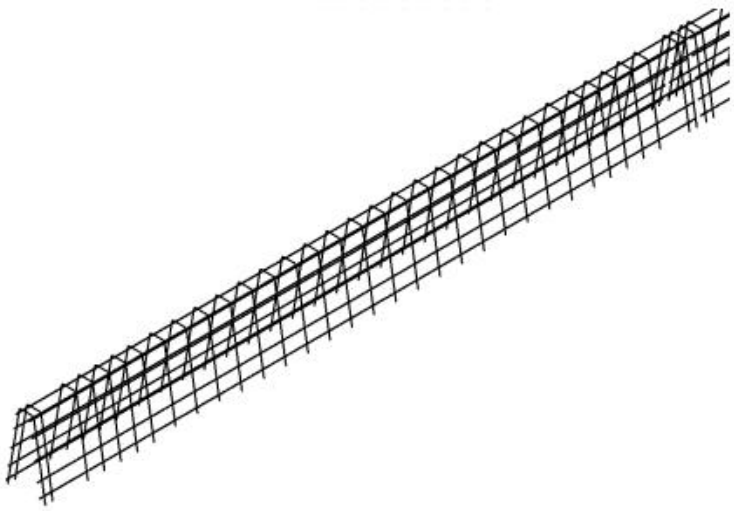

Figure 87. Isometric View of the Reinforcement Cage Consisting of Longitudinal Rebars and Stirrups.

7.2.2.3. Connection Components: JJ Hooks, Angle Plates and Welded Bars

The JJ hook was discretized using shell elements of thickness 0.4 in. Each JJ hook was divided into two parts, one part was contained inside the barrier (part Id 28, pink) and the other part protruded outside the barrier (part Id 27, blue). ELFORM was set to the value of 16 to allow LS DYNA to perform the very fast full integration of shell elements, corresponding NIP (Number of through shell thickness integration points) was kept as 5. Figure 88 and figure 89 show the cross section and the isometric view of the JJ hook, respectively.

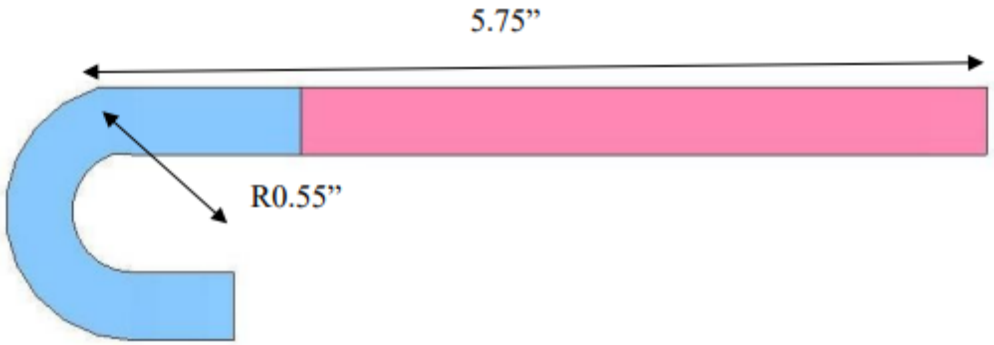

Figure 88. Cross Section of the JJ Hook

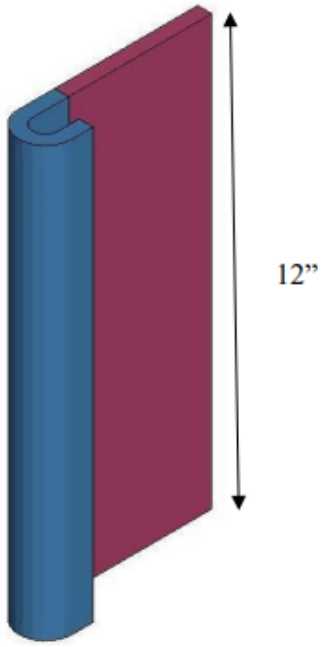

Figure 89. Isometric View of the JJ Hook

The angle plate discretized using shell elements of thickness 0.2 in. (geometry modelled by Aniruddha Zalani, TTI) and additional rebars (originally welded to JJ hooks in real life) were directly included into this assembly. One end of each angle plate was continuously connected to the JJ hook plate with the help of CNRB (Constrained Nodal Rigid Body).

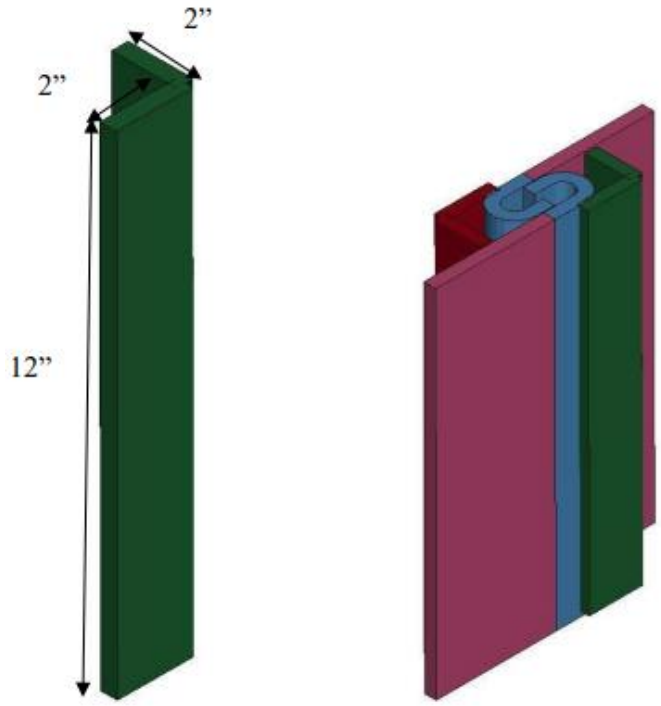

Figure 90. (i) Angle Plate (ii) Pair of Angle Plates Rigidly Connected to the Pair of JJ Hooks

7.2.2.4. 2018 Dodge RAM Quad Cab

The model of 2018 Dodge RAM Quad Cab was directly included in the combined assembly file at an angle of 25 degrees and CIP (Critical Impact Point) distance of 4.3 foot from the location which was targeted to be impacted. Initial linear velocity of 62.2 mph and angular velocity of 71 rad/s were provided to the pickup truck. Once the vehicle was rotated at an angle of 25 degrees in the combined assembly file, the initial velocity was resolved into two components, Vx = 56.4 mph and Vy= 26.3 mph. Radius of the wheel was measured as 15.4 in. thus giving an angular velocity of 71

rad/s. Figure 91 shows the isometric view of the vehicle model, Figure 92 shows the location of the vehicle with respect to the barrier assembly.

Figure 91. Isometric View of 2018 Dodge RAM Quad Cab, 4 door, 0.5-Ton.

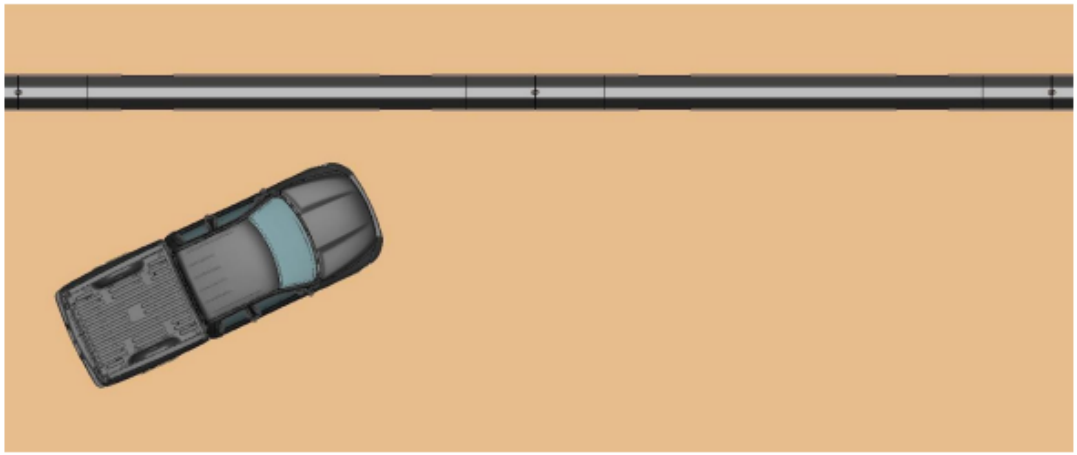

Figure 92. Initial position of RAM pickup truck

7.2.2.5. Toyota Yaris

Toyota Yaris model representing a 2420 lb. (1100 C) MASH small car test vehicle was directly included in the combined assembly file at an angle of 25 degrees and CIP (Critical Impact Point) distance of 3.6 foot from the location which was targeted to be impacted. Initial linear velocity of 62.2 mph and angular velocity of 71 rad/s were provided to the car. Once the vehicle was rotated at an angle of 25 degrees in the combined assembly file, the initial velocity was resolved into two components, Vx = 56.4 mph and Vy= 26.3 mph. Radius of the wheel was measured as 11.9 in. thus giving an angular velocity of 92 rad/s. Figure 93 shows the isometric view of the vehicle model, Figure 94 shows the location of the vehicle with respect to the barrier assembly.

Figure 93. Isometric View of Toyota Yaris Passenger Car

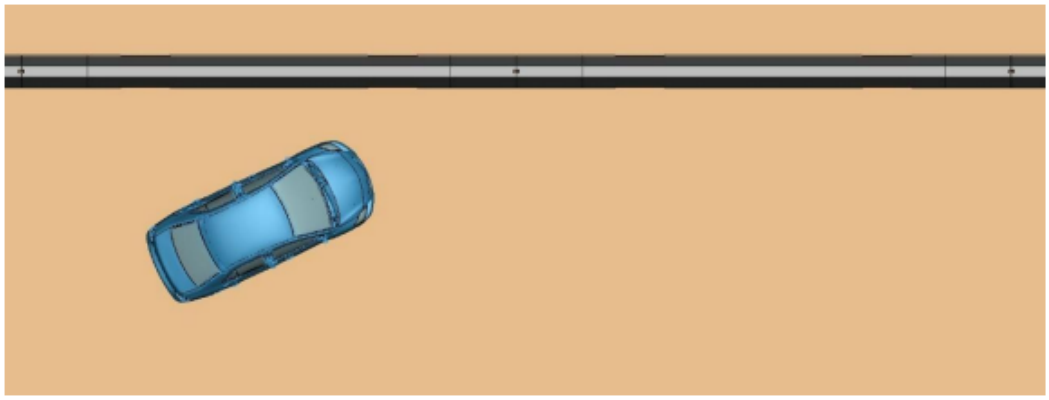

Figure 94. Initial position of Toyota Yaris passenger car

Both the models (RAM Pickup truck and Toyota Yaris car) have been made readily available to use by GMU. The keyword files for both the vehicles contain the appropriate part definitions, contacts, constraints, and connections.

7.2.2.6. 5000 lb. Bogie Model

A finite element model of the bogie nose was developed in LS DYNA. The researcher ran a simulation which consisted of the bogie nose impacting the single slope barrier assembly model perpendicularly at a speed of 18 mph. Figure 95 shows the bogie nose model.

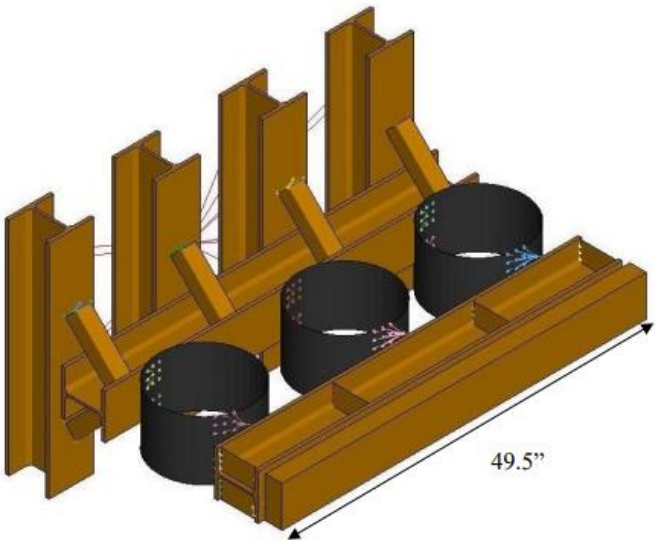

Figure 95. Bogie Nose

The bogie nose used in the real component crash test consisted of I girders, angle sections, crushable cylinders, transverse stiffeners, and a wooden block. In LS-DYNA, geometry of the above listed components was modelled as per the true dimensions (measurement data obtained from the TTI Laboratory) with the mesh size roughly around 1 in. by 1 in. The beams, angle sections and front wood piece were modelled with solid elements, whereas the cylinders and stiffeners were modelled with shell elements. Further, these were connected to each other by CNRB (Constrained Nodal Rigid Body). In the real world, these components were connected through welds of appropriate size. The total integrated mass of the bogie nose was 0.67 tons (1501 lb.). Since the total mass required to impact the barrier was 2.23 ton (5000 lb.), remaining mass of 1.56 tons (3494 lb.) was lumped at a node (ELEMENT_MASS) which was tied

to the back of the vertical I girders through CNRB. Thus, the total mass of this assembly was 3.79 tons (5000 lb.).

7.2.2.7. Rigid Ground

Rigid ground made up of shell elements of size 11.8 in. by 6.6 in. was provided beneath the barrier assembly and the vehicle. The shell elements had a thickness of 0.078 in (or 2 mm). ELFORM and NIP were set to the default value of 2. Model of the ground was readily made available to the researcher from the TTI FE model library. Figure 96 shows the plan of rigid ground.

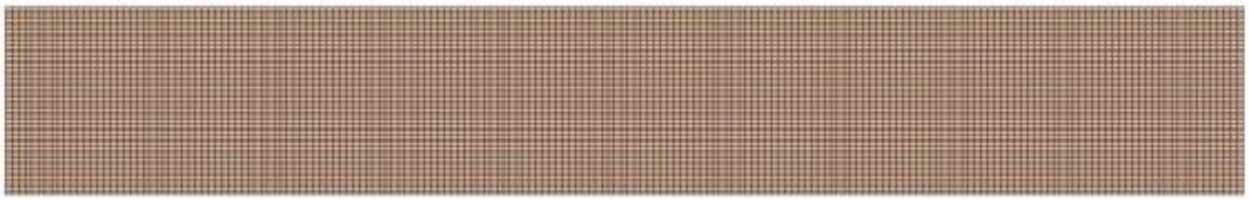

Figure 96. Rigid Shell Ground

7.2.3. Material Model

7.2.3.1. Concrete

The solid barrier was given the property of concrete using the material card 159_CSCM_CONCRETE. While there are two material models available for concrete, MAT_CSCM and 159_CSCM_CONCRETE, latter was chosen as it was more convenient to use and requested few default parameters such as unconfined compressive strength, maximum aggregate size and units. The model has been calibrated by FHWA through an extensive study of CEB-FIP Code and various impact tests for unconfined

compression strengths between 2.9 ksi and 8.4 ksi (or 20 MPa and 58 MPa) and aggregate sizes between 0.31 in. and 1.26 in. (or 8 mm and 32 mm). The unconfined compression strength affects aspects such as stiffness, three-dimensional yield strength, hardening and damage-based softening. The aggregate size affects the softening behavior of the damage formulation (1). Table 13 shows the parameters used for this material model:

Table 13. Parameters used to characterize concrete.

Parameter	Value input
Mass Density, RO	2.403e-09
Unconfined compression strength, FPC	24.821131 (Per the TxDOT drawing)
Maximum aggregate size, DAGG	19 (default)
UNITS	2 (EQ 2: MPa, mm, sec, Mg/mm^3, Nt)

7.2.3.2. Steel

As illustrated in section 7.2.2.2, reinforcement was modelled separately using beam elements. Beam elements of both longitudinal reinforcement and stirrups were given the property of steel using the material card 024_PIECEWISE_LINEAR_PLASTICITY. Table 14 shows the parameters used for this material model:

Table 14. Parameters used to characterize the steel reinforcement.

Parameter	Value input
Mass Density, RO	7.860e-09
Young's Modulus, E	2.070e+05
Poisson's Ratio, PR	0.29
Yield Strength, SIGY	420 (per the TxDOT drawing)
ETAN	2123

ETAN value is calculated as follows:

As given in the TxDOT drawing, the reinforcement shall be ASTM A-615 Grade 60. Per Table 2, ASTM A615/A615M,

Engineering Tensile Strength = 550 MPa

Percentage elongation = 9

Engineering Strain at Yield = Yield Strength/E

= 420/207000

= 0.00203

True Yield Strength = Yield strength*(1+Engineering strain at yield)

= 420*(1+0.00203)

= 420.85 MPa

True Strain at Yield = LN (1+True Yield Strength/E)

= LN (1+420.85/207000)

= 0.00203

Failure Strain = LN(1+elongation) = LN (1+9/100)

= 0.08618

True Tensile Strength = Engineering Tensile Strength*(1+elongation)

= 550*(1+9/100)

= 599.5 MPa

Tangent Young's Modulus, ETAN = (True Tensile Strength – True Yield Strength)/ (Failure Strain – True Strain at Yield)

= (599.5 – 420.85)/ (0.08618 – 0.00203)

= 2123 MPa

Same material card but with different input parameters was used for the constituent shell elements of JJ hook. Table 15 shows the input values for 024_PIECEWISE_LINEAR_PLASTICITY material card used for JJ hooks:

Table 15. Parameters used to characterize the JJ hooks.

Parameter	Value input
Mass Density, RO	7.860e-09
Young's Modulus, E	2.070e+05
Poisson's Ratio, PR	0.29
Yield Strength, SIGY	336
EPS1	0

Table 15. Continued.

Parameter	Value input
EPS2	0.024
EPS3	0.042
EPS4	0.05
EPS5	0.141
EPS6	0.213
EPS7	0.25
EPS8	0.259
ES1	336
ES2	336.7
ES3	401.2
ES4	434.3
ES5	537.2
ES6	589.6
ES7	675
ES8	677

The data points for plastic stress-strain curve were obtained from a laboratory test data provided by one of the TTI researchers. Figure 97 shows the plot of the data points (EPS, ES) listed in Table 16.

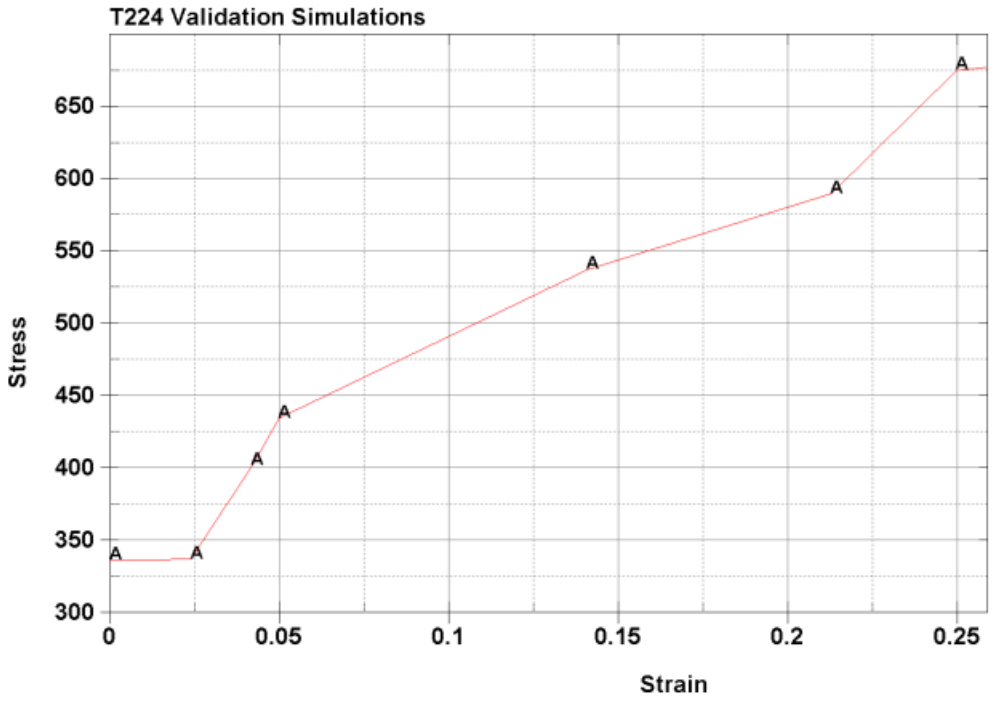

Figure 97. Plastic stress-strain curve for steel (Fy=336 MPa)

For the bogie model, except the crushable cylinders, all the other components were given the properties of a much denser steel material. Since these components were connected through CNRB, rigid material property could not be assigned to them as that could have given rise to numerical instability. Thus, steel of density twice as that of the actual density (2*7.860e-09=1.486e-08) was assigned to immolate the rigid behavior. The cylinders were assigned the property of steel of yield strength 336 MPa (48.7 ksi). The angle plates used to support the JJ hooks were also assigned the property of the steel with a density twice of that of the actual density as these plates were not expected to deform in the simulations.

7.2.4. Contacts

To let the various components of the barrier assembly and the vehicle recognize or "see" each other during an impact event, appropriate contacts should be provided in LS-DYNA. Following contacts were defined in the models developed for this research study:

7.2.4.1. Automatic Single Surface Contact

7.2.4.1.1. Between curved portion of JJ hook and concrete barrier

This contact was provided between the various parts of the concrete barrier body and the portion of the JJ hooks which protruded outside the barrier. The purpose of providing this contact was to allow the curved portions of the JJ hook protruding outside, to recognize each other and the barrier thickness while they rotated during an impact event.

Static coefficient of friction, FS and dynamic coefficient of friction, FD were set to a value of 0.15. Default values were used for SOFSCL (Scale factor for constraint forces of soft constraint option), MAXPAR (Maximum parametric coordinate in segment search), SBOPT (Segment based contact option), DEPTH (Search depth in automatic contact) and IGAP (Flag to improve implicit convergence behavior).

IGNORE was set as 1 to allow initial penetrations to exist. This was done so that if initial small initial penetrations do exist, they do not create any numerical issue in the simulation such as negative contact energy. SOFT was set to the value of 2 as this lets the program to take the element thicknesses into consideration. Not providing a SOFT value leads the components not seeing and penetrating through each other. Figures 98

and 99 illustrate the difference between automatic single surface contacts with “No SOFT” and “SOFT=2”.

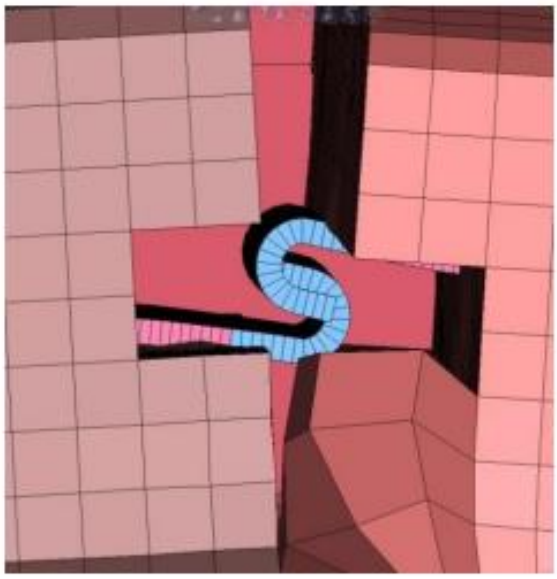

Figure 98. Automatic single surface contact between curved portions of JJ hooks and concrete barrier, No SOFT value provided.

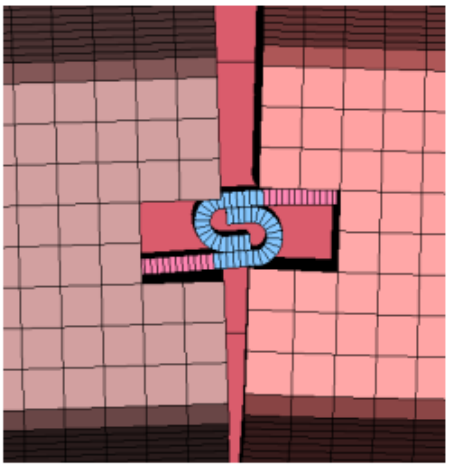

Figure 99. Automatic single surface contact between curved portions of JJ hooks and concrete barrier, SOFT=2

Table 16 summarizes the important parameters for the single surface contact:

Table 16. Parameters used for the contact between curved portion of JJ hooks and concrete barrier

Contact parameter	Value
FS	0.15
FD	0.15
SOFT	2
SOFSCL	0.1
MAXPAR	1.025
SBOPT	2.0
DEPTH	5
IGAP	1
IGNORE	1

In the simulation with the bogie vehicle, all parts of the bogie vehicle were also included in the above-mentioned contact.

7.2.4.2. Automatic Surface to Surface Contact

7.2.4.2.1 Between Barrier and Ground

This contact kept the barrier assembly standing/moving over the rigid shell ground during the various stages of all the simulations. Table 17 summarizes the

important parameters for the automatic surface to surface contact defined between the concrete barrier body and the ground:

Table 17. Parameters used for the contact between the concrete barrier body and the ground.

Parameter	Value
FS	0.46
FD	0.4
SOFT	2
SOFSCL	0.1
MAXPAR	1.025
SBOPT	2.0
DEPTH	5
IGAP	1
IGNORE	0

The values of 0.46 and 0.4 as fs and fd respectively gave a reasonable lateral displacement value in the simulation with the bogie vehicle. Using friction coefficient values higher than these values resulted in a much lower lateral displacement which did not conform to the actual bogie test result leading the researcher choose the former values for friction coefficient. In the past, DEPTH=5 has been validated for other

research projects of TTI, therefore the same value has been used for this research study.

7.2.4.2.1.2 Between Vehicle and Ground

This contact kept the vehicle (RAM/Toyota Yaris) running smoothly over the rigid shell ground. Table 18 summarizes the important parameters for the automatic surface to surface contact defined between the vehicle (RAM/Toyota Yaris) and the ground:

Table 18. Parameters used for the contact between the vehicle (RAM/Toyota Yaris) and the ground.

Contact parameter	Value
FS	0.46
FD	0.4
SOFT	1
SOFSCL	0.1
MAXPAR	1.025
SBOPT	2.0
DEPTH	2
IGAP	1
IGNORE	0

In the simulation with bogie, contact between the bogie and the ground was not required as the bogie parts were rigidly constrained to move in Y-direction (lateral) only. Movement of the bogie was restricted in both X and Z directions.

7.2.4.2.1.3 Between Vehicle and Barrier

This contact was provided so that the vehicle (RAM/Toyota Yaris) did not penetrate the barrier body and recognized its thickness during the impact event. Table 19 summarizes the important parameters for the automatic surface to surface contact defined between the vehicle (RAM/Toyota Yaris) and the barrier:

Table 19. Parameters used for the contact between the vehicle (RAM/Toyota Yaris) and the concrete barrier body.

Contact parameter	Value
FS	0.05
FD	0.05
SOFT	2
SOFSCL	0.1
MAXPAR	1.025
SBOPT	2.0
DEPTH	5
IGAP	1
IGNORE	0

Per 7.2.4.1.1., automatic single surface contact was provided between the bogie vehicle, concrete barrier body and curved portion of JJ hooks in the simulation with the bogie vehicle.

7.2.5. Constraints

7.2.5.1. Lagrange in solid

"Lagrange in solid" constrained the various connection components originally embedded inside the concrete barrier as well as the cage of longitudinal rebars/stirrups to the outer barrier body. Straight portion of JJ hooks, angle plates, longitudinal rebars and stirrups were constrained to the concrete barrier body.

7.2.5.2. Constrained Nodal Rigid Body

Constrained nodal rigid body or CNRB was provided to model connection between two components. CNRB connections were made between the various parts of the bogie nose frame. Also, CNRB connections were made between the angle plates and JJ hooks as well as the welded bars and the straight portion of JJ hooks.

7.2.6. Gravity

Table 20 summarizes the mass of the various components of the 210-foot-long barrier assembly, as measured in LS-DYNA.

Table 20. Mass of the various components of the 210-foot-long barrier assembly.

Part	Mass (Tons)
Concrete Barrier	65.463

Table 20. Continued.

Part	Mass (Tons)
JJ-Hooks	0.063
Angle Plates	0.027
Rebars	1.528

Total mass comes out to be 67.081 Tons. To avoid the dynamic effects associated with large loads, gravity was applied gradually as per the load curve values in Table 21:

Table 21. Load curve for applying gravity.

A1	O1	Load applied
0.0	0.0	0.0
0.025	0.2	13.416
0.05	0.5	33.541
0.075	0.9	60.373
0.085	1.0	67.081
1.5	1.0	67.081

Figure 100 represents the load curve for the abscissa and ordinate values given in Table 21.

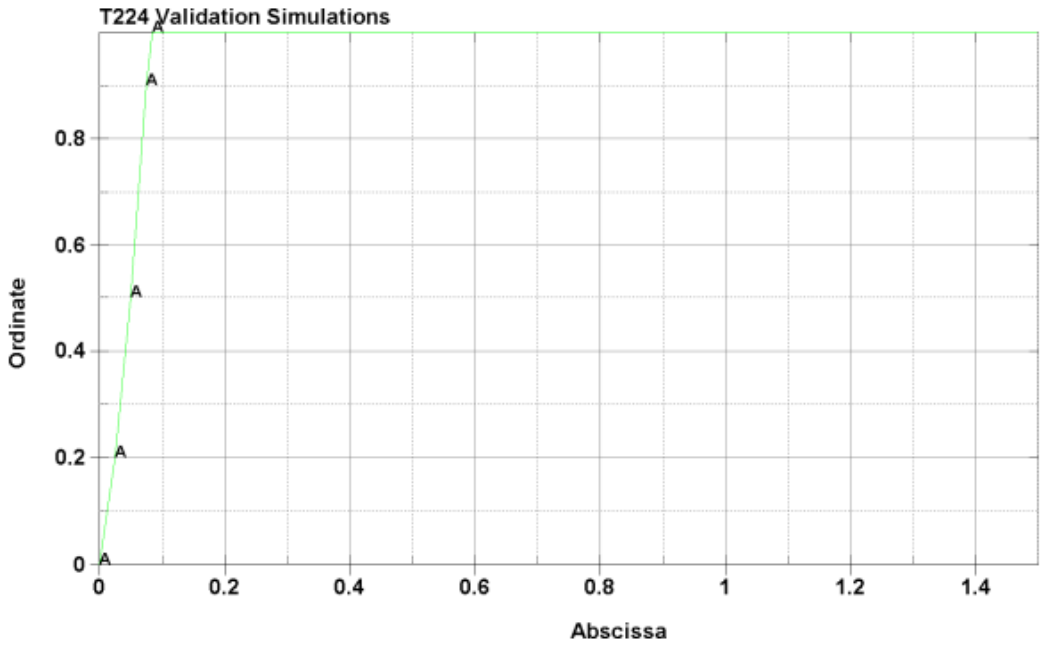

Figure 100. Load curve used for applying gravity

It was ensured in all the simulations that the vehicle impacted the barrier assembly at t=0.09 sec, once the entire weight of the barrier assembly was applied at t=0.085 sec.

7.2.7. Hourglass

Non-physical, zero-energy modes of deformation that produce zero strain and zero stress are known as hourglass modes. These modes occur in under-integrated solid, shell, and thick shell elements (2). They can be completely eliminated by adopting fully-integrated or selectively reduced integration element formulation. For example, type 2 solids can be used in place of the default option of type 1 constant stress solid element, but this selection can be very computationally expensive. Also type 2 solids are much more unstable in large deformation applications such as vehicle impact, thus type 1 solid

was used to formulate the concrete elements in the barrier. LS-DYNA has many algorithms to inhibit hourglass modes, hourglass control type (IHQ) 5 was used for the type 1 solid elements in the single slope barrier model developed for this research study. Hourglass coefficient of 0.08 was used for IHQ=5. Using a too high value for the hourglass coefficient may overly stiffen the response, while using a too low value for the coefficient may result in visible hourglass modes of deformation. Figures 101 and 102 illustrate the difference between the barrier without hourglass and with hourglass card used, respectively.

Figure 101. Single slope barrier simulation without hourglass card

Figure 102. Single slope barrier simulation with hourglass card

Table 22 summarizes the parameters associated with the hourglass card used for type 1 solid concrete elements.

Table 22. Parameters associated with the hourglass card used for type 1 solid concrete elements.

Parameter	Value
Hourglass control type, IHQ	5
Hourglass coefficient, QM	0.08
Bulk viscosity type, IBQ	0
Quadratic bulk viscosity coefficient, Q1	1.5
Linear bulk viscosity coefficient, Q2	0.06
Hourglass coefficient for shell bending, QB/VDC	0.1
Hourglass coefficient for shell warping, QW	0.1

7.2.8. Simulation Time

The simulation was run for 1 second with time interval between outputs equal to 0.01 second. Thus, 100 d3plots were generated for a simulation.

7.3. Simulation for Calibration with Bogie Test

7.3.1. Description

A bogie model weighing 5000 lb. was made to impact perpendicularly at the center of a 4-segment barrier assembly with a nominal speed of 18 mph. Height of the top edge of the frontal piece attached to the bogie nose frame was kept 26.5 inches above the ground, in conformance with the bogie vehicle used in the actual component crash test. Figure 103 shows the initial set up of the bogie and barrier assembly.

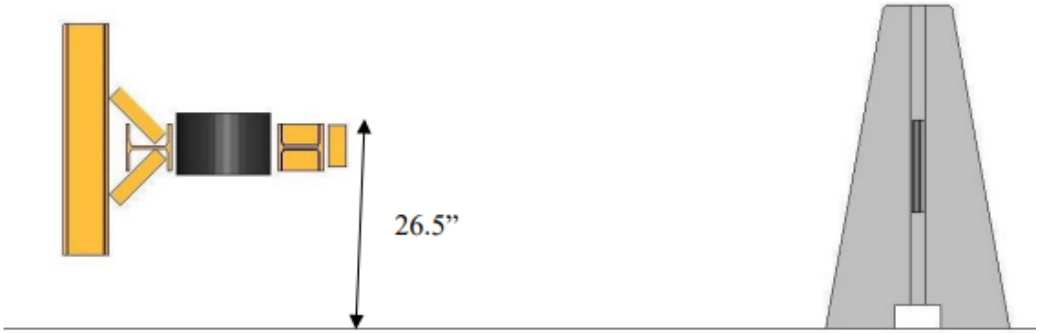

Figure 103. Bogie positioned to impact perpendicularly at the center of the 4-segment barrier assembly, nominal speed= 18 mph.

7.3.2. Results

D3plots obtained were compared with the frames of the crash videos from the actual component crash test and a significant correlation was observed. Figure 104 shows the comparison of the actual crash test (left) and the simulation (right) illustrating the similar barrier segment behavior after the impact.

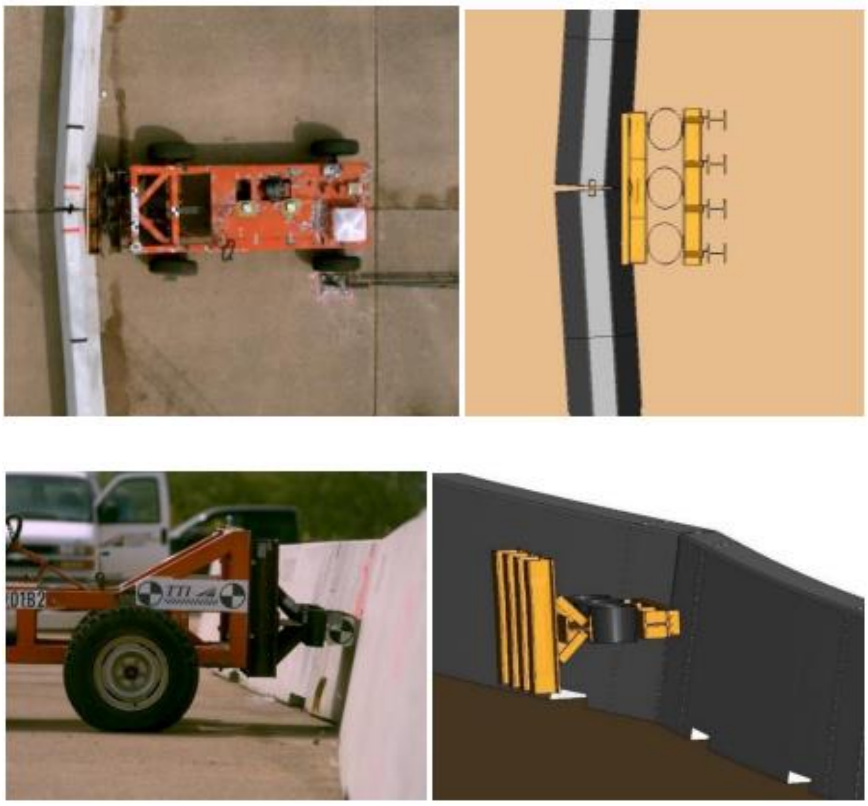

Figure 104. Comparison of actual bogie test (left) and bogie-barrier impact simulation (right) in LS-DYNA.

From the above comparison of frames from the actual test and the simulation, we can say that the model closely replicates the actual behavior of the barriers in terms of the following results:

1. Lateral Displacement at the impacted joint in the simulations compared well with the actual test displacement. The displacement value was obtained as 14 inches which deviated by 8% from the actual displacement value of 15.25 inches.

2. General behavior of barrier toes.

3. Opening in the back of the impacted joint. Thus, the model was considered calibrated with the component crash test, this model was further used in the predictive simulations with the RAM pickup truck and Toyota Yaris passenger car.

7.4. Predictive Simulations

After validating the behavior of the barriers in the crash simulation with the bogie nose, a 210-foot-long barrier assembly was modeled in LS DYNA and pre-existing spalls were introduced into it by deleting the appropriate number of solid elements. The pre-damaged barrier system was impacted by the RAM pickup truck model and Toyota Yaris passenger car model. Each vehicle model was positioned at an angle of 25 degrees and given an initial impact velocity of 62 mph. Purpose of the simulations was mainly focused on finding the occupant impact velocity (OIV), ride down acceleration (RA) as well as assessing the crashworthiness of the barrier system and the post impact vehicle trajectory quantified in terms of roll, pitch, and yaw angles. Since the full-scale crash test barrier arrangements shall be decided based on the findings of the results of these simulations, these simulations are 'predictive' in nature. The predictive simulations were carried out after achieving a realistic behavior of the barrier segments, JJ hook connectors and the vehicle during and after the impact. The process of getting the realistic behavior was not simple, the researcher faced numerous challenges in validating the behavior of the barrier-vehicle system. In the initial stages, the barriers were kept partially rigid (in the middle) and partially flexible (on the ends) but when this barrier model was impacted by the pickup truck/bogie at a speed of 18 mph or beyond, it was found that the connection between the impacted barriers opened which was not

expected at all to happen in the real life. This was a numerical issue since when the material of the barriers was changed to concrete (flexible) from the usual partially rigid and partially concrete (flexible) material, the connection though deformed, did not open out and was found consistent with the actual behavior. There was an excessive deformation of the concrete at the ends during the impact. Multiple attempts were made to eliminate the distortion such as refining the mesh size from 1 in. by 1in. to 0.6 in. by 0.6 in., changing the model of the connection, use of hourglass card and so on.

It was seen that using the hourglass card alone made a considerable difference and eliminated the hourglass modes. The mesh size was changed back to the original 1 in. by 1 in. with hourglass property which ensured that there was no excessive distortion at the barrier ends. Different combinations of contacts were tried for the overall system. An inappropriate contact/ contact property yielded odd behavior such as torsion in the reinforcement even before the vehicle impacted the barrier, inter-penetration between JJ hooks or JJ hook and barrier during the impact, barrier toes not touching each other when they should have been touching and so on. Thus, multiple simulations were run with change of contact parameters to get the most precise behavior of the JJ hook connection and barrier segments. The thesis documents the results of the latest simulations.

7.4.1 Predictive Baseline Simulations with Undamaged Single Slope Barrier

7.4.1.1. Description

The purpose of this simulation was to ascertain the baseline values of OIV (Occupant Impact Velocity), RA (Ride down Acceleration), roll, yaw and pitch values

and lateral displacement of the undamaged barrier. Results from all the subsequent simulations with pre-existing damage(s) in the barrier assembly were compared with the values obtained from the baseline simulation.

7.4.1.1.1. Simulation of undamaged barrier impacted by RAM model representing a 5,000-lb (2270P) MASH pickup truck test vehicle.

A baseline simulation was carried out with the RAM pickup truck model weighing 5000 lb., positioned 4.3 foot upstream of the joint at an angle of 25 degree with the undamaged barrier system to impact at a speed of 62 mph. Figure 105 shows the initial position of the pickup truck with respect to the barrier.

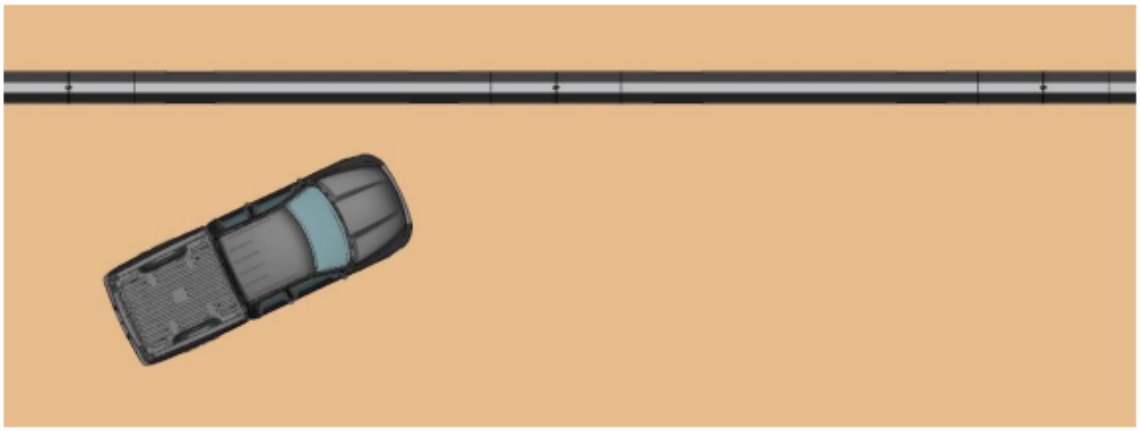

Figure 105. Initial position of RAM pickup truck

Figures 106 illustrates the interaction between the barrier and the vehicle at various time instants.

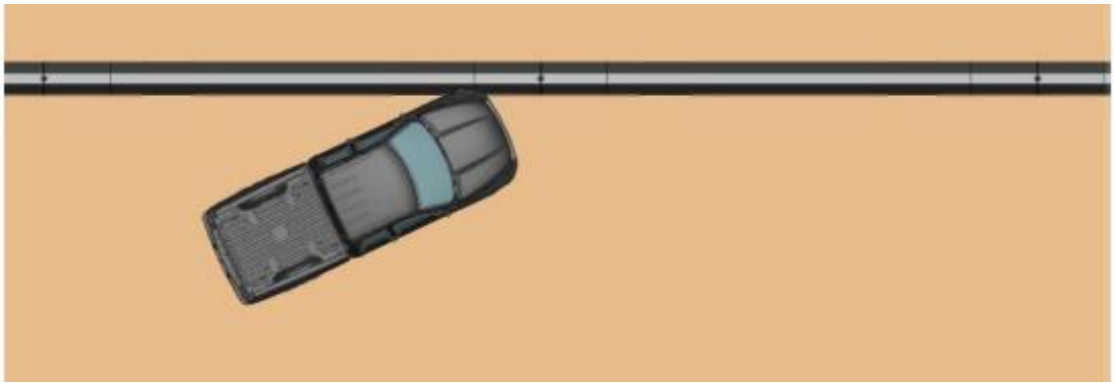

t = 0.090 s, event = Pickup truck strikes the barrier

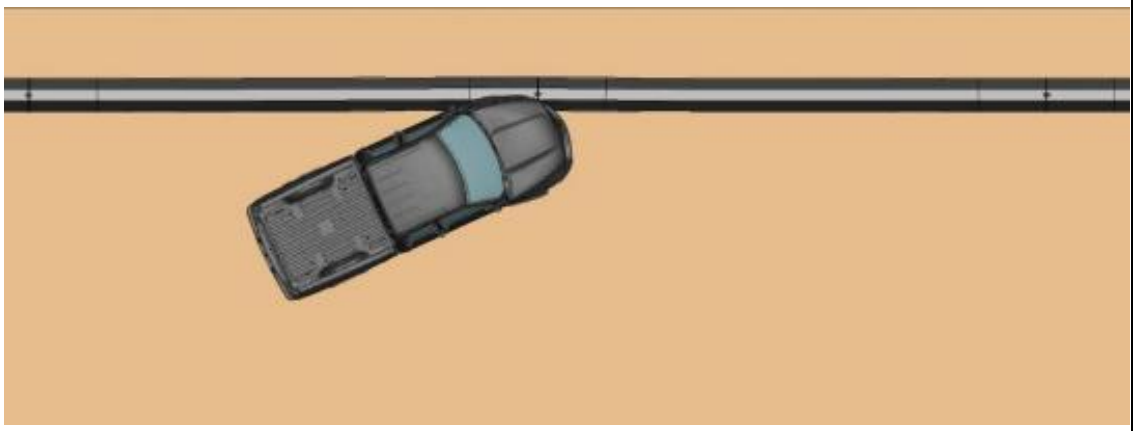

t = 0.13 s, event = Pickup truck contacts the joint

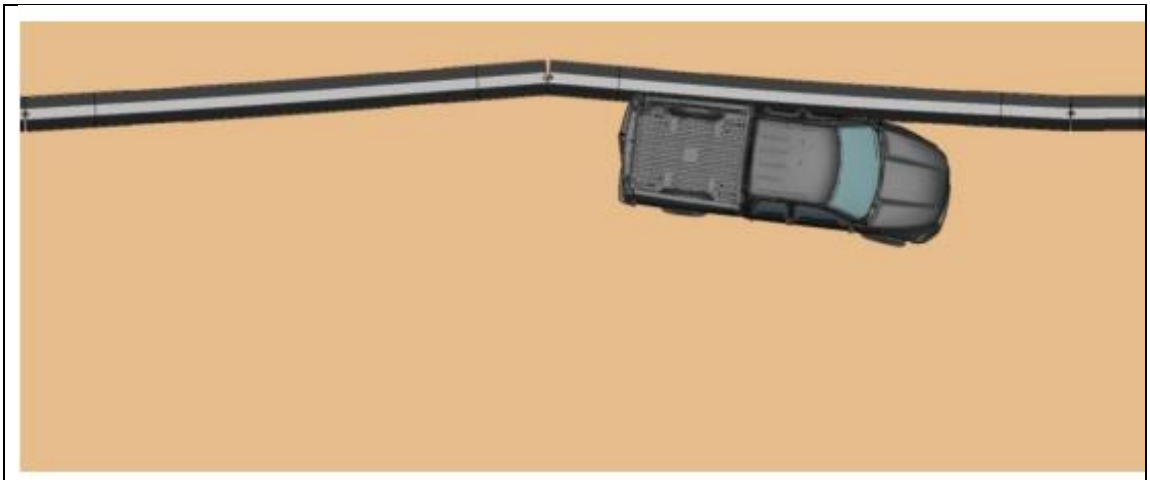

t = 0.40 s, event = Pickup truck redirected by the barrier

Figure 106. Truck-barrier interaction through various stages

Figure 107 illustrates the behavior of RAM pickup truck at various time instants

t = 0.10 s, event = front right tire contacts the barrier

t = 0.31 s, event = rear right tire contacts the barrier

t = 0.54 s, event = front right tire touches ground

Figure 107. Post impact trajectory of the RAM pickup truck

Lateral displacement of the impacted barrier was obtained as 28 inches. TRAP analysis was performed to calculate OIV, RA, pitch, roll and yaw. Table 23 summarizes the results from TRAP.

Table 23. TRAP values for RAM pickup truck impacting an undamaged single slope barrier.

Parameter	Absolute Value
OIV (ft/s)	23.6
RA (g's)	14.4
Yaw (deg.)	31.6
Pitch (deg.)	7.5
Roll (deg.)	16.5

7.4.1.1.2. Simulation of undamaged barrier impacted by Toyota Yaris model representing a 2,420-lb (1100C) MASH small car test vehicle.

A baseline simulation was carried out with the Toyota Yaris passenger car model weighing 2420 lb., positioned 3.6 foot upstream of the joint at an angle of 25 degree with the undamaged barrier system to impact at a speed of 62 mph. Figure 108 shows the initial position of the car with respect to the barrier.

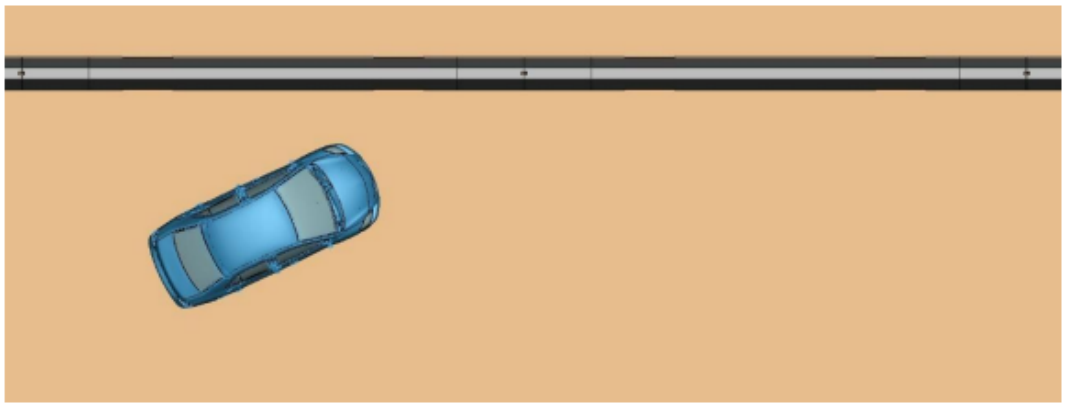

Figure 108. Initial position of Toyota Yaris passenger car

Figures 109 illustrates the interaction between the barrier and the car at various time instants.

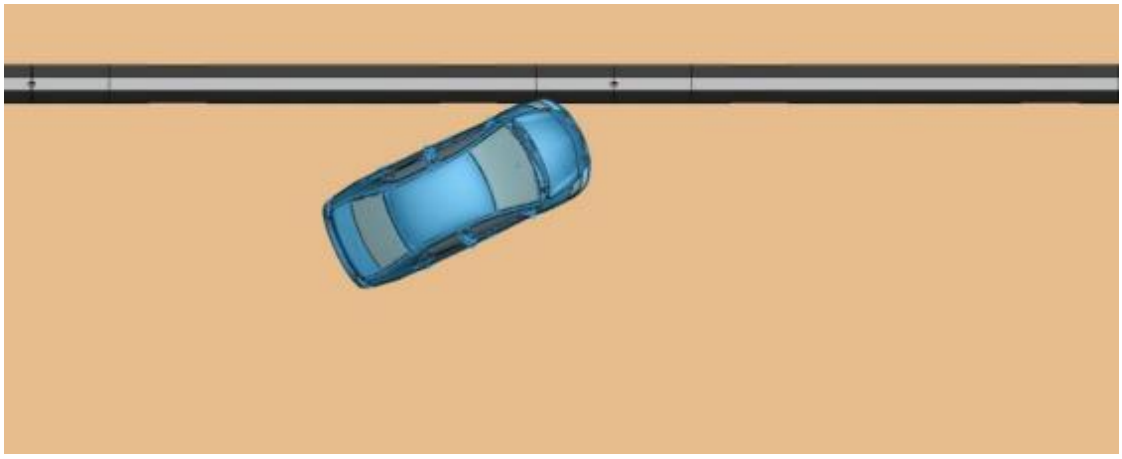

t = 0.090 s, event = Car strikes the barrier

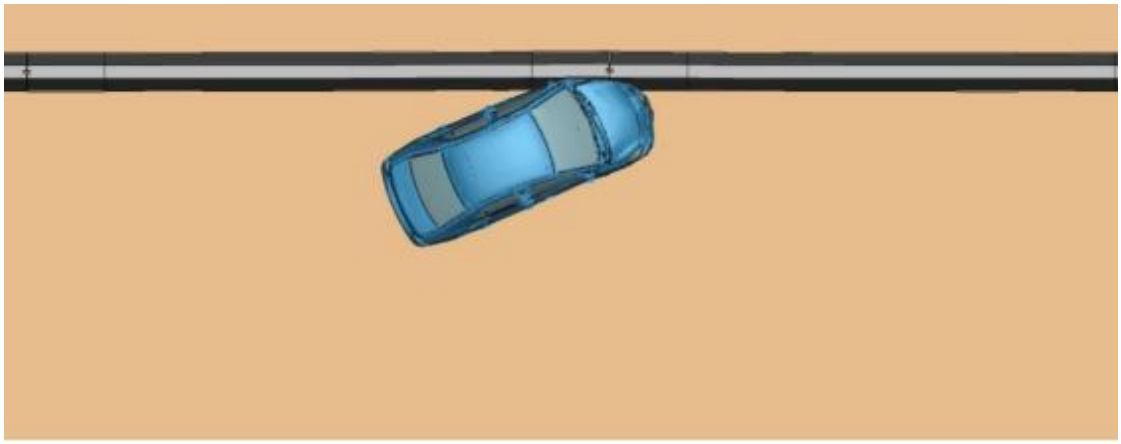

t = 0.13 s, event = Car contacts the joint

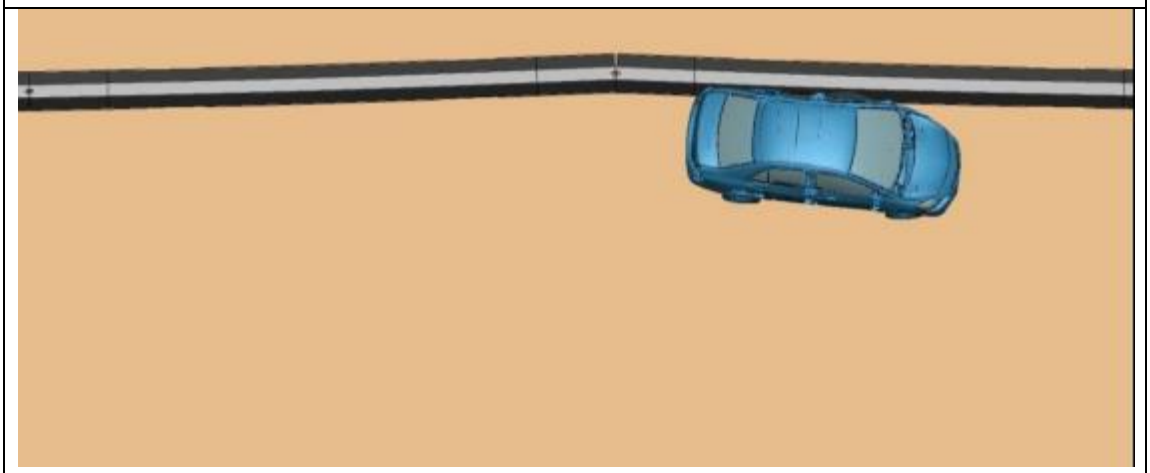

t = 0.33 s, event = Car redirected by the barrier

Figure 109. Car-single slope barrier interaction through various stages

Figure 110 illustrates the post impact trajectory of the car.

t = 0.10 s, event = front right tire contacts the barrier

t = 0.23 s, event = rear right tire contacts the barrier, windowpane snags against the barrier

t = 0.45 s, event = front right tire touches ground

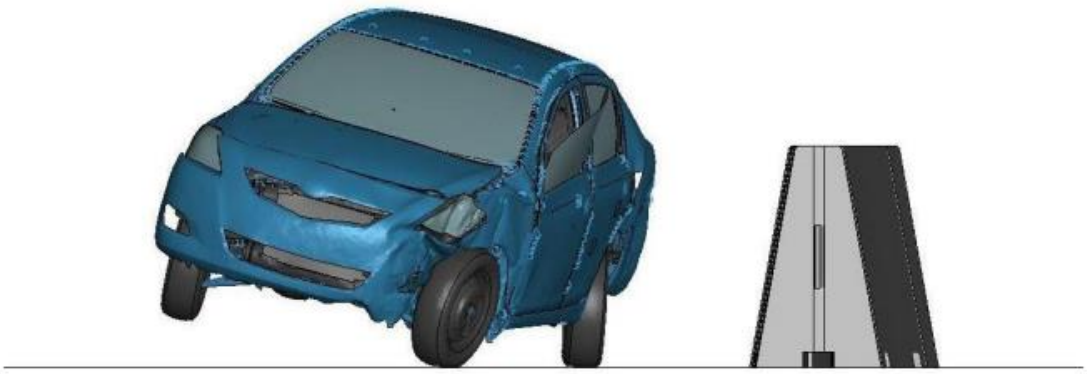

t = 0.91 s, event = rear right tire stabilizes on ground

Figure 110. Post impact trajectory of the Toyota Yaris passenger car.

Lateral displacement of the impacted barrier was obtained as 11 inches. TRAP analysis was performed to calculate OIV, RA, pitch, roll and yaw. Table 24 summarizes the results from TRAP.

Table 24. TRAP values for Toyota Yaris Passenger Car impacting an undamaged single slope barrier.

Parameter	Absolute Value
OIV (ft/s)	24.6
RA (g's)	17.2
Yaw (deg.)	37.2
Pitch (deg.)	8.2
Roll (deg.)	27.7

7.4.2. Predictive Simulations with Pre-Damaged Single Slope Barrier

7.4.2.1. Description

The purpose of these simulations was to ascertain the values of OIV (Occupant Impact Velocity), RA (Ride down Acceleration), roll, yaw and pitch values and lateral displacement of the damaged barrier. Pre-existing damage was introduced into the barrier system by deleting elements to make a spall of certain size.

7.4.2.1.1. Simulation of the pre-damaged barrier (13 in. x 4 in. x 2 in. spall on toe) impacted by RAM model representing a 5,000-lb (2270P) MASH pickup truck test vehicle.

Pre-existing damage in the form of a 4 in. by 13 in. by 2 in. spall was created on the toe of one of the barriers. Figure 111 illustrates the damage created in the barrier.

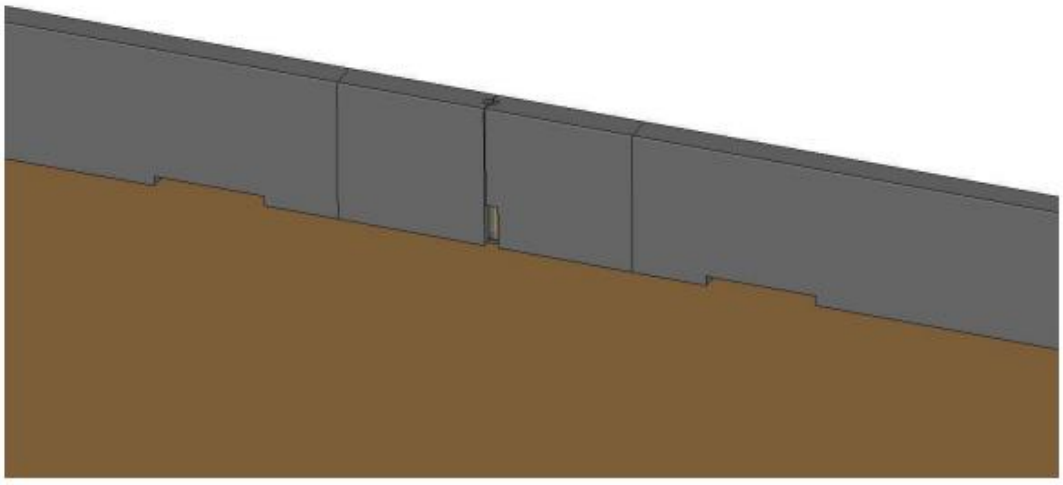

Figure 111. Pre-damaged barrier with a spall on toe with length= 13 in., width= 4 in., depth=2 in.

Lateral displacement of the impacted barrier was obtained as 29 inches. TRAP analysis was performed to calculate OIV, RA, pitch, roll and yaw. Table 25 summarizes the results from TRAP.

Table 25. TRAP values for RAM pickup truck impacting a single slope barrier with 1 spalled toe.

Parameter	Absolute Value
OIV (ft/s)	23.5
RA (g's)	14.7
Yaw (deg.)	32
Pitch (deg.)	7.2
Roll (deg.)	13

7.4.2.1.2. Simulation of the pre-damaged barrier (13 in. x 4 in. x 2 in. spall on toe) impacted by Toyota Yaris model representing a 2420-lb (1100C) MASH small car test vehicle.

Lateral displacement of the impacted barrier was obtained as 11.1 inches. TRAP analysis was performed to calculate OIV, RA, pitch, roll and yaw. Table 26 summarizes the results from TRAP.

Table 26. TRAP values for Toyota Yaris passenger car impacting a single slope barrier with 1 spalled toe.

Parameter	Absolute Value
OIV (ft/s)	25.2
RA (g's)	16.3
Yaw (deg.)	40.4
Pitch (deg.)	8.2
Roll (deg.)	28.1

7.4.2.1.3. Simulation of the pre-damaged barrier (13 in. x 4 in. x 2 in. spall on adjacent toes) impacted by RAM model representing a 5,000-lb (2270P) MASH pickup truck test vehicle.

Pre-existing damage in the form of a 4 in. by 13 in. by 2 in. spall was created on adjacent toes of the two barriers at the center. Figure 112 illustrates the damage created in the barrier.

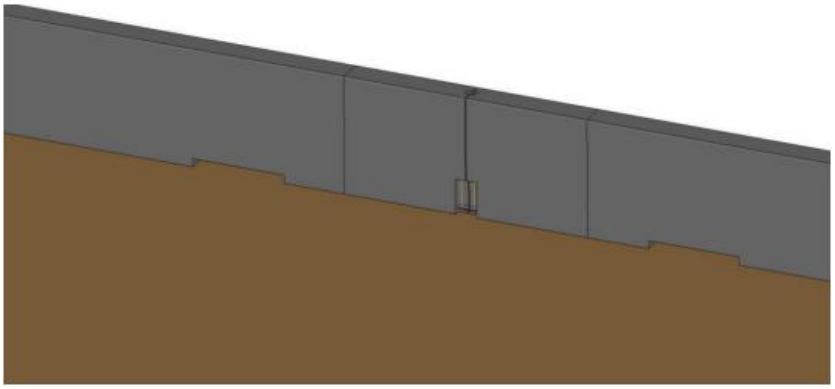

Figure 112. Pre-damaged barrier with adjacent toes having spalls of length= 13 in., width= 4 in., depth=2 in.

Lateral displacement of the impacted barrier was obtained as 29 inches. TRAP analysis was performed to calculate OIV, RA, pitch, roll and yaw. Table 27 summarizes the results from TRAP.

Table 27. TRAP values for RAM pickup truck impacting a single slope barrier with 2 spalled toes.

Parameter	Absolute Value
OIV (ft/s)	23.4
RA (g's)	14.2
Yaw (deg.)	32.0
Pitch (deg.)	6.1
Roll (deg.)	16.6

7.4.2.1.4. Simulation of the pre-damaged barrier (13 in. x 4 in. x 2 in. spall on adjacent toes) impacted by Toyota Yaris model representing a 2420-lb (1100C) MASH small car test vehicle.

Lateral displacement of the impacted barrier was obtained as 11 inches. TRAP analysis was performed to calculate OIV, RA, pitch, roll and yaw. Table 28 summarizes the results from TRAP.

Table 28. TRAP values for Toyota Yaris Passenger Car impacting a single slope barrier with 2 spalled toes.

Parameter	Absolute Value
OIV (ft/s)	25.2
RA (g's)	16.9
Yaw (deg.)	32.9
Pitch (deg.)	8.2
Roll (deg.)	30.8

7.4.3. Observations and Discussion

The researcher evaluated the crashworthiness of the full-scale single slope barrier assembly through FEA simulations under MASH TL-3 impact conditions. Baseline simulations were carried out with the RAM pickup truck and Toyota Yaris passenger car. The results of the baseline simulation with the pickup truck were compared with the results from the subsequent simulations of (i) damaged single slope barrier assembly with 1 spalled toe impacted by the pickup truck and (ii) damaged single slope barrier assembly with 2 adjacent spalled toes impacted by the pickup truck. Size of the spall was selected as 13 inches (height) by 4 inches (width) by 2 inches (depth) based on two reasons:

(i) Firstly, from the review of the guidelines given by other DOTs, usually a portable concrete crash barrier is considered unacceptable if it has a spall of a

size equal to or greater than 12 inches in any surface dimension and a depth greater than the cover.

(ii) Secondly, nearby spall sizes were witnessed in the barriers damaged during crash testing done at the TTI proving ground.

Therefore, the researcher decided to evaluate this particular spall size through FEA simulations.

Since the spall on the ends could make a barrier rotate more in case of a vehicle impact with the threat of tire getting snagged, the spall was strategically created on the toe(s). But despite of the damaged toe, it was found that the single slope barrier maintained its crashworthiness without any considerable difference in vehicle occupant risk (OIV, RA) and stability values (yaw, pitch, roll). For the envelope of FEA simulations with the single slope barrier and pickup truck, maximum and minimum absolute values of OIV, RA, yaw, pitch and roll along with the % variation are summarized below:

Table 29. Comparison of TRAP results for simulations involving pickup impacting the single slope barrier.

Parameter	Maximum absolute value	Minimum absolute value	%Variation =100*(Max.-Min.)/Min.
OIV (ft/s)	23.6	23.4	0.9
RA (g)	14.7	14.2	3.5
Yaw (deg.)	32	31.6	1.3
Pitch (deg.)	7.5	6.1	23.0
Roll (deg.)	16.6	13	27.7
Deflection	29	28	3.6

From Table 29, we see that the OIV of 23.6 ft/s is less than the corresponding preferred value of 30 ft/s and the RA of 14.7 g's is less than the corresponding preferred value of 15 G's. Pitch and roll values are much less than the MASH limit of 75 degrees. Similar comparisons were done for the corresponding FEA simulations with the passenger car. For the envelope of FEA simulations with the single slope barrier and passenger car, maximum and minimum absolute values of OIV, RA, yaw, pitch and roll along with the % variation are summarized below:

Table 30. Comparison of TRAP results for simulations involving passenger car impacting the single slope barrier.

Parameter	Maximum absolute value	Minimum absolute value	%Variation =100*(Max.-Min.)/Min.
OIV (ft/s)	25.2	24.6	2.4
RA (g)	17.2	16.3	5.5
Yaw (deg.)	40.4	32.9	1.3
Pitch (deg.)	8.2	8.2	22.8
Roll (deg.)	30.8	27.7	11.2
Deflection	11.1	11	0.9

From Table 30, we see that the OIV of 25.2 ft/s is less than the corresponding preferred value of 30 ft/s and the RA of 17.2 g's is less than the corresponding maximum value of 20.49 G's. The maximum roll of the car is observed as 30.8 degrees which is less than the limit of 75 degrees but is still considerable. Although, as per the latest literature review, the behavior of a portable single slope barrier with JJ hooks has not

been investigated with full-scale crash testing in the past, the level of instability in terms of roll that the simulations appear to show is still questionable. The reason for this concern is that when similar predictive simulations were carried out by another Graduate Assistant Researcher, Aniruddha Zalani on a full-scale assembly of F shape barrier segments (which is much less heavy than the robust single slope barrier), the lateral deflection was more than double that of the single slope barrier deflection, yet the car was observed to be much more stable. This makes the researcher suspect that a potential modelling characteristic of the available passenger car might be causing the observed discrepancy in the roll angle. The researcher further suggests investigating some modifications in the passenger car model to depict impact behavior best realistically against the single slope barrier.

7.4.4. Effect of Pre-Deformed JJ Hook Connectors on the Crashworthiness of Barrier Systems.

In general, single slope shape barrier is known to be the most crashworthy barrier out of all the different shapes of barriers. Since F shape barrier is less heavy than the single slope barrier and thus, more critical from safety point of view, this series of predictive simulations with pre-deformed JJ hook connectors was carried out on a fullscale assembly of F shape barrier segments. The model of the F shape barrier assembly was prepared by Graduate Assistant Researcher, Aniruddha Zalani (TTI). The researcher of this project introduced deformations in the JJ hooks by making changes in the original geometry. Figure 113 shows a pair of undeformed hooks (diameter=1.10 in.)

and a pair of JJ hook connectors where each hook is opened to 1.41 in. from the original diameter of 1.10 in.

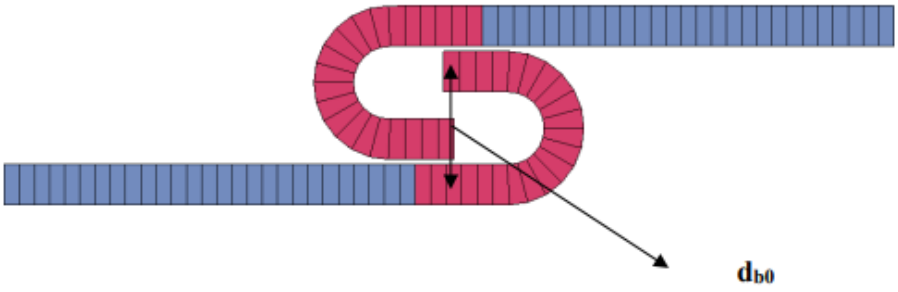

Figure 113 (a). Undeformed JJ hook connectors with db0=1.10 in.

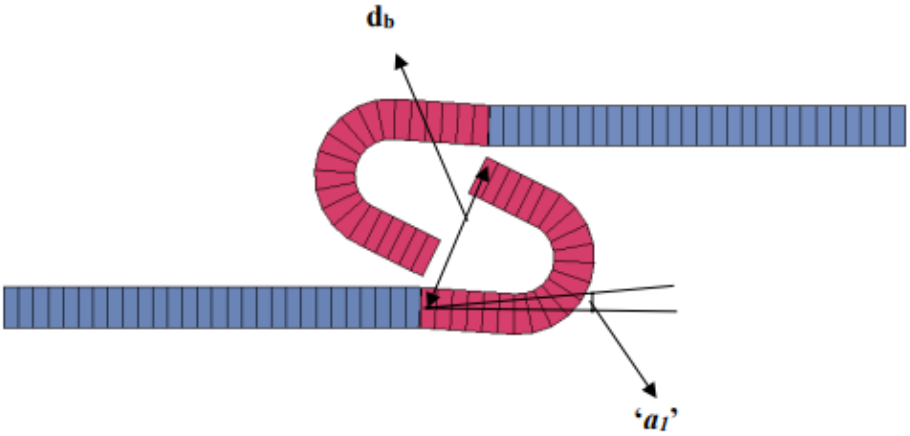

Figure 113 (b). Pre-deformed JJ hook connectors with db1=1.41 in. and rotation angle 'a1' = 4 deg.

This deformation was comparable to the maximum JJ hook deformation recorded at the end of the predictive FEA simulation replicating MASH Test 3-11. A second predictive FEA simulation was conducted to replicate MASH Test 3-11with inclusion of

the above recorded JJ hook deformation. Critical impact point was chosen as suggested by MASH (4.3 foot upstream of the joint). Results of the second predictive FEA simulation showed that JJ hook connectors increased their deformation as expected (Figure 114). The pre-impact distance db1 increased from 1.41 in. to 1.54 in.

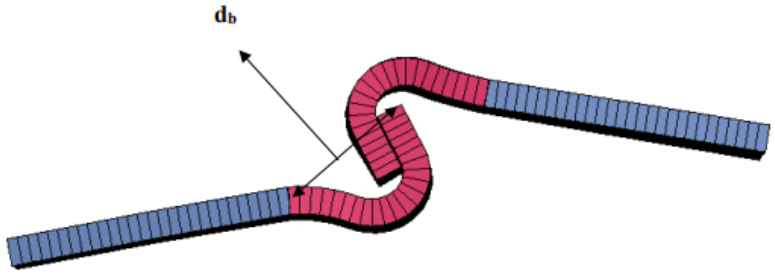

Figure 114. Pre-deformed JJ hook connectors with db1= 1.41 in. open to db2=1.54 in. and rotation angle increases from 4 deg.

Further, the deformation in JJ hook connectors was increased by complimenting the opening of the hook with maximum hook rotation. Figure 115 illustrates the next deformation level which was introduced in the JJ hook connectors.

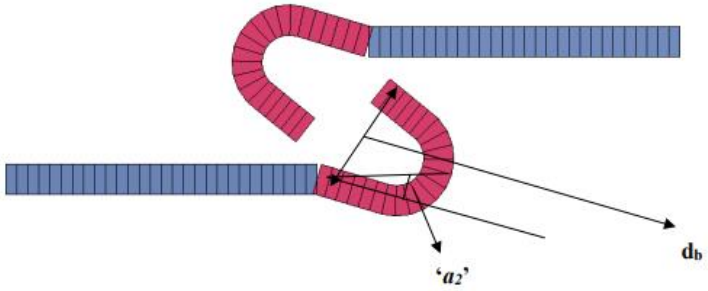

Figure 115. Pre-deformed JJ hook connectors with db1=1.41 in. and rotation angle 'a2'= 16.4 deg.

When barrier system with pre-deformed JJ hook connectors shown in Fig. 115 was impacted by RAM pickup truck, JJ hook connectors opened to a maximum distance of 2.06 in. Figure 116 shows the resulting deformation in the JJ hook connectors.

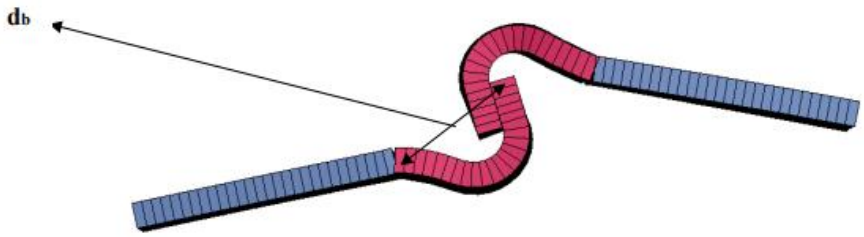

Figure 116. Pre-deformed JJ hook connectors with db1=1.41 in. open to db4=2.06 in. and rotation angle increases from 16.4 deg.

Since it is also possible to have the individual JJ hooks in a pair to be rotated by different angles, a simulation was run with the RAM pickup truck and a barrier system with one undeformed JJ hook and another rotated JJ hook. Figure 117 shows the JJ connector pair with an undeformed hook and a deformed hook.

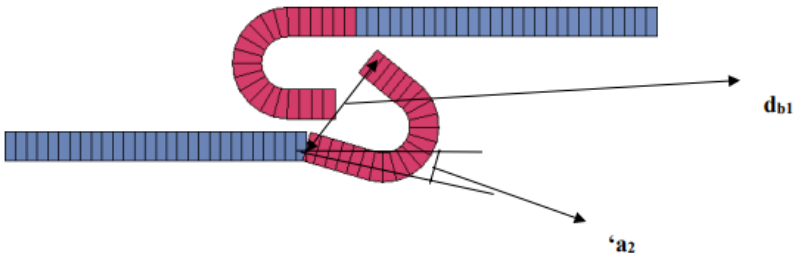

Figure 117. Pair of undeformed and pre-deformed JJ hook connectors. db1 = 1.41 in., 'a2'=16.4 deg.

Figure 118 illustrates the resulting deformation in the JJ hook connectors at the end of the simulation.

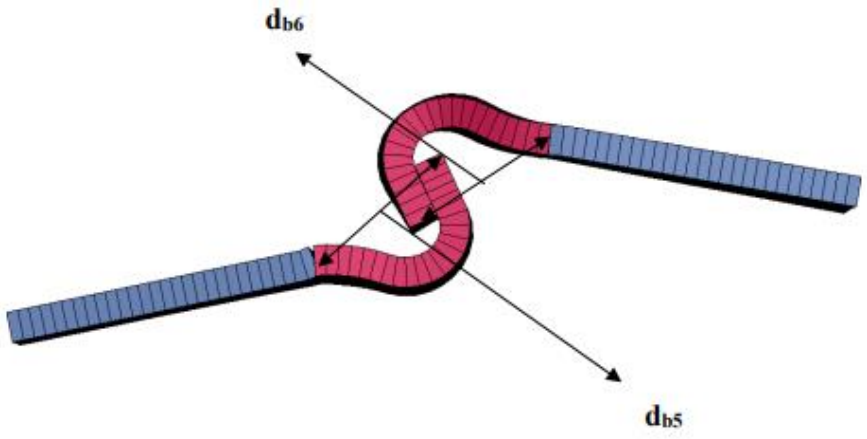

Figure 118. Pre-deformed JJ hook opens to db5 = 1.99 in. whereas the originally undeformed hook opens to db6 = 1.97 in.

Table 31 summarizes the system deflection, opening of the barrier segments at the back and TRAP values for F shape barrier systems with the different cases of pre-deformed JJ hook connections, impacted by RAM pickup truck. An erode value of 1.1 was used in all these simulations.

Table 31. F shape barriers with pre-existing deformations in JJ hooks.

Parameter	Pre-deformed JJ hook connectors with db1=35.8 mm and rotation angle 'a1'=4 deg. (Case 1)	Pair of undeformed and pre-deformed JJ connectors with db1=35.8 mm and rotation angle 'a2'= 16.4 deg. (Case 2)	Pre-deformed JJ hook connectors with db1 = 35.8 mm and rotation angle 'a2'= 16.4 deg. (Case 3)	Pre-deformed JJ hook connectors with db1=35.8 mm and rotation angle 'a2'= 16.4 deg. combined with 2 spalls on toes (Case 4)
Deflection (in.)	55.7	57.2	59.2	61
Opening at back (in.)	7.9	8.3	8.6	8.4
OIV (ft/s)	22.2	22.2	22.1	21.7
Ridedown Acceleration	13.9	13.9	13.4	12.9
Roll (deg.)	13	10.6	12.3	12.7
Pitch (deg.)	12.8	12	12.7	13.2
Yaw (deg.)	48.7	46.2	48.7	49.5

From Table 31, we can observe that the deflection of the barrier system increases from 55.7 inches (when pre-deformed JJ hook connectors had the hook open to a diameter of 1.41 in.) to 61 inches (when the maximum deformation level in JJ hooks was complemented by spalls on the adjacent toes). TRAP values for OIV, RA, roll, pitch, and

yaw are comparable and within the prescribed limits given in MASH. Table 32 gives the comparison of the deflection, opening and TRAP values for the simulation with F shape barrier system with pre-deformed JJ hook connectors (db1=1.41 in.) and the two MASH vehicles (RAM pickup truck and Toyota Yaris passenger car).

Table 32. RAM pickup truck vs Toyota Yaris passenger car with F shape barrier system having pre-existing deformations in JJ hooks.

Parameter	F-shape barrier system with RAM pickup truck, ERODE=1.1	F-shape barrier system with Toyota Yaris passenger car, ERODE=1.1
Deflection (in.)	55.7	27.8
Opening at back (in.)	7.9	4.7
OIV (ft/s)	22.2	24.3
Ridedown Acceleration	13.9	16.7
Roll (deg.)	13	13.4
Pitch (deg.)	12.8	6.0
Yaw (deg.)	48.7	37.8

From Table 32, we can observe that the TRAP values are within the prescribed limits given in MASH.

7.4.5. Observations and Discussion

As discussed in section 7.4.3., pre-existing spalls alone did not show any detrimental effect on the crashworthiness of the full-scale single slope barrier system. F shape barrier being lighter and less crashworthy shape deflects more than the single slope barrier during vehicle crash and therefore has a higher risk of causing instability to the vehicle. For this reason, the combined effect of JJ hook deformations and pre-existing spalls was studied by carrying out FEA simulations with the F shape barrier.

In the simulations involving the pickup truck and F shape barrier with pre-deformed JJ hook connections, the deflection increases from 55.7 inches (when pre-deformed JJ hook connectors had the hook open to a diameter of 1.41 in.) to 61 inches (when the maximum deformation level in JJ hooks was complemented by spalls on the adjacent toes) but there is not much difference in the values of OIV, RA, roll, pitch and yaw of the pickup truck. Also, the TRAP values (Table 11) are within the prescribed limits given in MASH implying that the barrier maintains its crashworthiness. In the simulation involving the F shape barrier having deformed JJ hook connection combined with two spalled toes, OIV and RA values of the passenger car are found as 24.3 ft/s and 16.7 g's respectively which are higher than the corresponding values for the pickup truck which are found as 22.2 ft/s and 13.9 g's. The roll of the passenger car is 13.4 degrees which is higher than the roll of the pickup truck (13 degrees), although the difference is not appreciable. As part of the scope of future investigation, it is suggested to verify the most critical combination checked for F-shape barrier (Case 4, Table 31) on the single slope barrier assembly.

7.5. References

1. US Department of Transportation Federal Highway Administration, User's Manual for LS-DYNA Concrete Material Model 159, Publication No. FHWAHRT-05-062, May 2007.

2. Hourglass, LS-DYNA Support, Last accessed on October 28, 2021. https://www.dynasupport.com/howtos/element/hourglass

8. CONCLUSION

Portable concrete barriers (PCBs) are roadway safety hardware designed to protect workers in construction zones from traffic. Continuing to use severely damaged barriers and not replacing them in a timely manner can pose a safety risk, while replacing them too early underestimates their design life and adds to the overhead cost of the project. At present, PCBs used in the state of Texas do not have standardized guidelines governing their inspection, use and repair. The aim of this research study is to develop preliminary guidelines for the evaluation and repair of TxDOT PCBs. The procedure is quite involved and consists of multiple research steps: literature review, bogie testing, non-destructive testing, engineering analysis (predictive simulations) and full-scale crash testing.

The tasks independently carried out by the researcher involved reviewing the latest literature on the guidelines given by other state DOTs, studying about repair materials and different repair method statements for concrete spalls and cracks, observing various damage modes in component (crash) testing, conducting non-destructive testing of selected PCB segments, proposing evaluation and repair guidance based on the literature review and observation from the component tests and evaluating the critical guidelines (identified earlier) by carrying out predictive FEA simulations of calibrated barrier model under MASH TL-3 impact conditions. Based on the findings of the predictive analysis, critical barrier arrangements shall be identified and tested in the future on the TTI proving ground.

Guidelines laid down by different state DOTs on the usage and repair of PCBs were studied and compared. A literature review was already carried out by TTI researchers which was considered by the researcher of this project. Further the different acceptability criteria for spalls, cracks, and JJ hook deformations, were reviewed and it was seen that not only the guidelines by the various state DOTs differed from each other but were also very subjective to the experience of the inspector. The researcher intends to give a standardized guidance for TxDOT PCBs and wherever possible attempts to define acceptability criteria in terms of threshold values for different damage modes. To complement the findings from the review of guidelines given by other state DOTs, the researcher also used her observations from component testing to come up with the evaluation guide which would classify a given barrier as acceptable, acceptable with repair or unacceptable. Selected PCB segments damaged during component testing were tested non-destructively using sophisticated devices namely, low frequency ultrasonic tomography device and ground penetrating radar. Images taken from these devices were further processed using specialized computer software. Investigation carried out with the low-frequency ultrasonic tomography gave important clue about the underlying reinforcement arrangement of the barrier. However, corresponding to the damages seen on the surface (cracks, spall), no change could be traced back to the internal structure of the barrier. Though there were some large red bands observed in the C scans (other than the rebar lines), but a definite conclusion could not be drawn. The researcher recommends investigating the significance of these red bands.

Ground Penetrating Radar (GPR) additionally gave information on the cover depth and potential voids that might be present inside the barrier(s). Reinforcement layout found through the results from both the devices were compared with each other as well as compared with the standard TxDOT drawings. For the middle region of the barriers, the reinforcement arrangement was found consistent throughout the results of tests done using both the devices and matched with the reinforcement arrangement shown in the standard drawings as well. However, for the end region near the joint, the vertical rebar arrangement was found slightly different from the one shown in the drawings.

A repair guidance has been proposed for the PCBs based on the suggestions given in the TxDOT Concrete Repair Manual 2021 as well as the latest practices adopted/preferred for common concrete damages namely, spalls and cracks. The most important part of the research study is the engineering analysis where the least conservative or the most critical threshold value for the acceptability criteria for pre-existing spalls, coming from the guidelines of other state DOTs have been evaluated by carrying out predictive FEA simulations under MASH TL-3 impact conditions.

Finite element model of the single slope barrier along with the connection details was developed in LS-DYNA. The model was calibrated against the bogie tests and then predictive simulations were performed with the MASH vehicle models, 0.5-ton 4 door quad RAM pickup truck and Toyota Yaris passenger car.

The finite element analyses were kept restricted to evaluate the effect of pre-existing damage in barriers in the form of spalls and deformed JJ hooks. Cracks were

excluded from this study as the researcher made the recommendations on cracks in the preliminary guidelines based on the overriding concern of durability.

The barrier model was considered validated as it replicated the bogie test results in terms of the connection behavior, relative rotation of segments and lateral displacement of the barrier system at the impacted joint. The lateral displacement obtained was 14 in. which deviated from the actual lateral displacement value of 15.25 in. by only 8%. Different damage modes such as pre-existing spalls and deformed JJ hooks were assessed.

Angular velocities and linear acceleration values from the predictive simulation (with an undamaged barrier system and barrier system with a specific damage mode) were extracted and processed further in the TRAP (Test Risk Assessment Program) software. Results from TRAP gave the pitch, roll, yaw angles, occupant impact velocities (OIV) and ride down accelerations (RA) for the RAM pickup truck and Yaris passenger car. The TRAP values were compared with the corresponding limits prescribed for TL 3 in MASH.

Simulations indicated that the maximum spall of dimensions 13 inches (height) by 4 inches (width) by 2 inches(depth) did not alter the crashworthiness of the single slope barrier when impacted under MASH TL-3 conditions. Simulations that were conducted with the various deformation levels in the F shape barrier indicated that the maximum JJ hook deformation considered by the researcher did not have a detrimental effect on the crashworthiness of the barrier system. Further, the researcher recommends verifying the case of maximum JJ hook deformation combined with pre-existing spalls

with a single slope barrier system through another predictive FEA simulation under MASH TL-3 impact conditions.

As part of the scope of future FEA simulations, the researcher additionally recommends evaluating the effect of pre-existing damage near the scupper for both single slope barrier and F shape barrier. The low-profile barrier system with the X bolt connectors is much different in terms of crash behavior than the single slope barrier/F-shape barrier with JJ hooks, thus its investigation through finite element modelling shall be of great computational interest.

There have been some limitations in the modelling process. The deformation in JJ hooks was introduced by making changes in the original geometry of the JJ hook. The material properties of the JJ hook were not changed from the original i.e., no prestress or prestrain was included in the material input whereas this might not be the case in the real life. JJ hook deformations are accompanied with damage in the concrete surrounding the hooks but in the model such modification was not made.

Keeping in mind the modelling limitations discussed above, the researcher recommends conducting full-scale crash testing to verify the results recorded from the FEA simulations. Physical full-scale crash testing results will also provide additional material that can be used for additional future predictive simulations involving similar damage mode characteristics.